

Two case studies of fractured upper mantle peridotite from the Western Gneiss Region (Norway) and Lherz (French Pyrenees): did reaction-induced fracturing play a role?



Renske Lambert

December, 2010

MSc thesis Geology
Supervisor: prof. dr. Martyn Drury

Faculty of Geosciences
Department of Earth Sciences



Universiteit Utrecht

Contents

Abstract.....	3
1. Introduction.....	4
1.1 Background.....	4
1.2 Research questions.....	4
1.3 Outline thesis.....	5
2. Serpentinization and fracturing history of upper mantle peridotites in the Western Gneiss Region (Norway).....	6
2.1 Introduction.....	6
2.2 Research area.....	7
2.2.1 Geological history peridotites on Otrøy.....	7
2.2.2 Field area.....	8
2.3 Method.....	9
2.4 Fracture networks at outcrop scale.....	11
2.4.1 Morphology.....	11
2.4.2 Orientation.....	15
2.5 Fractures on microscopic scale.....	22
2.5.1 Fractures in peridotite.....	22
2.5.2 Fractures in pyroxenite layers.....	27
2.6 Serpentinization and volume change.....	29
2.6.1 Key reactions.....	29
2.6.2 Volume expansion due to serpentinization.....	29
2.6.3 PT conditions.....	30
2.6.4 Thermal contraction.....	31
2.7 Discussion.....	32
2.7.1 Development of fracture networks.....	32
2.7.2 Evolution of peridotite bodies.....	38
2.8 Conclusions.....	39
3. Breccia development and carbonation in the Lherz peridotite (French Pyrenees).....	40
3.1 Introduction.....	40
3.2 Geological setting.....	40
3.3 Method.....	41
3.4 Field observations: types of breccias.....	43
3.4.1 Peridotite breccia with calcite matrix.....	43
3.4.2 Peridotite breccia with peridotite matrix.....	46
3.4.3 Polymictic breccias with peridotite matrix.....	47
3.5 Mineralogy and microstructures.....	49
3.5.1 Peridotite breccia with calcite matrix.....	49
3.5.2 Internal and matrix-supported peridotite breccia.....	52
3.5.3 White homogeneous material.....	53
3.6 Discussion.....	60
3.6.1 Geological implications of classified breccias.....	60
3.6.2 Serpentine or white olivine?.....	63

3.6.3	General model for breccia development.....	64
3.7	Conclusions	67
4.	Summary	68
5.	References	70
	Appendix A: List of mineralogy	72
	Appendix B	73
	Appendix C: Volume change calculations	74
	Appendix E: EBSD patterns	77
	Acknowledgements	79

Abstract

The possibility of in situ CO₂ sequestration in mantle rock is widely investigated (Kelemen & Matter (2008) amongst others). The process involves infiltration of CO₂-rich fluids into the mantle rock through initial cracks, which react with the main constituents of the host rock (olivine and pyroxene) to form serpentine and carbonates. Hereby the CO₂ content in the atmosphere is reduced. A volume increase during both serpentinization and carbonation could cause further fracturing of the rock. In this case, the fractures would enhance the process by creating additional reaction surface and allowing fluids to penetrate deeper into the rock. Studying naturally fractured mantle rocks gives insight in the mechanisms that play a role in the formation of fracture networks and fracture propagation. Two case-studies of fractured peridotite bodies in the Western Gneiss Region (Norway) and the brecciated Lherz body (French Pyrenees) were done. The development of fracture networks and the role of serpentinization and carbonation in fracturing were investigated by studying the geometry and scale of fracture patterns in the field and performing optical and electron microprobe (EMP) analyses on thin sections.

The peridotite bodies of Raudhaugene and Ugelvik in Norway are characterized by a variety of fracture networks at different scales. A homogeneous serpentine network is observed at micro-scale. At outcrop scale, fracture networks consist of thin (1 mm) extensional fractures filled with serpentine. Fractures cut each other and the compositional banding fairly randomly, although fractures at angles of 60, 90 and 120 degrees also occur. At some localities thick serpentine veins with a second generation of perpendicular fractures were found and parallel talc veins have been observed. Pyroxenite layers are characterized by a regular fracture pattern of equally spaced fractures (sub)perpendicular to the pyroxenite layer. The fractures show a dominant orientation. Crack-seal vein microstructures are observed within the fractures.

The homogeneous serpentine network indicates widespread fluid infiltration, most likely via a micro-fracture network that formed in an earlier stage. As there is no gradient in the degree of serpentinization throughout the peridotite body, the micro-fracture network is not likely to be the result of reaction-induced fracturing. It is more plausible that the micro-scale fracture network has formed due to thermal cracking. The crack-seal structure observed in the fractures in the pyroxenite layers shows that extension has taken place during serpentinization. The regularly spaced fractures are partly explained by differential volume expansion due to serpentinization. The predicted volume change in the adjacent peridotite is large enough to cause the observed extension in the pyroxenite layers. The dominant orientation of the fractures in the pyroxenite layers is explained by influences from regional stress. Outcrop-scale fractures in the peridotite do not show evidence for reaction-induced fracturing. More likely they formed due to multiple phases of regional stress and hierarchical fracturing.

Different breccias are recognized in the Lherz peridotite body, which are characterized by angular or rounded peridotite clasts, a calcite or peridotite matrix, and the presence of exotic clasts. Cross-cutting relations reveal that serpentinization occurred before fracturing and the formation of carbonate veins. Rotated angular clasts and calcite geodes cannot be explained by reaction-induced fracturing, rather they have a sedimentary origin. This is confirmed by lamination in the matrix consisting of calcite and peridotite particles. Rounded clasts and the incorporation of exotic clasts in the breccia also indicate a sedimentary setting. The Lherz body was most likely intensely fractured due to tectonic stress and subsequently reworked by sedimentary processes.

The absence of Mg-rich carbonates in both geological settings, indicate that in situ carbonation has not taken place. Carbonates are present in the form of calcite in fractures, but their origin is most likely outside the system and no evidence has been found that they are involved in fracturing. In this study insights were gained in fracture patterns and various mechanisms of fracture development. Clear evidence for reaction-induced fracturing, resulting in peridotite fracture networks, was not observed.

1. Introduction

1.1 Background

There is currently great interest in the possibility of sequestration of CO₂ in mantle rock. The principle is derived from natural peridotite hydration (serpentinization) and carbonation. Near the Earth's surface, the main constituents of mantle peridotite, olivine and pyroxene, react with H₂O and CO₂ to form serpentine and carbonates (calcite, magnesite, dolomite). Hereby the CO₂ content in the atmosphere is reduced. Natural examples are found at the Semail ophiolite in Oman (Kelemen & Matter, 2008) and Atlin in British Columbia (Hansen et al., 2005).

To keep up with the anthropogenic CO₂ production, these processes can be stimulated by creating more reaction surface and optimal PT-conditions. Two concepts have been proposed: ex situ, where peridotite is crushed into fine material (Schuiling & Krijgsman (2006a) amongst others) and in situ, where self-propagating reactions and mechanisms take place within a peridotite body (Kelemen & Matter, 2008). The latter concept is based on the exothermic reactions of serpentinization and carbonation, under self-sustaining high temperatures. Mantle rocks are initially hydrofractured at depth. Hot fluid is subsequently pumped into the system to heat up the fractured peridotite to an optimal temperature (185°C) and pure CO₂ is injected. Further fracturing may occur as a result of thermal expansion during heating, volume increase during hydration, and volume increase during carbonation. This would allow fluids to penetrate further into the rock mass and enhance the process.

Whether or not volume expansion actually occurs during hydration of mantle rock and to what extent is subject of debate. Serpentine is a water-bearing mineral and chemically similar to olivine. It has a lower density than olivine which may be the result of a volume increase. However, the lower density can also be caused by a decrease in mass, due to the removal of elements by fluids. It is generally agreed upon that a volume increase occurs as a result of serpentinization (O'Hanley, 1992; Mével, 2003; Iyer et al., 2008; Jamtveit et al., 2008). The volume expansion could produce enough stress to fracture the rock. Pore fluid pressure may also play a role in building up stress resulting in fracturing of peridotite. When the infiltrating fluids have a high CO₂-content, carbonation may take place. Mg⁺- and Ca⁺-ions, dissolved from the mantle rock, react with CO₃⁻ ions to form magnesite, dolomite and calcite. Precipitation causes an increase in volume of the rock, which may induce fracturing. Since serpentinization and carbonation are exothermic reactions, they may provide suitable conditions for further reactions to occur. The process continues and fractures may propagate to form a complex fracture network. Instead of fracturing the rock however, the growth of new minerals could also cause a strong decrease in permeability. Fluid infiltration is hampered and the process eventually ceases, as was found in experiments in the High Pressure and Temperature Laboratory at Utrecht University (Van Noort, pers. comm.).

Both the Semail ophiolite in Oman and peridotite rock in Atlin, British Columbia (Canada), contain carbonates within the rock and in veins that form dense fracture networks. These observations indicate that the mantle rock was chemically involved and that in situ mineralization may have induced the formation of fractures. Studying the geometry, scale and chemistry of naturally fractured mantle rocks gives insight in the fracture mechanisms that lead to the development and propagation of fracture networks. In particular the role of serpentinization and carbonation, that may result in reaction-induced fracturing due to volume expansion, is identified. Two field areas with fractured peridotite have been studied to investigate the role of reaction-induced fracturing. First, two peridotite bodies in the Western Gneiss Region in Norway were investigated. Fractures are found throughout the bodies, although carbonates are not abundantly present. Second, the Lherz body in the French Pyrenees was studied. This peridotite body is heavily brecciated and calcite veins are abundant.

1.2 Research questions

What general types of fracture patterns are found in the peridotite bodies in the Western Gneiss Region and Lherz? What do they reveal about the process(es) that formed them? Did reaction-induced fracturing play a role in the development?

1.3 Outline thesis

On the island of Otrøy in the Western Gneiss Region (Norway), two strongly serpentinized and naturally fractured upper mantle peridotites were investigated. The results of this study are presented in **chapter 2**. The aim was to determine whether the fractures are reaction- or stressed-induced. Determining different generations of fractures and the timing of serpentinization could provide more insight on the mechanism of formation. Chemical analyses were performed on several samples to determine the mineral assemblages and to indicate the possible presence of carbonates. Field- and laboratory work was carried out together with Karen Oud, who focused on late stage PT-conditions of the two peridotite bodies.

In **chapter 3**, the results of the research done on the Lherz peridotite in the French Pyrenees are presented. This is the main peridotite body of several in the Northern Pyrenean Fault Zone. Different types of breccias are distinguished, which can be the result of different mechanisms. On the edges of the peridotite body, calcite veins between breccias are prominent. The main research questions are: Do the breccias represent fault breccias or did they form as a result of reaction-induced fracturing through CO₂ infiltration? Did sedimentary processes play a role in the formation of the breccias? Studying thin section studies and performing chemical analyses using the microprobe provide more insight in the nature of these breccias.

A summary of the findings of both studies is given in **chapter 4**. A comparison and interpretation of the two case studies results in general conclusions on the process of reaction-induced fracturing.

The chapters consist of individual researches. Therefore, some subjects may be treated more than once.

2. Serpentinization and fracturing history of upper mantle peridotites in the Western Gneiss Region (Norway)

2.1 Introduction

Fractures can form as a result of various processes. These include regional stress as a result of tectonics, thermal cracking and weathering amongst others. Various researchers have also associated hydration processes to fracturing (Iyer et al., 2008; Jamtveit et al., 2008; Kelemen & Matter, 2008). Serpentinization of peridotite and accompanying volume expansion is a prominent example of this process. Whether or not volume expansion and the resulting fracturing actually occurs in this process and to what extent is subject of debate.

The original and resulting products of serpentinization, olivine and serpentine respectively, contain nearly the same constituent elements, Mg, Fe and Si. The resulting serpentine is a softer water-bearing mineral and less dense than the original olivine. A decrease in density can be caused by a volume increase, as mentioned above, or by a decrease in mass. Elements can both have been added or removed from the system along with the water. The resulting question is: Is the change in density during serpentinization directly caused by volume expansion and/or to what extent can the removal of mass have played a role in this process?

Most authors agree that, in general, a volume increase occurs as a result of serpentinization (O'Hanley, 1992; Mével, 2003; Iyer et al., 2008; Jamtveit et al., 2008). The volume increase could produce enough stress to fracture the rock. Pore fluid pressure may also have played a role in building up stress resulting in fracturing of peridotite. The development of fractures allows further infiltration of water and serpentinization. Since serpentinization is an exothermic reaction, suitable conditions for this reaction are maintained and fractures may propagate to form a complex fracture network.

Alongside, when CO_2 is taken up by the water that infiltrates peridotite rock, carbonation may take place. Mg^{2+} - and Ca^{2+} -ions, dissolved from the peridotite rock, presumably react with CO_3^{2-} ions to form magnesite, dolomite and calcite. Precipitation causes an increase in volume of the rock, which may induce fracturing. Compared to serpentinization this reaction is even more exothermic, causing the reactions to continue.

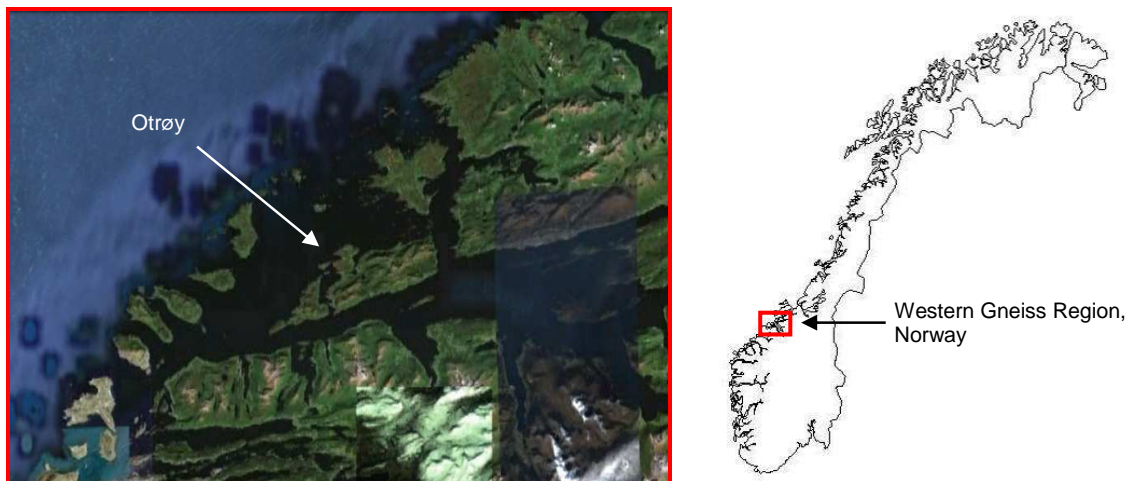


Figure 2-1: Otrøy in the Western Gneiss Region, Norway.

Fractures are found throughout the strongly serpentinized peridotite bodies on the island of Otrøy (Western Gneiss Region, Norway; Figure 2-1). The question is how did these form? Could they indeed be reaction-induced, the result of serpentinization or did regional stress play an important role? What was the relative timing of serpentinization and fracturing? Are carbonates found, implying that CO₂ is present in the system? If so, did the formation of carbonates play a role in fracturing? With these questions in mind Karen Oud and I performed fieldwork on the two peridotite bodies. Geometry and orientation of fracture networks were investigated to gain insight on the mechanism of formation. Samples were taken and analyzed microscopically to gain insight in small scale fractures and the process of serpentinization. These investigations were set to find evidence for reaction-induced fracturing.

2.2 Research area

2.2.1 Geological history peridotites on Otrøy

The origin and evolution of the orogenic peridotites on Otrøy have been studied by numerous geologists (Carswell, 1968, 1973; Van Roermund and Drury, 1998; Van Roermund et al., 2000, 2001; Drury et al., 2001; Spengler, 2006). In Spengler (2006) an extensive overview of the geological history of these bodies is given. They are thought to represent upper mantle lithologies that have originated at a depth of ≥ 350 km in the Archaean (Figure 2-2). An extremely hot plume transported the mantle rocks to a depth of about 150 km and caused partial melting. Cr-rich melts subsequently infiltrated the melt depleted peridotite and the residual mantle rocks formed a cratonic root (3.3-2.9 Ga). The sub-cratonic emplacement of the peridotites was most likely accompanied by strong deformation. Mechanical mixing of garnet-rich and garnet-poor lithologies could explain the strongly pronounced compositional layering that is present. Probably in the early-Proterozoic, the peridotites were exhumed to shallower levels (~150 km). During the Caledonian orogeny (490-390 Ma) the mantle rocks are thought to have been emplaced into the crust and underwent UHP metamorphism as is imprinted into the rocks. This was accompanied by strong deformation which resulted in (isoclinal) folding and recrystallization of the compositional layers and pyroxenite dykes. The emplacement in the crust is reconstructed as follows: as Laurentia and Baltica collided, Baltica subducted beneath Laurentia temporarily. Hereby, fragments of the base of the Laurentic plate were emplaced into the Baltic crust, which was subsequently subducted to deeper levels, far into the diamond stability field. Thereafter, due to processes of buoyancy and extension, the mantle fragments were uplifted and exhumed to the surface.

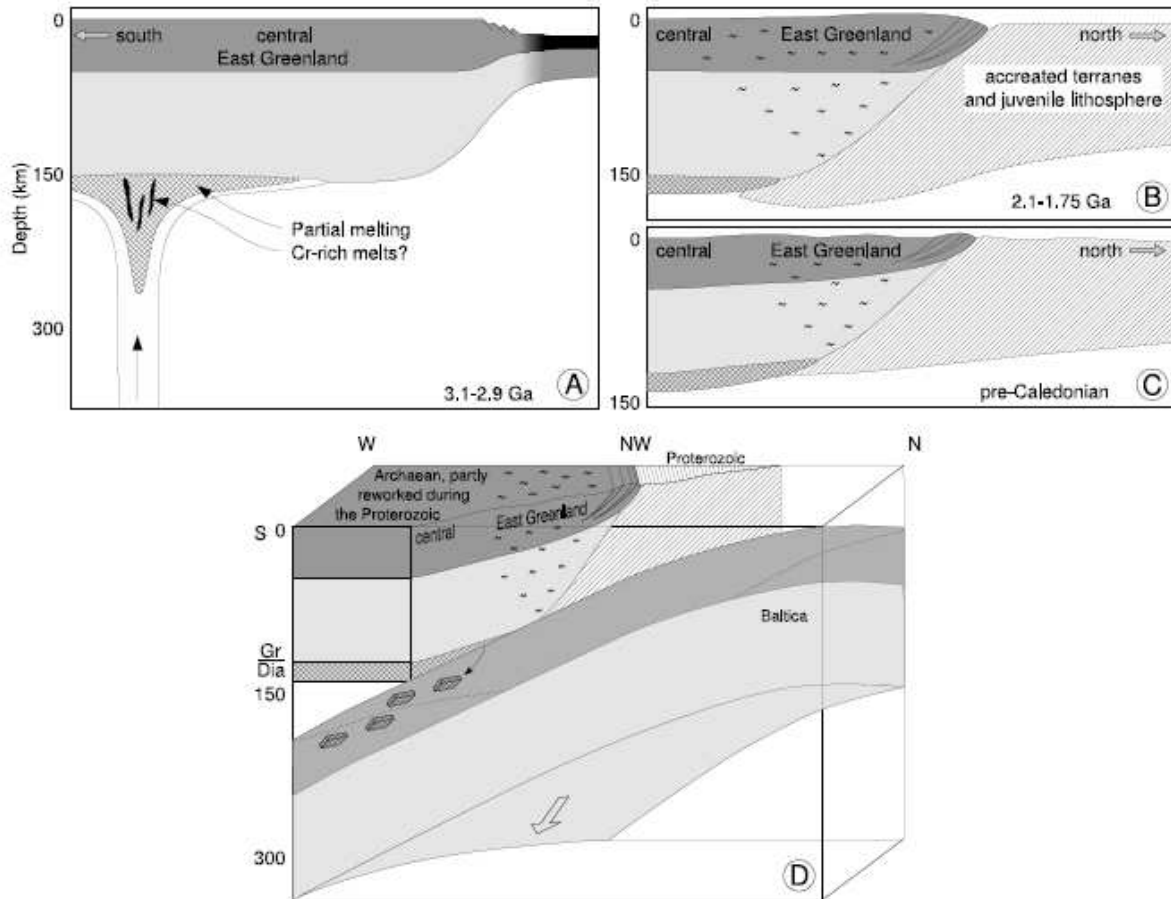


Figure 2-2: Schematic model for the origin and evolution of orogenic peridotite on Otrøy (Spengler, 2006).

2.2.2 Field area

The two grt-peridotite bodies on the island of Otrøy which are subject of this study are named Raudhaugene and Ugelvik. They can be found on the west coast of the island, 3 km northeast of the village Midsund (Figure 2-3). They are both ~1 km in diameter and are embedded in (U)HP gneisses. These grt-peridotite bodies consist mainly of dunites and harzburgites. Occasionally a pyroxenite layer is found. Compositional banding can be distinguished through the presence of garnets. In some parts compositional banding is clearly visible, in other parts not, despite the presence of garnets. The pyroxenite layers are parallel to the compositional banding. The peridotite bodies are strongly serpentinized. Compared to other peridotites in the Western Gneiss Region they have a relatively high degree of serpentinization of 50% and more. The peridotite bodies can easily be recognized by their typical yellow-brown weathering colour.

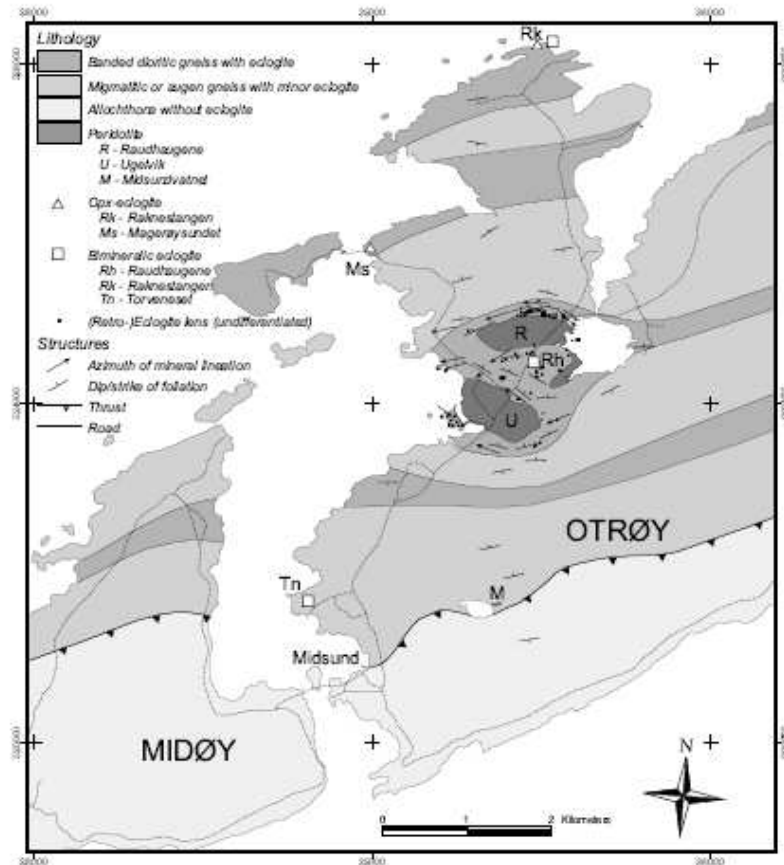


Figure 2-3: Simplified geological map of western Otrøy showing peridotite bodies Raudhaugene (R) and Ugelvik (U) within (U)HP gneisses (Spengler, 2006).

2.3 Method

To investigate the origin of the fractures in the peridotite bodies on Otrøy, the fracture geometry has been studied in the field. Orientations of fracture planes were measured. Moreover, the extent of fracture propagation was studied; the angles between fractures, cross-cutting relationships, different generations and their morphology. Attention was also paid to the mineralogy inside the fractures and at the rim. Fracture patterns were studied 3D and 2D, also in relationship with the compositional banding. Pictures of the different phenomena were taken in the field as well as samples. Thin sections were analysed optically to determine the mineralogy and to examine them on deformation features using a light microscope. Chemical analyses were done using the electron microprobe (EMP) and scanning electron microscope (SEM). To examine the possible volume expansion that may have taken place in the peridotite bodies as they were serpentinized, the contact of the peridotite bodies and the surrounding (U)HP gneiss has been examined as well.

2.4 Fracture networks at outcrop scale

2.4.1 Morphology

Fractures in peridotite bodies

Fractures can be found throughout the two peridotite bodies, forming different types of fracture networks. The fracture density varies from widely spaced fractures to dense networks. The fractures show different morphology including: the dimensions of the fractures, opening width, presence and extent of a rim, mineralogy inside the fracture, straight or curved fractures, the orientation of fractures relative to each other and the. Fractures may extent for decimetres to tens of metres. Figure 2-5 shows examples of characteristic fracture networks. Due to limited outcrop not all fractures could be followed and examined.



Figure 2-5: Different types of fracture networks. (a) Intensely fractured peridotite outcrop. Most fractures are open, some are closed and have a rim (not clearly visible); (b) Fractured peridotite along coast with dominant fracture plane orientation dipping north (inland); (c) Fracture network consisting of fractures that cut compositional banding at low and high (perpendicular) angles. Fractures have a clear rim, some are open but most are closed; (d) Fractures, cm-scale, with rim. Vertical fracture branches out into horizontal fractures.

The fracture networks in Raudhaugene and Ugelvik consist of fractures that cut each other at high or low angles. Some fractures end at another fracture, indicating (at least) two generations of fractures and the order of formation. However, in most cases cross-cutting relationships are not visible. In several outcrops the compositional banding is quite obvious. Some fractures formed perpendicular to the compositional layering, others at angles of 60° or 120° (Figure 2-6), or at very low angles. The fractures may end at or cut through the compositional banding. The tip or end of fractures simply dies out.

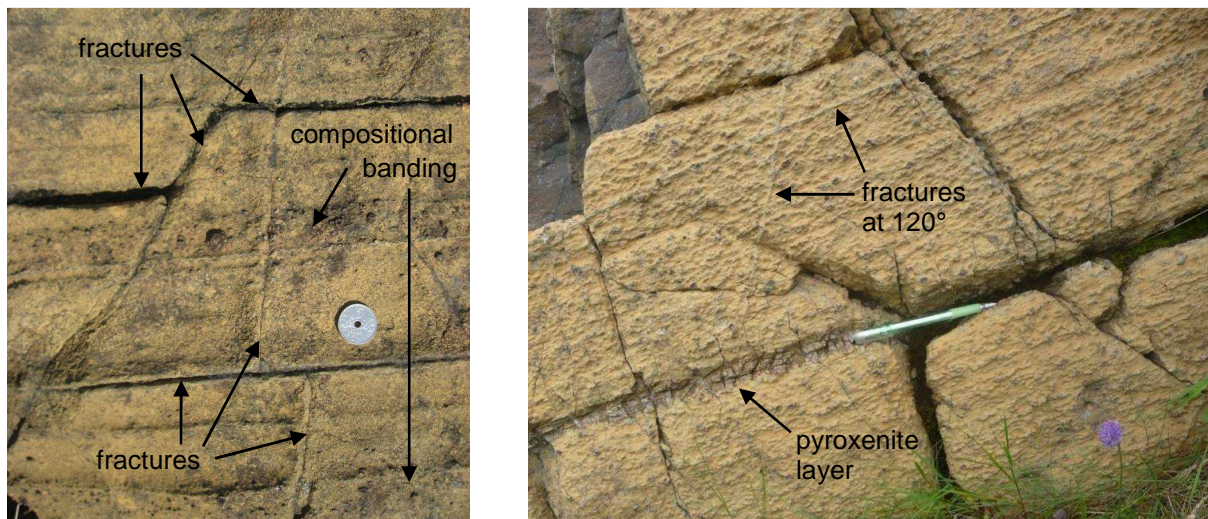


Figure 2-6: Fracture networks consisting of fractures parallel to the compositional banding and fractures at 60°, 90° and 120°.

The fractures are most often filled with serpentine, forming veins. The colour of the serpentine can be green or white (Figure 2-7 left). In some cases it looks very dark and it may also appear in its weathered colour orange. For the greater part they occur as straight veins for several meters. However, curved veins are abundant as well. By far the most veins are about 1 mm thin and have an amorphous texture. In some locations, much thicker veins of ~1 cm are present. The texture of these veins is fibrous. The thick veins are cut by small, regularly spaced fractures sub-perpendicular to the thick vein (Figure 2-7 right). Furthermore, calcite is often found inside fractures. At another locality on Ugelvik, many fibrous talc veins were found, nearly parallel to each other (Figure 2-8 left). They are not as straight as the serpentine veins found throughout the two peridotite bodies and do not have clear rims. Some talc veins are split by a fracture running parallel through the vein.

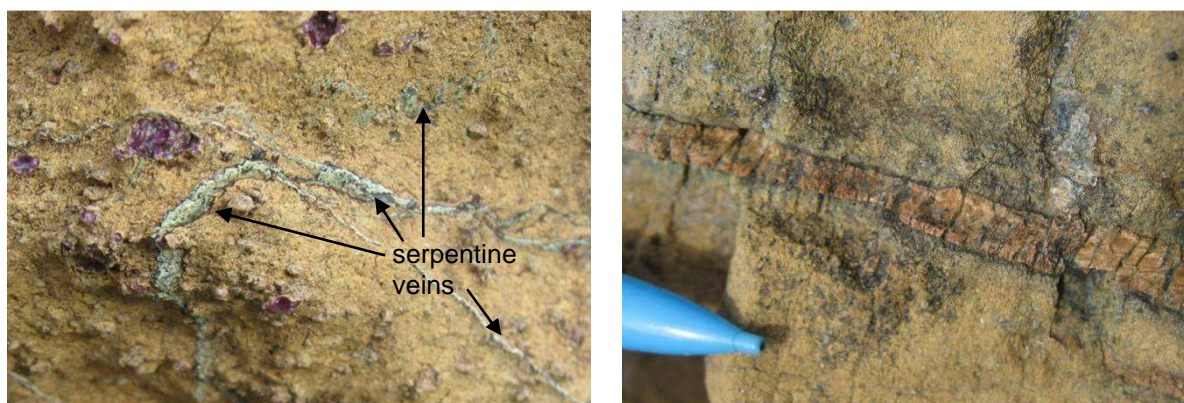


Figure 2-7: Thin, light-green serpentine veins with amorphous texture (left). Thick fibrous serpentine vein cut by smaller fractures, sub-perpendicular to the thick vein (right).

One feature that makes the different fracture networks distinct from each other is the presence of rims around the fractures. They may be as thick as 1 cm or as thin as 1 mm, or absent. Many fractures look weathered, widening towards the surface and showing no minerals inside. Especially along the coast, large blocks of peridotite have formed. Often, following such fractures leads to a part where the fracture is filled with serpentine. At one particular location in the Ugelvik peridotite, fractures can be found that are only a few centimetres long and have a rim in the form of 'lips'. Two generations can be distinguished (Figure 2-8 right).



Figure 2-8: Fibrous talc veins (left). Two generations of lip-shaped fractures (right).

Fractures in pyroxenite layers

Pyroxenite layers are found throughout the two peridotite bodies, in most cases straight and parallel to the compositional banding. An isoclinally folded pyroxenite layer has been found as well, however, and not all pyroxenite layers present may have been observed. Most of the pyroxenite layers show a remarkable fracture pattern. They are cut by regularly spaced, parallel fractures of about 1 mm wide, that cut the pyroxenite layer (sub-)perpendicular (Figure 2-9 left). Both the fracture thickness and the fracture spacing correlate with the layer thickness of the pyroxenite layer. The thinner the pyroxenite layer, the thinner the cracks and the smaller the distance between them. The fractures are centered in the pyroxenite layers. They may cut across the pyroxenite-peridotite boundary or may not. They may be perpendicular or at a high angle to the layer. These properties differ per pyroxenite layer. Signs of a possible second generation were visible as fractures with a slightly different angle to the pyroxenite layer at one location. In general, the fractures are filled with serpentine in a symmetrical pattern (Figure 2-9 right). However, in some cases calcite is present as well. Parallel fracture patterns have been found in pyroxenite layers of the Raudhaugene peridotite body (Figure 2-10a,b). At the coast of the Ugelvik peridotite body several top views of pyroxenite layers could be observed. These show parallel fractures extend for several meters along the pyroxenite layer, but only in one particular direction (Figure 2-10 c-e). One case was observed though, where the fractures do not seem to run parallel to each other. This is shown in a thin pyroxenite layer found in Ugelvik (Figure 2-10f).



Figure 2-9: Pyroxenite layer with regularly spaced fractures along the coast of Ugelvik (left). On the left side of the picture the top of the pyroxenite layer and adjacent peridotite is missing. This reveals a top view on the parallel fractures. On the right of the picture only a side view can be observed; Symmetrical pattern of serpentine inside fractures in pyroxenite layer (right).



Figure 2-10: (a) Regular fracture pattern in pyroxenite layer perpendicular to the layer. (b) Fracture pattern in pyroxenite layer at slight angle. (Raudhaugene); (c)-(e) Top view of pyroxenite layer with one set of parallel fractures; (f) Thin pyroxenite layer with fractures perpendicular to layer, but most likely not parallel to each other. (Ugelvik)

Contact with (U)HP gneisses

As both peridotite bodies are strongly serpentinized, volume expansion due to this reaction may have taken place. In that case, signs of this expansion could be expected at the contact of the peridotite body and the neighbouring gneiss. Volume expansion of the peridotite body may have caused pressure on the surrounding gneiss, producing radial cracks for instance. Or fluid may have passed from the peridotite into the gneiss, carrying dissolved serpentine. In their present position, both peridotite bodies are partially surrounded by water and for the greater part covered by vegetation. The

outcrops at the northern rim of the Raudhaugene peridotite body are closest to the neighbouring (U)HP gneisses, they are ~10 meters apart. A direct contact of the peridotite could not be found due to vegetation. Barely any fractures were found in the gneiss and the orientation of the few fractures did not appear to correspond to nearby fractures in the peridotite. The rock was too hard to take any samples, so a study on possible microstructures or chemical analyses could not be done unfortunately. No signs of fractures due to expansion of the enclosed peridotite body were observed in the embedding gneiss.

2.4.2 Orientation

Raudhaugene and Ugelvik

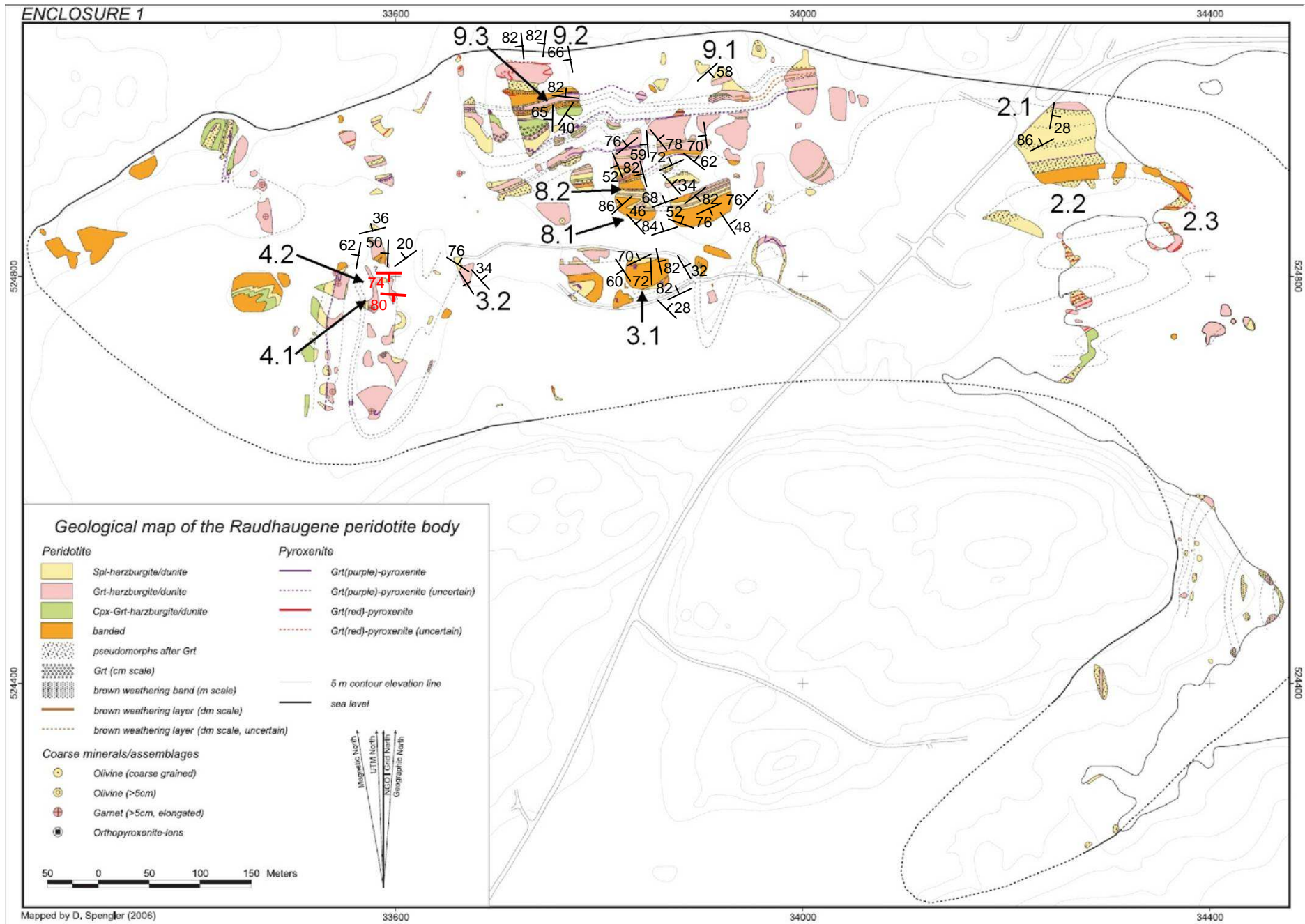
The orientation of the main fractures was measured and plotted in the field map of both Raudhaugene and Ugelvik (Figure 2-11 and Figure 2-12). Note that strike-dip indications are not on their exact location; often several orientations were measured within 10 metres or so at one field location. In Raudhaugene two pyroxenite layers were found close to each other, at field locations 4.1 and 4.2. The orientations of the fractures that cut these layers are similar for both pyroxenite layers, both dipping steeply to the south. The fracture planes that were measured in the surrounding peridotite, however, have different orientations. At other localities in this peridotite body, the fracture orientations appear to be more or less random. In the west of Ugelvik, several pyroxenite layers were found with fractures that have similar orientations, dipping about 70° to 75° to the northwest. At field location 5.1, the fractures in a pyroxenite layer have a similar strike orientation but they dip 56° to the southeast. Fractures in the peridotite that were measured at this location have similar strikes, with varying dip orientations. Except for one or two fracture orientations, in the west of the Ugelvik peridotite body, fracture planes have all different orientations. In the southeast of Ugelvik, pyroxenite layers with fracture orientations perpendicular to each other were found, their orientations differ compared to the west. Most of the other fractures in this part of the peridotite body have similar strikes, but the dip varies.

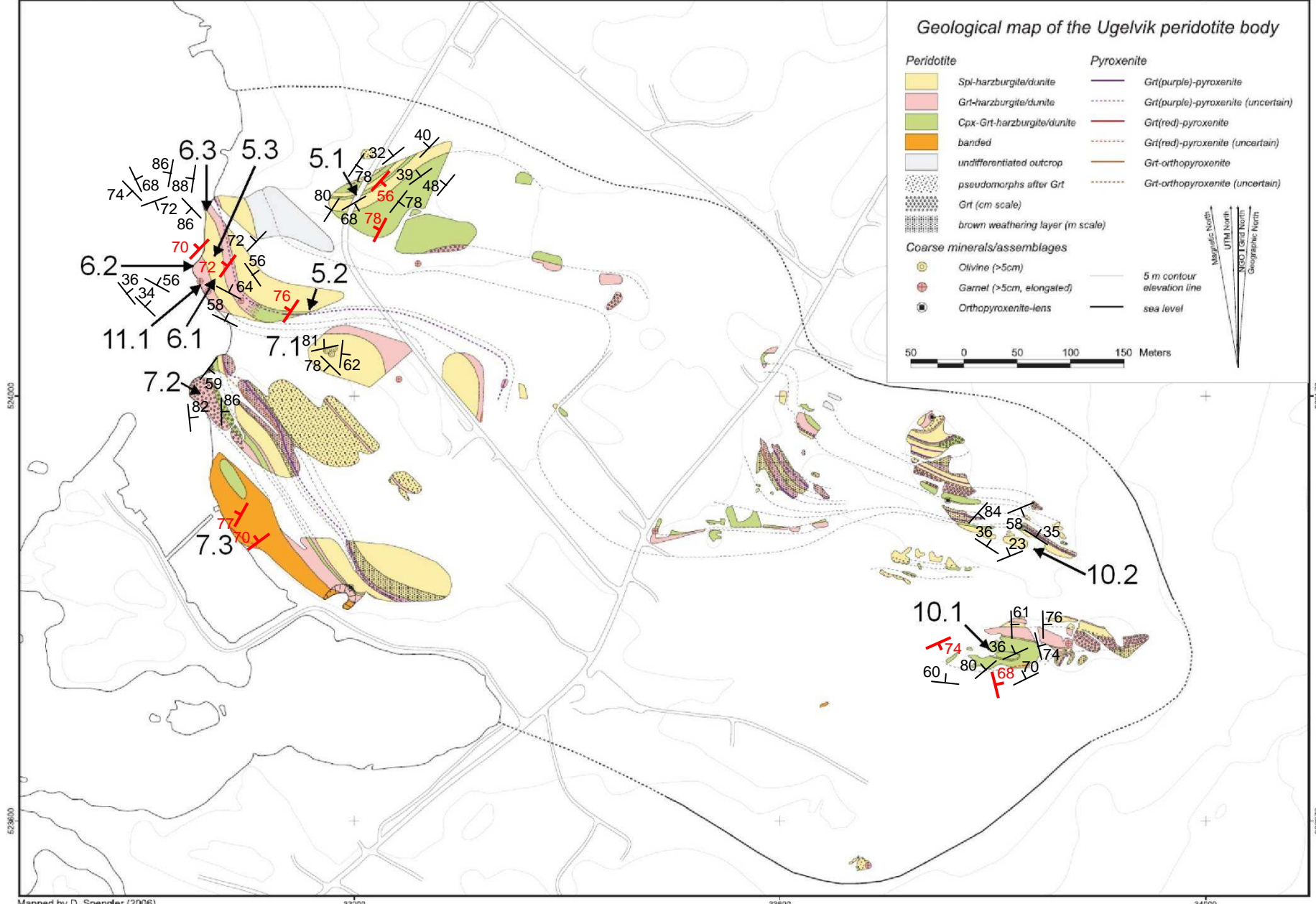
The poles of the fracture orientations were plotted in Stereo32 for the two peridotite bodies separately (Figure 2-12 a-d). The distribution over each body is visualized by different colours. In complicated fracture networks, only the most representative fracture orientations were determined. Figure 2-12 e-h shows plots of only the peridotite fractures. This set of data is 'corrected' to give additional insight in the orientations: extra weight has been given to data representing a dominant fracture orientation and double measurements (when not representative) have been excluded. The fractures in pyroxenite layers are not included in these plots, they will be considered separately.

In Figure 2-12a, among widespread data points three clusters can be observed for Raudhaugene. These can be recognized in the density plot (Figure 2-12c) as three peaks. Ugelvik clearly lacks poles in the first quadrant (azimuth 0-90°). The density plot for Ugelvik (Figure 2-12 d) shows only one peak and a small sub-peak. The peak nearly corresponds to one of the peaks of Raudhaugene. For both peridotite bodies the patterns are slightly different for the peridotite data set (Figure 2-12e,f). The intensity of the three peaks of Raudhaugene has reduced (Figure 2-12g). Ugelvik now has two peaks and two sub-peaks (Figure 2-12h). Raudhaugene and Ugelvik have in common that they both have almost no poles with azimuth between 0 and 45°. The comparison of Figure 2-12 a-d and Figure 2-12 e-h can also be regarded as a sensitivity analysis. Going from around 50 to about 40 data points has a substantial effect on the resulting pattern. For Ugelvik, this is mostly due to the exclusion of fractures in pyroxenite layers. Therefore, interpretations should be made carefully when analyzing these plots.

Figure 2-11: Fracture orientations for Raudhaugene (page 16) and Ugelvik (page 17). Orientations of fractures in pyroxenite layers are indicated in red.

Figure 2-12: Page 18–19: Orientation of fractures in peridotite bodies of Raudhaugene (left) and Ugelvik (right) represented by poles. (a-d) complete data set, (e-h) peridotite fracture data set.



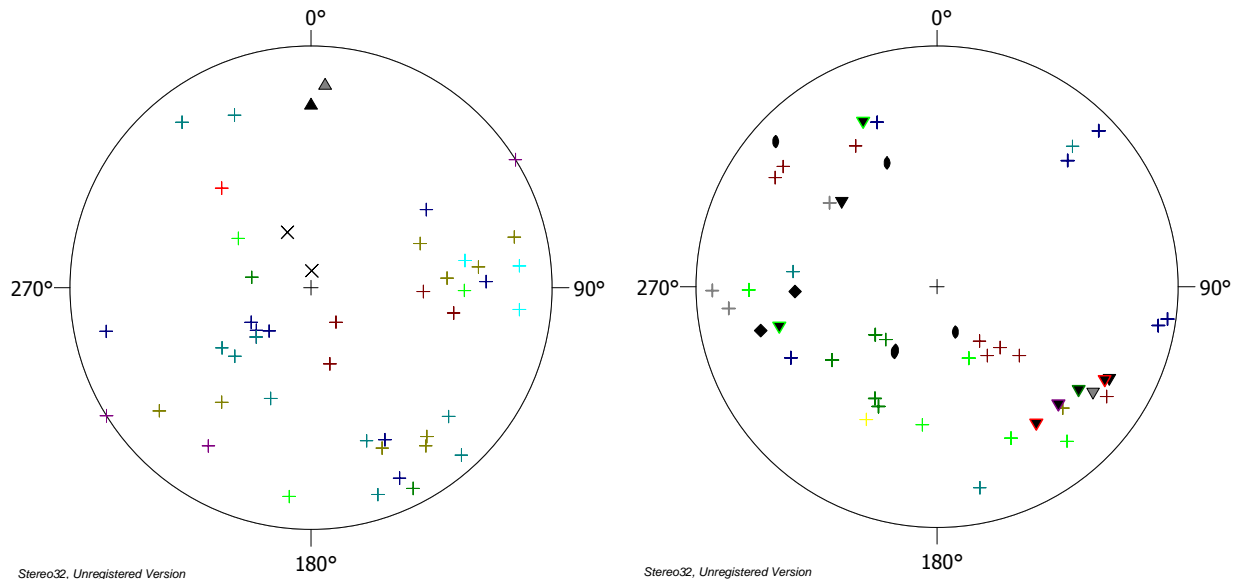


Mapped by D. Spengler (2006)

33200

33600

34000



Stereo32, Unregistered Version

N total = 47

- + n=2 (planar) R2.1 FR
- × n=2 (planar) R2.2 FR (loose blocks?)
- + n=8 (planar) R3.1 FR
- + n=3 (planar) R3.2 FR
- ▲ n=1 (planar) R4.1 FR in pyr.
- + n=4 (planar) R4.1 FR
- ▲ n=1 (planar) R4.2 FR in pyr.
- + n=10 (planar) R8.1 FR
- + n=9 (planar) R8.2 FR
- + n=1 (planar) R9.1 FR
- + n=3 (planar) R9.2 FR
- + n=3 (planar) R9.3 FR

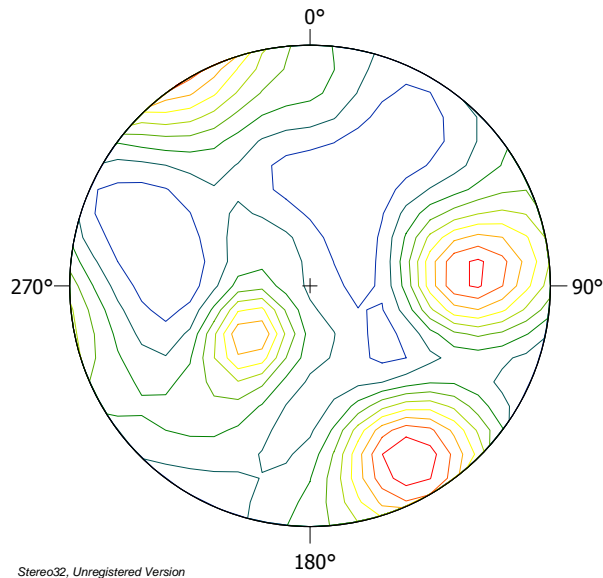
Stereo32, Unregistered Version

N total = 49

- ▼ n=2 (planar) U5.1 FR in pyr.
- + n=8 (planar) U5.1 FR
- ▼ n=1 (planar) U5.2 FR in pyr.
- + n=5 (planar) U5.3 thick FR
- ▼ n=1 (planar) U5.3A FR in pyr.
- + n=1 (planar) U611 (sample)
- + n=6 (planar) U6.2 dominant FR
- ▼ n=1 (planar) U632 FR in pyr.
- + n=3 (planar) U7.1 FR
- + n=3 (planar) U7.2 dominant FR
- ▼ n=2 (planar) U7.3 FR in pyr.
- ◆ n=2 (planar) U1011 (sample)
- ▼ n=2 (planar) U10.1 FR in pyr.
- + n=6 (planar) U10.1 thick FR
- n=5 (planar) U10.2 FR, thick rim
- + n=1 (planar) U1111 (sample)

(a) all data in projection

(b) all data in projection



Stereo32, Unregistered Version

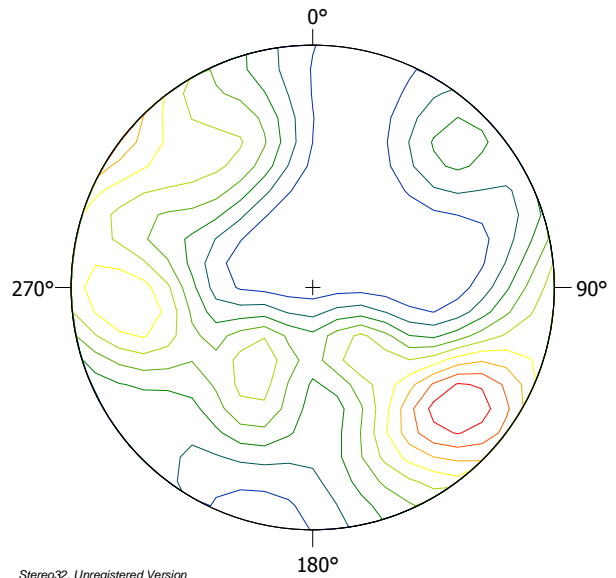
N = 47

Maximum density = 7.45

Minimum density = 0.19

Mean density = 2.24

(c) all data in density plot



Stereo32, Unregistered Version

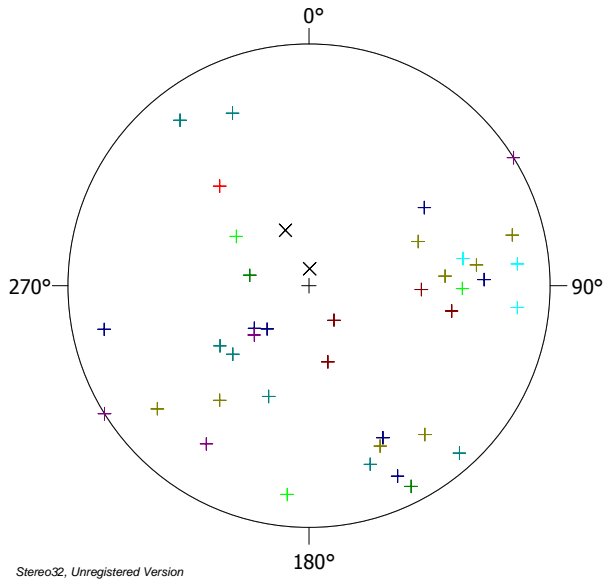
N = 49

Maximum density = 8.03

Minimum density = 0.00

Mean density = 2.33

(d) all data in density plot

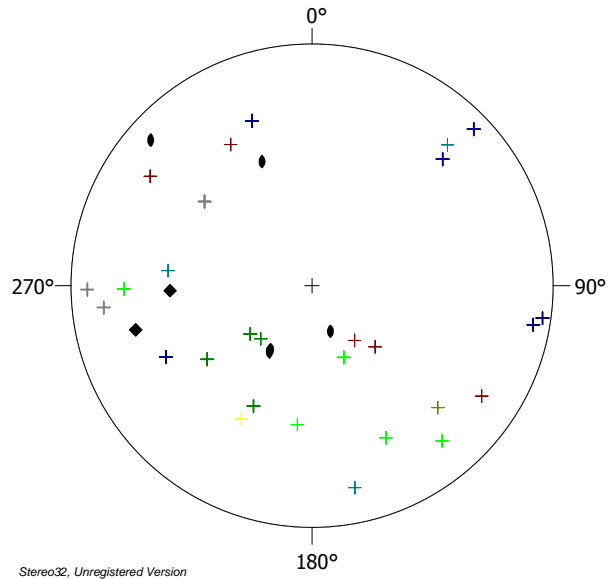


Stereo32, Unregistered Version

N total = 40

- + n=2 (planar) R2.1 FR
- × n=2 (planar) R2.2 FR (may be loose blocks)
- + n=7 (planar) R3.1 FR
- + n=3 (planar) R3.2 FR
- + n=4 (planar) R4.1 FR
- + n=7 (planar) R8.1 FR
- + n=8 (planar) R8.2 FR
- + n=1 (planar) R9.1 FR
- + n=3 (planar) R9.2 FR
- + n=3 (planar) R9.3 FR

(e) peridotite data set in projection

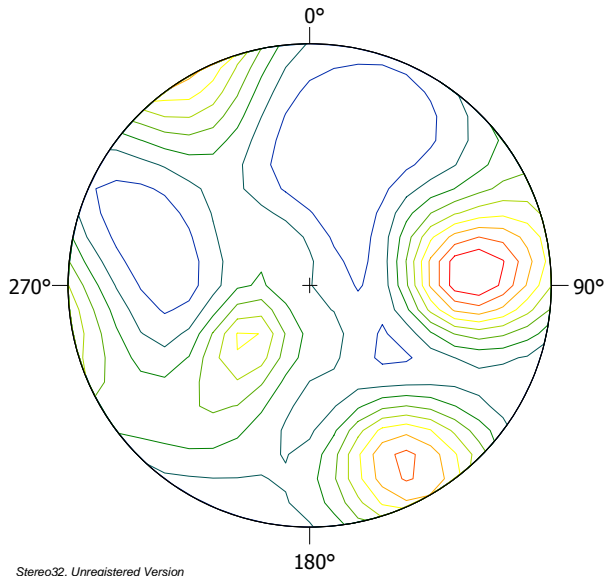


Stereo32, Unregistered Version

N total = 39

- + n=5 (planar) U5.1 FR
- + n=4 (planar) U5.3 thick FR
- + n=1 (planar) U611 (sample)
- + n=8 (planar) U6.2 dominant FR
- + n=3 (planar) U7.1 FR
- + n=4 (planar) U7.2 dominant FR
- ◆ n=2 (planar) U1011 (sample)
- + n=6 (planar) U10.1 thick FR
- n=5 (planar) U10.2 FR with thick rim
- + n=1 (planar) U1111 (sample)

(f) peridotite data set in projection



Stereo32, Unregistered Version

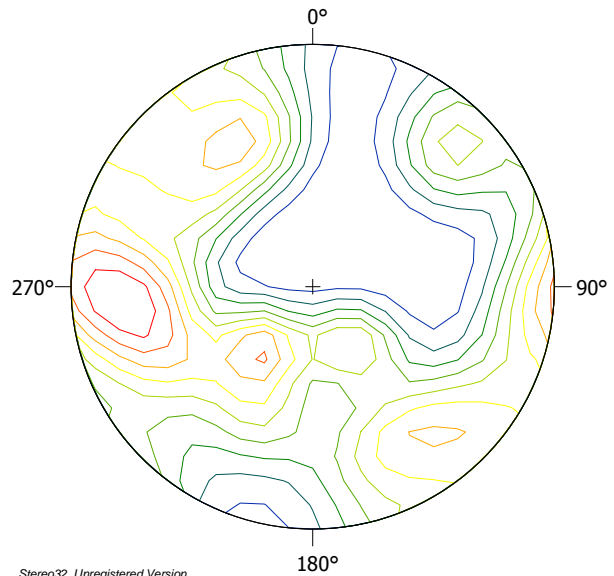
N = 40

Maximum density = 6.86

Minimum density = 0.05

Mean density = 1.90

(g) peridotite data set in density plot



Stereo32, Unregistered Version

N = 39

Maximum density = 5.10

Minimum density = 0.00

Mean density = 1.86

(h) peridotite data set in density plot

In Figure 2-13, the angles of fractures with respect to compositional banding have been plotted in a histogram. Both acute and corresponding obtuse angles have been plotted, which results in symmetrical patterns. For Raudhaugene there is a clear peak of around 90° between fractures and the compositional banding (Figure 2-13). Angles of about 35°, 55° and 75° also occur quite frequently. For Ugelvik the angles are more homogeneously spread, although there is a tendency for high angles.

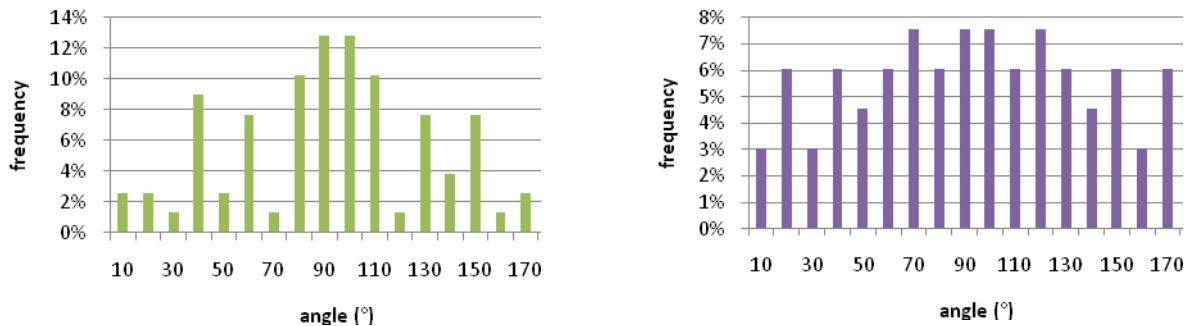


Figure 2-13: Angles of fractures with respect to compositional banding for Raudhaugene (left) and Ugelvik (right).

Pyroxenite layers

Plots have been made for the orientation of the pyroxenite layers and their fractures in both peridotite bodies (Figure 2-14). Two pyroxenite layers in Raudhaugene were found close to each other in the field. They are steeply dipping and their orientations are nearly parallel. The angle between the fractures and the pyroxenite layers differ for both cases (Figure 2-15), but the actual orientation of the fractures is about the same. The orientations of the pyroxenite layers found in Ugelvik differ. They are horizontal and also nearly parallel to each other. In the pyroxenite layers found at the coast, the fractures plot very close to each other. At three other localities, the fractures plot differently, they are indicated by different colours. To be able to compare all of the data spatially, the intersections of the pyroxenite layers and their fractures have been calculated and plotted. As Figure 2-14 shows, these linear orientations plot quite close to each other. More pyroxenite layers can be found in both peridotite bodies, but these were not measurable.

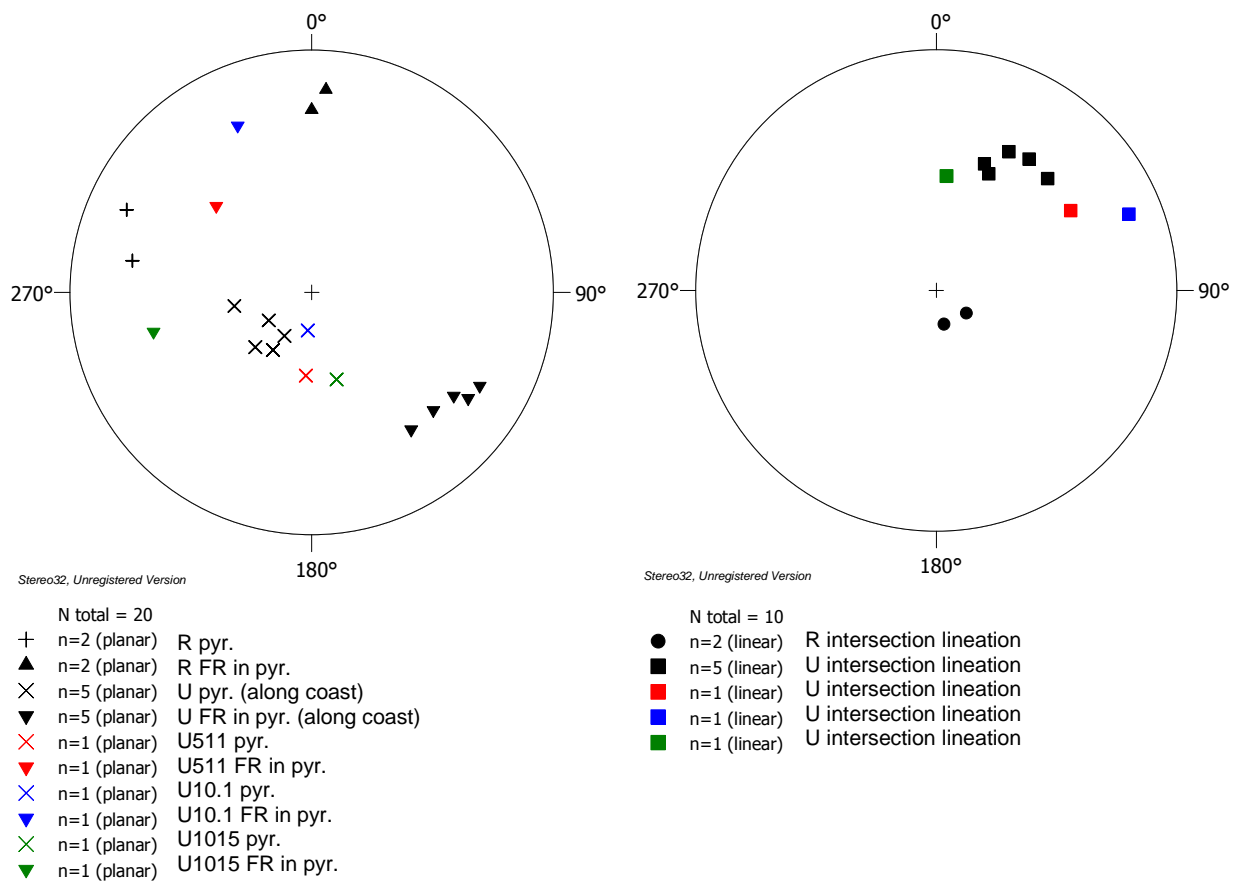


Figure 2-14: Orientation of fractures in pyroxenite layers represented by poles (left). Intersection lineations of the fractures and the pyroxenite layers represented by poles (right).

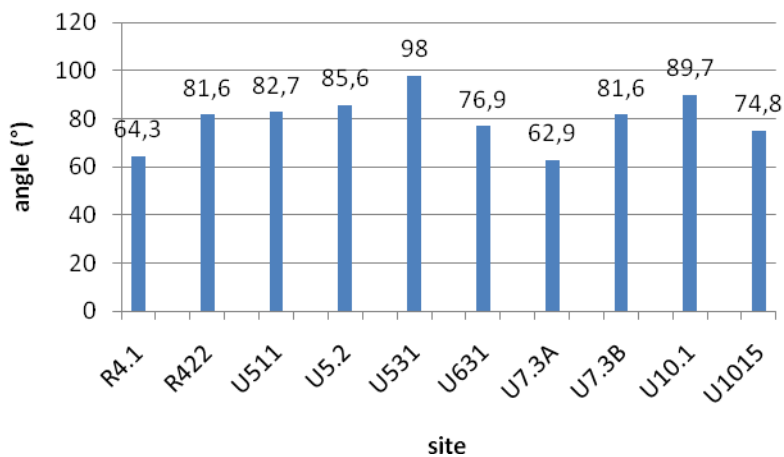


Figure 2-15: Angles between pyroxenite layers and their parallel fractures.

2.5 Fractures on microscopic scale

19 thin sections of selected samples have been made to investigate the mineralogy and microstructures in and near the rim of the fractures. In the following sections the thin sections showing the clearest and most representative features are described.

2.5.1 Fractures in peridotite

Serpentine network

The peridotite bodies, mainly consisting of garnet-bearing harzburgite and dunite, consist to a lesser extent of olivine primarily and orthopyroxene. Furthermore, garnets or spinel crystals may be present. At some localities the garnet crystals have reacted to form amphibole and subsequently chlorite crystals. Several chlorite flakes are present in some of the thin sections. The rock has been serpentinized extensively, the extent of which differs slightly from locality to locality. Optical analyses show that olivine crystals have been replaced by serpentine crystals at the rim, forming a serpentine network (Figure 2-16a). This is often described as a mesh structure. A mesh is defined as an area enclosed by a network; an olivine grain that has been or is being replaced by serpentine (Prichard, 1979). The back-scattered image below (Figure 2-16b) shows the microstructure produced by serpentinization. Olivine relicts are surrounded by a serpentine network. In the serpentine network, another reaction product, magnetite (small white crystals) is visible. The large white mineral is a spinel. In general, serpentine crystals are too small to be distinguished. There are three polymorphs: lizardite, chrysotile and antigorite. Although they appear in various forms, chemically they are nearly the same. In this study, no distinction between the polymorphs will be made.

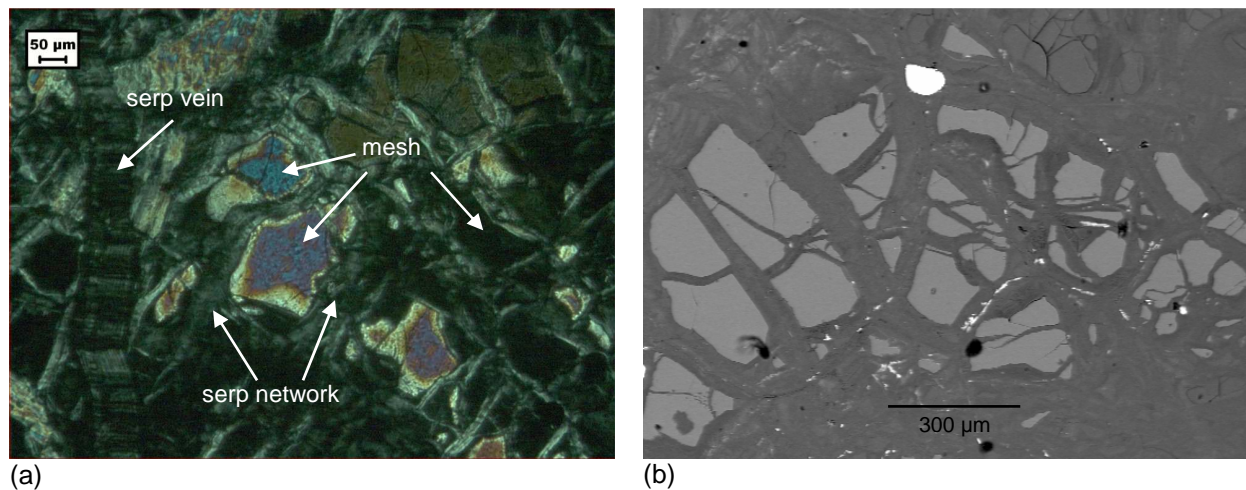


Figure 2-16: (a) Light microscope photo (XPL) of olivine crystals that have partially been replaced by serpentine and a serpentine vein on the left. (b) Back-scattered EMP image of olivine relicts and a serpentine network. A line of magnetite in the middle of the vein is visible.

As water is involved in serpentinization, the serpentine networks are interpreted as fluid pathways, often following grain boundaries. Serpentinization appears to have occurred everywhere, despite low porosity and permeability of these dense mantle rocks. Orthopyroxenes are usually less serpentinized than olivine crystals. Pyroxenes that are replaced by serpentine are called bastites. They usually keep their original shape.

EMP analyses have pointed out that the system is a Mg-rich system with a small percentage of Fe (Table 2-2). In olivine and serpentine the molar proportion of magnesium and iron is 9:1.

	ol	opx	serp mesh	serp vein
Si	19.14	18.94	19.27	19.52
Al	0.00	0.09	0.04	0.04
Fe	6.92	7.43	2.64	5.07
Mn	0.07	0.10	0.00	0.20
Mg	30.14	15.18	23.57	22.41
Ca	0.00	0.17	0.03	0.03
Na	0.00	0.00	0.00	0.01
Ti	0.00	0.00	0.00	0.00
Cr	0.00	0.00	0.00	0.00
Ni	0.33	0.28	0.26	0.04
O	43.74	33.96	38.35	38.56
Total	100.34	76.15	84.17	85.88

Table 2-1: Mineral compositions in weight percentage.

The serpentine network and mesh have been investigated for crystal growth patterns, volume expansion and deformational features. No large scale textures can be distinguished (Figure 2-17), but there are notable features. Serpentine appears with an aligned texture, perpendicular to the olivine crystals. It appears as straight bars as well. Commonly, symmetrical textures can be observed, as indicated in the figure.



Figure 2-17: Mesh texture in peridotite (light microscope picture).

Several thin sections have been examined to see if there is a preferred orientation within the serpentine network or elongated grains. This could reflect the orientation of a regional stress field and furthermore could indicate the direction of fracture formation. The method is limited as it is only a 2-dimensional analysis. Most thin sections do not reveal a preferred orientation. Only a thin section of a serpentine network close to a talc vein shows a dominant orientation (horizontal in Figure 2-18). Talc veins were found perpendicular to the orientation that is shown (Figure 2-23; note that this image is rotated and that the dominant orientation is vertical).

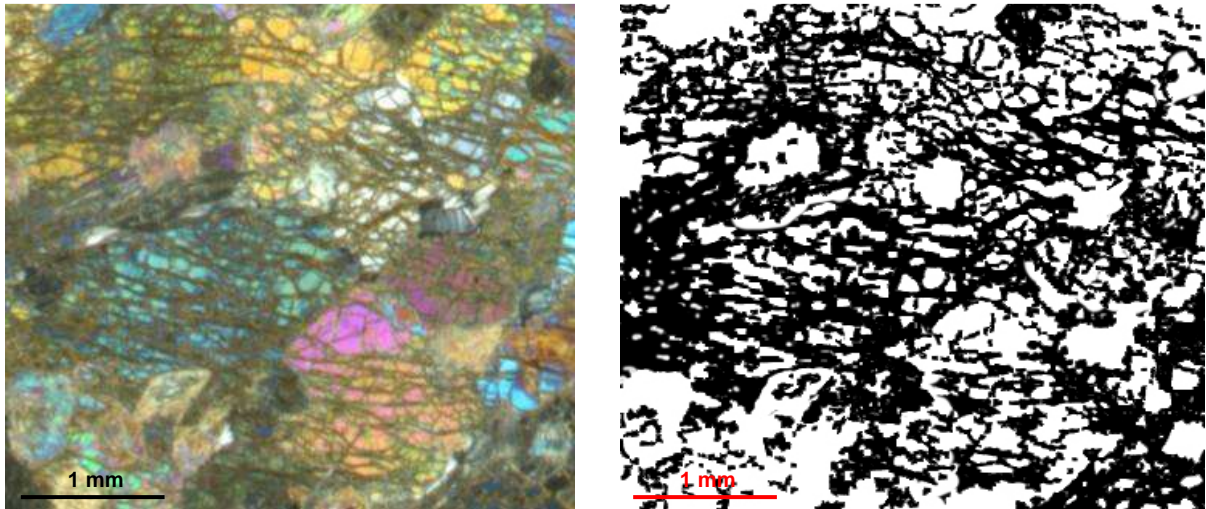


Figure 2-18: Thin section of serpentine network (left) and the orientation of the network in black and white (right).

Common fracture

Both empty fractures, without mineral growth inside, and filled fractures, thus forming veins, were found. Both field observations and microscopical studies show that fractures simply 'die out' at their tips. No special deformational features are visible in the mesh just next to the fractures. Furthermore, when fractures have a rim visible in the field, at microscopical level nothing special can be observed.

Ordinary serpentine-filled fractures are either filled by serpentine crystals that appear to have grown at random orientations, or they are aligned, perpendicular to the vein wall (Figure 2-19 left). In this light microscopic picture there is even a symmetrical pattern from the center of the vein towards the vein wall. Between the serpentine crystals in the fracture and the serpentine network a gradual transition is observed. Figure 2-19 (right) shows a fracture in a thin section in XPL of a harzburgite sample (R931) which is empty. It cuts through the mesh, consisting mostly of olivine grains and some enstatite grains, and the serpentine network. The shape of the rock on both sides of the fracture is completely similar.

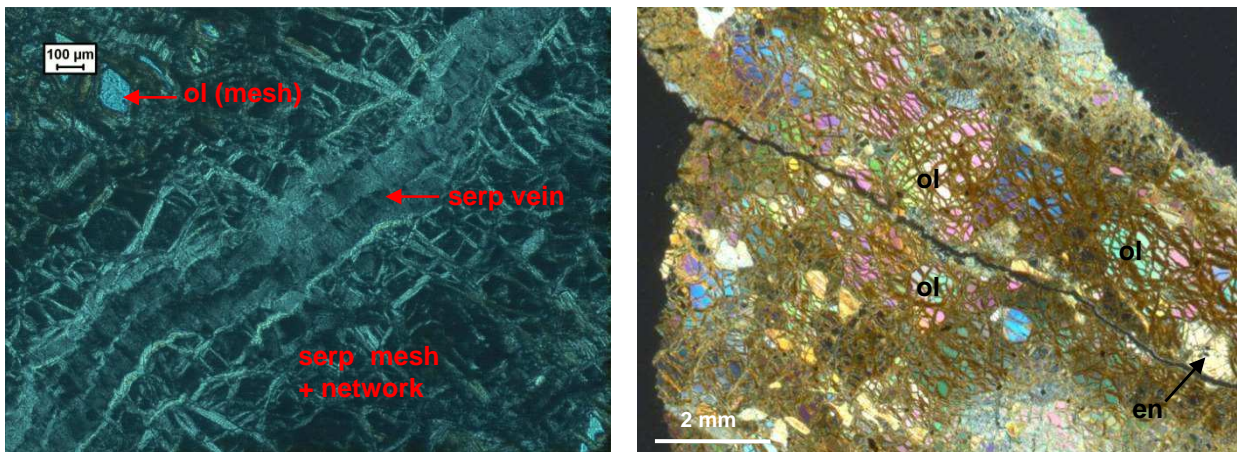


Figure 2-19: Thin sections of a serpentine vein (left) and an open fracture (right).

Figure 2-20 shows a thin section of a fracture with a thick rim (R931B). This rim is on the left side of the figure, which represents the surface. It should not be confused with the brown-coloured oxidation rim along the surface and the fracture. This sample is harzburgitic in composition, with some chlorite flakes. No differences in mineralogy are found between the thick rim and away from this rim. No deformation features are visible either. Again, the fracture cuts through the minerals in the mesh. There are no indications that minerals were dissolved and no shearing is observed. As the brown oxidation rim follows the fracture as well as the surface, this may point to fluid pathways.

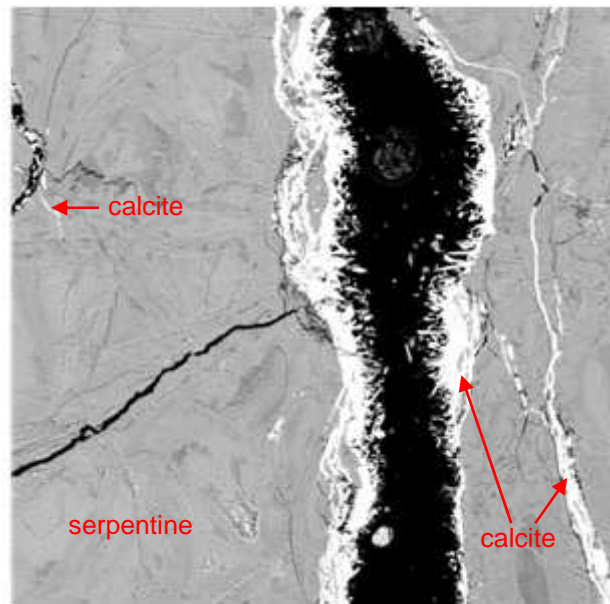
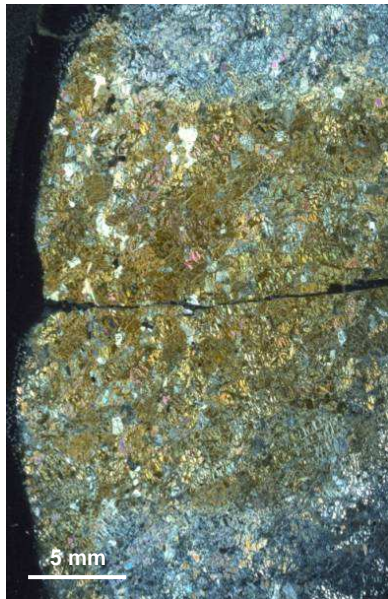


Figure 2-20: Thin section of open fracture in peridotite with rim and brown oxidation colour (left). Calcite along fracture walls and inside small adjacent fractures (white in back-scattered image, right).

Many fracture surfaces show a white mineral together with serpentine on the surface. Reactions with HCl point out that this is calcite. EMP analyses have also indicated the presence of calcite in several fractures and side-branches of these fractures (Figure 2-20 right). Magnesite was not observed in any of the thin sections.

Thick vein

At the coast of the Ugelvik peridotite body, rather thick serpentine veins (0.5-1.5 cm) were found. The fibrous structure of the serpentine inside these fractures is remarkable and different from the serpentine in other fractures. Furthermore, small fractures perpendicular to the thick vein cut the thick vein. Occasionally, the thick vein is cut by a longer fracture. Figure 2-21 shows a fibrous serpentine vein and another vein which cuts the thick vein. (Appendix B shows an overview of the veins and the surrounding peridotite.) It is obvious that the smaller fracture was formed after the thick vein was formed. Within the vein also different generations of serpentine growth are visible. Star-shaped serpentine crystals have grown over the fibrous serpentine crystals (Figure 2-22). EMP results have pointed out that these crystals, although different in shape, are all serpentine crystals. They may be different polymorphs of serpentine (lizardite, chrysotile or antigorite), but these are very difficult to distinguish. Even though the fibres of serpentine have grown in a certain direction (oblique to the orientation of the fracture itself), it is difficult to determine the opening direction (perpendicular or oblique to the fracture plane). The rim of the large vein is characterized by a band of star-shaped serpentine crystals. The vein that cuts the thick vein consists of serpentine crystals with a different structure. They are aligned perpendicular to the vein wall. The vein shows small kinks and does not have a clear rim. It cuts the band of star-shaped serpentine crystals and has thus formed later.

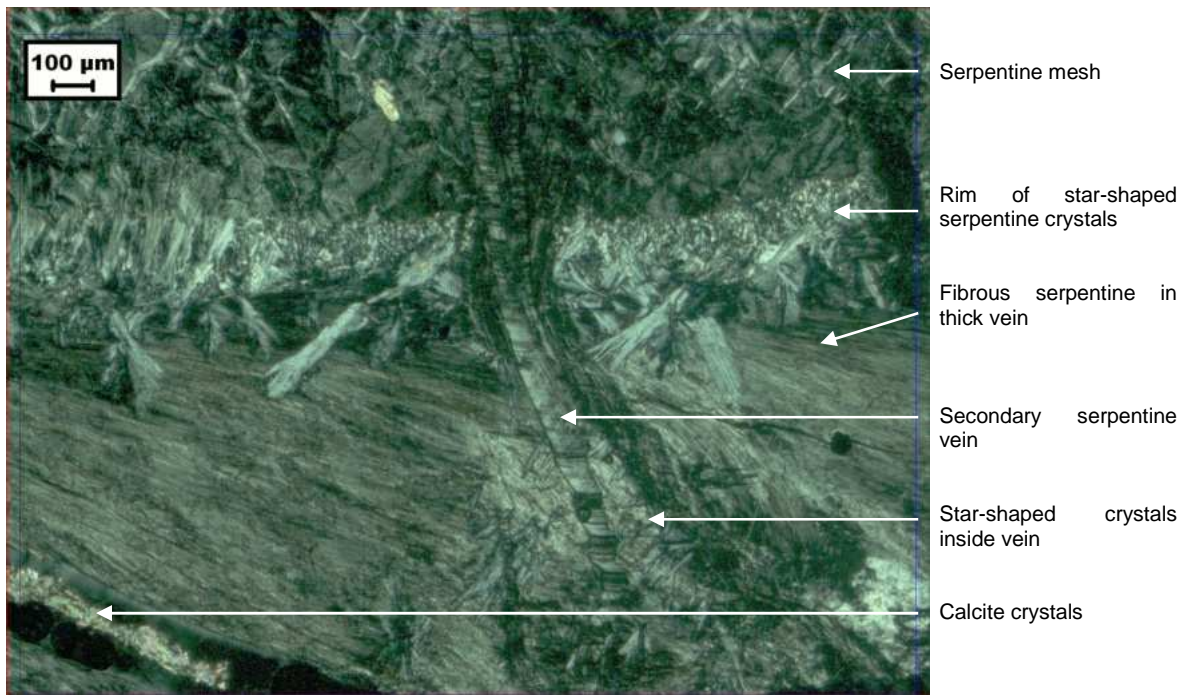


Figure 2-21: Structures in and along thick fibrous serpentine vein.

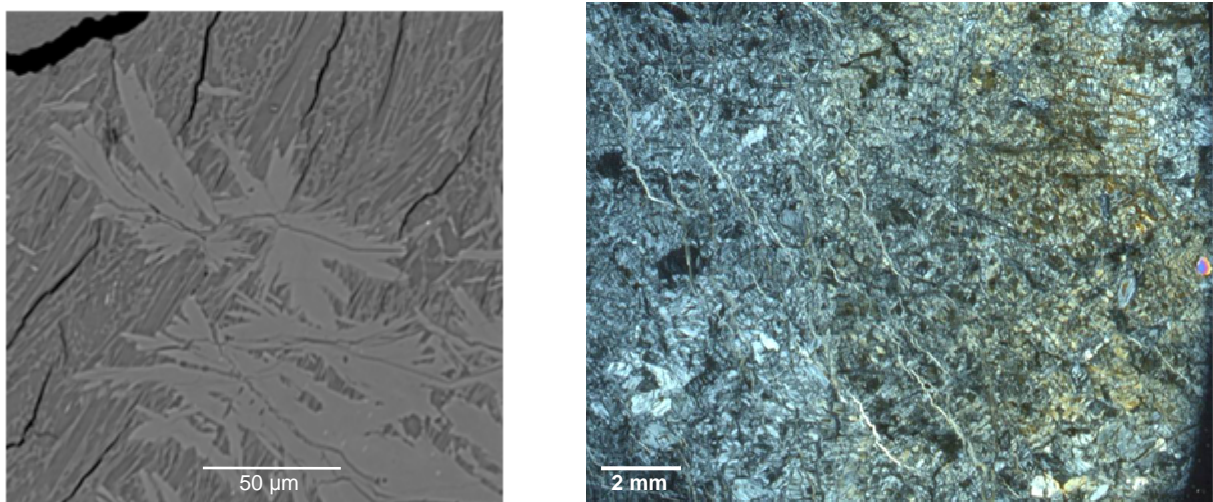


Figure 2-22: Star-shaped serpentine crystals on serpentine fibers in thick vein (left). Network of small, thin veins (right).

Network of small veins

At one particular locality in the Raudhaugene peridotite body, a network of very small parallel veins was observed (Figure 2-22). An optical analysis shows that they have a very homogeneous texture and that they are likely serpentine veins. They show a similar orientation. Some of them are connected.

Talc veins

Figure 2-23 shows a talc vein and the mesh of the peridotite rock. The talc veins do not have a clear rim, they appear to have grown over the minerals in the peridotite next to this vein. Some amphibole crystals were found in the vein as well, as indicated by measurements done using SEM. Furthermore, a single zircon mineral was found within the talc vein. Garnet relicts are present within the peridotite, consisting of amphibole and chlorite. Some chlorite flakes appear in the mesh.

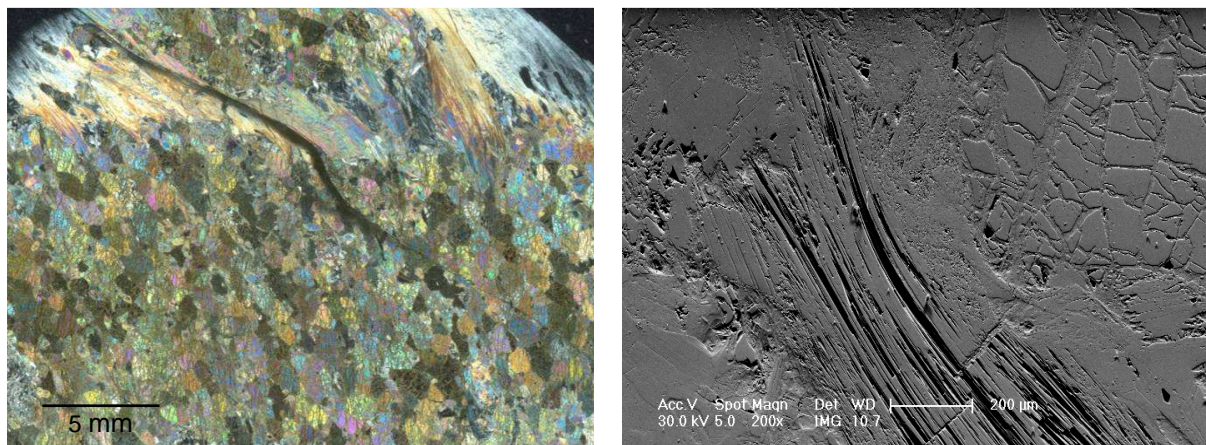


Figure 2-23: Thin section of a talc vein (left). Talc fibres on SEM image (right).

2.5.2 Fractures in pyroxenite layers

Figure 2-24 (top) shows a thin section of fractures in a pyroxenite layer in the Raudhaugene peridotite. The pyroxenite layer consists primarily of clino-, orthopyroxenes and garnets. Fractures end at the pyroxenite-peridotite boundary. Serpentine crystals have grown along the rim, perpendicular to the vein wall. Inside the fracture, within this rim, there is open space or calcite crystals have grown. The calcite crystals show twinning and appear undeformed. This piece is serpentinized quite heavily. The serpentine network has extended into the pyroxenite layer and affected the clino- and orthopyroxenes. The garnet crystals have remained relatively intact, they merely have a kelyphitic rim.

In Figure 2-24 (bottom), a thin section shows fractures in a pyroxenite layer in Ugelvik, which are filled with only serpentine crystals. The rock is relatively fresh, showing intact clino-, orthopyroxene crystals and unaltered garnets. The fractures end at the boundary of the pyroxenite layer and the peridotite. Serpentine crystals have grown inside the fracture, showing a symmetrical growth pattern perpendicular to the vein wall. It is remarkable that the serpentine veins branch out, suggesting several fracturing opening stages. No shear features are present. The fractures cut through minerals. Characteristic microstructures of dissolution (e.d. grain indentations and sutured grain boundaries) were not observed.

When we take a closer look at the vein in the pyroxenite layer in Ugelvik, we see that the texture of the vein consists of micro-bands (Figure 2-25). These are characteristic for a so-called crack-seal type of vein. The bands show distinct kinks. Another crack-seal structure is observed in the secondary serpentine vein that cuts the thick fibrous vein (Figure 2-21). The bands are visible in Figure 2-16. This vein also shows kinks.

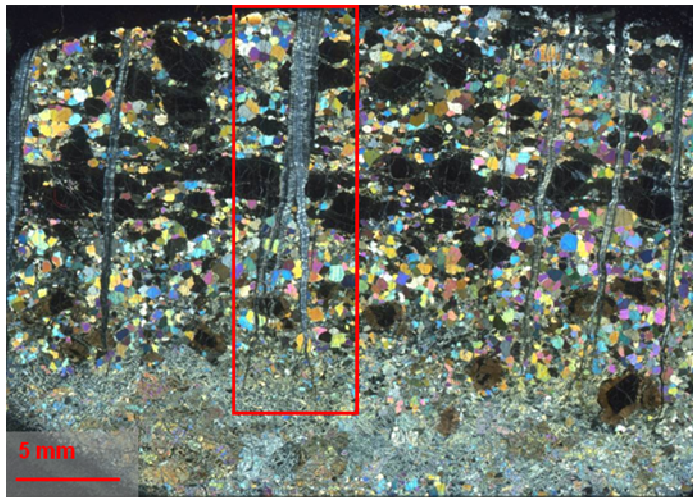
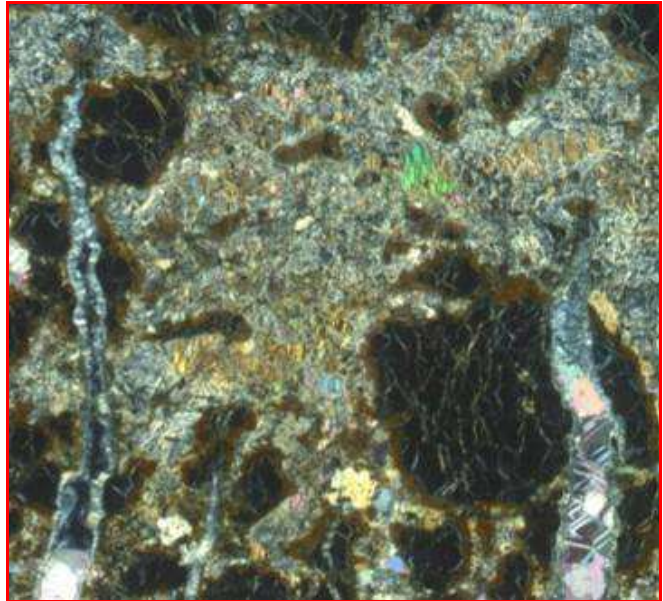
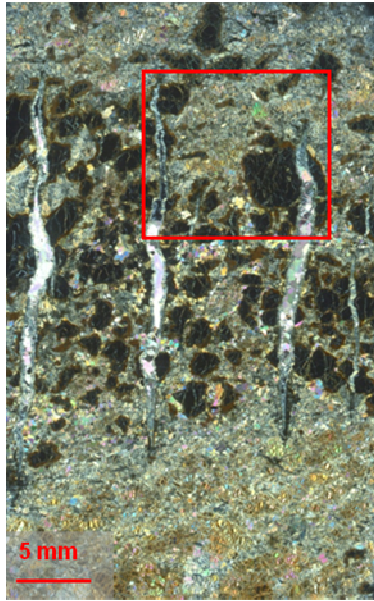


Figure 2-24:
Thin sections of fractures in a pyroxenite layer in Raudhaugene (top) and in Ugelvik (bottom).

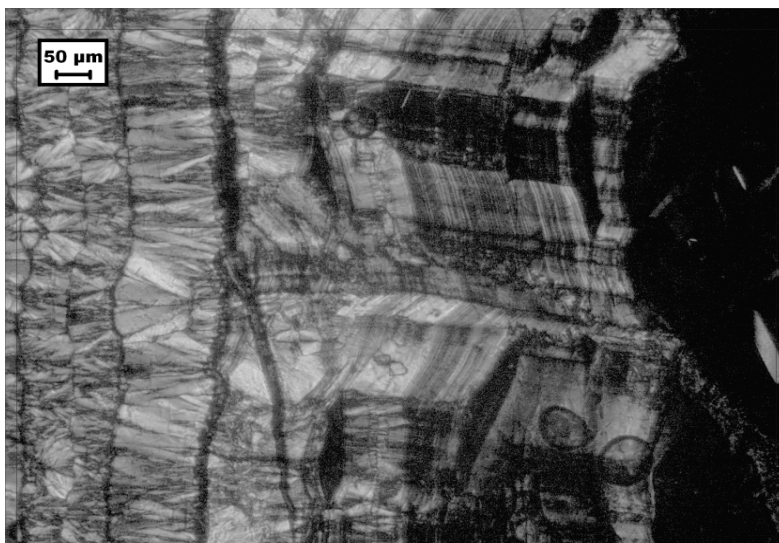
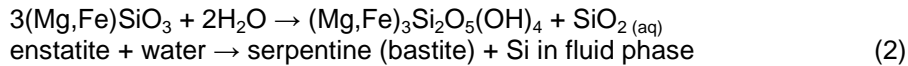
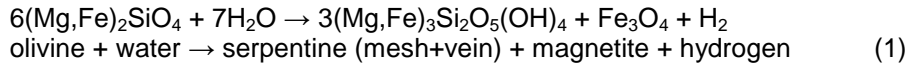


Figure 2-25 (left):
Crack-seal fracture in pyroxenite layer.

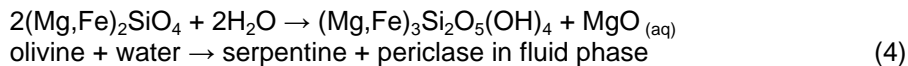
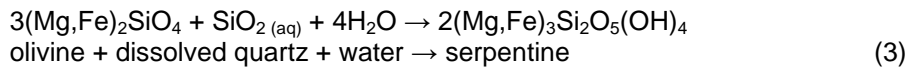
2.6 Serpentinization and volume change

2.6.1 Key reactions

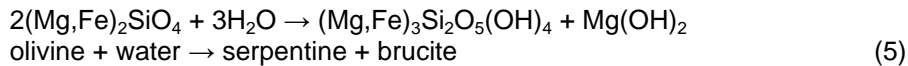
From the mineral assemblages in the thin sections and from the literature (Andreani et al., 2007; Mével, 2003; O'Hanley, 1992) reactions were derived. A list of mineralogy, including chemical formulas, is given in Appendix A. The process of serpentinization can be described by the following reactions:



The presence of magnetite and the incorporation of a small but significant amount of Fe in serpentine indicates that it is likely that some iron was dissolved in the water. Other reactions that replace olivine by serpentine in this particular setting are also plausible:

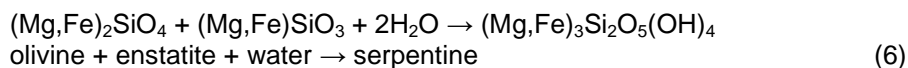


Fresh peridotite could have reacted with water and the addition of Si through a Si-rich fluid penetrating in peridotite, perhaps coming from the neighbouring gneiss, to form serpentine (reaction 3). Or twice as much olivine formed serpentine and the excess of Mg as periclase, dissolved in water (reaction 4). The Mg-excess could be incorporated in a solid as well, like periclase or brucite, however no traces of these minerals have been found. The reaction that is often used for hydration of olivine is:



In this case brucite is also a reaction product, growing between serpentine crystals. This mineral has not been observed, though the crystals may be too small to be recognized.

Reactions (2) and (3) combined yields:



This reaction fits best with the minerals observed. The proportions of olivine and orthopyroxene correspond with a harzburgite with 2/3 olivine and 1/3 orthopyroxene. The modal compositions in Raudhaugene and Ugelvik consist of more olivine and less orthopyroxene.

2.6.2 Volume expansion due to serpentinization

The reactions all lead to different volume expansions, depending on the molar proportions and phases of the reactants and products. Especially, pyroxenites respond differently to the process of serpentinization, they expand much less. The consequence of a difference in volume increase between peridotite and pyroxenite may lead to an accommodation problem in the pyroxenite layers (Figure 2-26). The expected volume change has been calculated for both peridotite and pyroxenite to investigate if the regular fracture pattern observed in pyroxenite layers is the result of this difference in volume increase. For these calculations two samples were used (one for each peridotite body). Both consist of a pyroxenite layer with fractures and adjacent peridotite rock. Figure 2-24 shows thin sections of these samples.

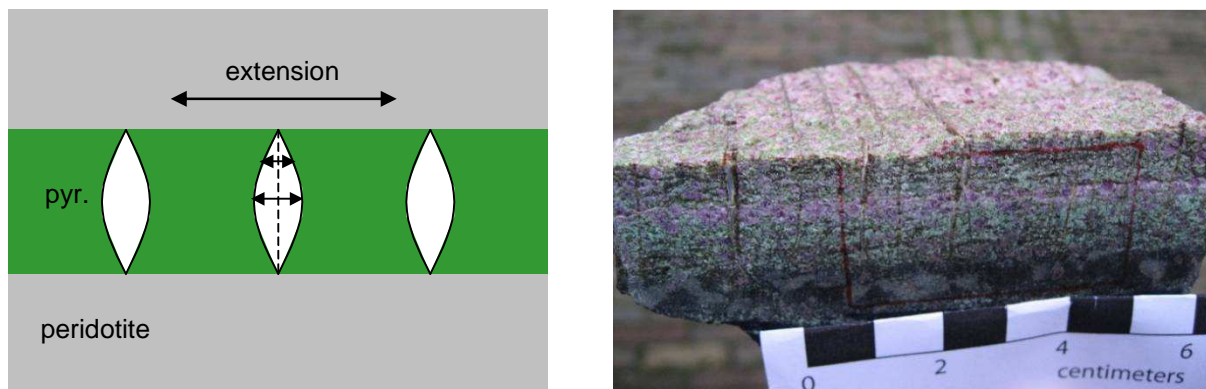


Figure 2-26: Schematic drawing of extension causing extensional fractures in pyroxenite layer (left). Sample showing fracture pattern in pyroxenite layer (right).

For both samples, the volume increase due to serpentinization in the peridotite adjacent to the pyroxenite layer was determined. This was done by estimating to which extent serpentinization has taken place, and calculating the molar volume of solids before and after the reaction. As it is not clear which reactions have occurred exactly, this was done for several reactions.

An isotropic volume increase is assumed in this simplified expansion model. The volume increase was resolved into equal components from which the linear expansion was derived. The extension in two samples of pyroxenite layers with fractures was measured and compared to the expected linear expansion in the peridotite. Calculations can be found in Appendix C, the results are presented in Table 2-2. For all reactions the linear expansion in the peridotite is less than the extension in the pyroxenite layer.

Sample R422 (Raudhaugene)

Reactions	Linear expansion peridotite (%)	Linear expansion pyroxenite (%)
Formation of brucite (1+5)	7	13
Formation of magnetite (2+5)	10	
Addition of silica (3+5)	5	
Discharge of periclase (4+5)	9	

Sample U631 (Ugelvik)

Reactions	Linear expansion peridotite (%)	Linear expansion pyroxenite (%)
Formation of brucite (1+5)	5	11
Formation of magnetite (2+5)	8	
Addition of silica (3+5)	5	
Discharge of periclase (4+5)	7	

Table 2-2: Results of calculations for linear expansion in pyroxenite layer and surrounding peridotite.

2.6.3 PT conditions

The peridotite bodies emerged from the upper mantle towards the surface, following a retrograde path (Figure 2-27). Serpentine forms at relatively low temperatures, from approximately 500 to 200°C. The three polymorphs of serpentine could indicate more specific temperature conditions (Andreani et al., 2007), but they have not been identified in this study. In addition, the presence of other minerals like garnet, amphibole, chlorite, talc and zircon could give indications which conditions the peridotite bodies have experienced. Karen Oud has focussed on this topic in her MSc thesis.

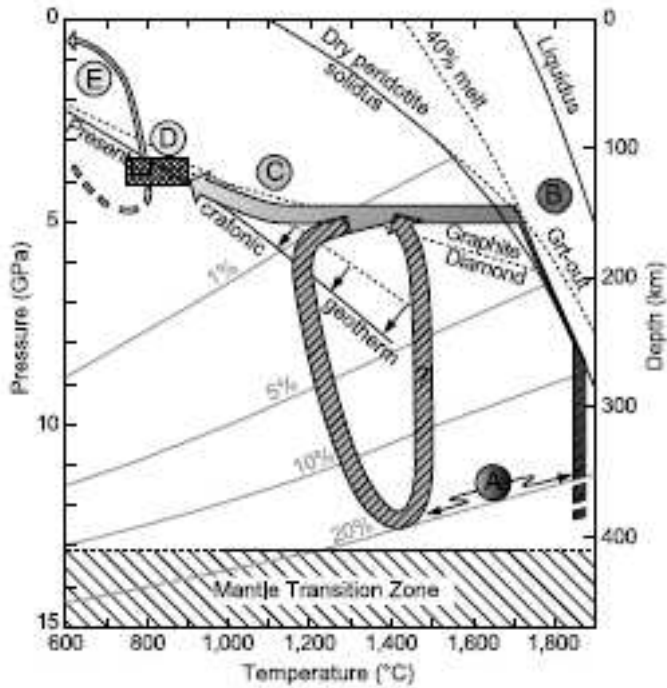


Figure 2-27: P-T diagram of the Otrøy peridotites (Spengler, 2006). For the early part of the evolution of the peridotites he proposes two possible models.

2.6.4 Thermal contraction

As the peridotite bodies were exhumed towards the Earth's surface, thermal contraction may have taken place. The peridotite rock and the pyroxenite layers may have reacted differently to the enormous drop in temperature. The corresponding thermal contraction (fractional change in volume) was calculated for both peridotite and pyroxenite rock (Appendix D). A contraction of 0.35% was determined for peridotite and a contraction of 0.30% for pyroxenite. According to the simplified model in section 2.6.2, the linear contraction was found to be about 0.12% for peridotite and 0.10% for the pyroxenite layers.

2.7 Discussion

2.7.1 Development of fracture networks

Serpentine network (grain-scale)

Thin sections reveal that serpentine networks are present throughout the two peridotite bodies. The network structure and density seems to be very consistent on outcrop scale. Between outcrops the extent of serpentinization varies slightly but the overall network appears to be remarkably homogeneous. Similar observations were noted by Rudge et al. (2010) in oceanic settings, where peridotites are exposed on the seafloor near mid-ocean ridges. Between depths of 100 to 200 m no significant gradient in the degree of serpentinization has been observed.

In order for serpentinization to take place, water infiltration must have occurred throughout the whole peridotite body. The exact mechanisms with which this occurs are not yet fully understood. Generally, fluids may be transported via diffusion along grain boundaries. This is, however, a very limited means of transport and may not account for impermeable, dense mantle rock. Grain boundary diffusion is not sufficient to explain the extent of serpentinization that is observed. Transport by means of cracks is a much more effective process. Micro-scale cracks in samples were found to be present along grain boundaries, but also splitting grains into pieces. These cracks form an intrinsic part of the serpentine network.

The micro-fracture network is not likely to be the result of reaction-induced fracturing, as there is no gradient in the degree of serpentinization throughout the peridotite body. Reaction-induced fracturing would propagate from the edge further into the rock. Therefore a higher degree of serpentinization is expected near the edge. Rather the peridotite bodies show a homogeneous serpentine network. The origin of micro-scale cracks is found in thermal contraction that, according to Viti and Mellini (1998) can lead to almost isotropic fracturing of the peridotite. The transport of water through these fractures has enabled the development of a homogeneous serpentine network.

Serpentine is a sheet-silicate and is pliable in multiple forms. The observed aligned serpentine texture may be formed by the alignment of numerous individual serpentine crystals (Figure 2-17). This would indicate that serpentine crystals grow perpendicular to olivine grains. Occasionally, such an alignment occurs on both sides of a straight line, that may represent the nucleus points in the middle of a crack. Thus, perpendicular growth of serpentine crystals occurred towards the olivine grains.

No convincing deformation features on micro-scale are observed that suggest a volume increase or indicate fracturing. There is no clear relation between serpentinization and fracture formation in the form of a fracture lying in the extension of aligned serpentine crystals. No transitional forms from the serpentinization network to a fracture, that might occur in the process of serpentinization, were detected either.

The mesh was studied for a preferred orientation in the serpentine network or elongated grains that could provide information on the nature and orientation of stress in the peridotite rock. In most of the thin sections no preferred orientation was found. Only the serpentine network near the talc veins in the east of Ugelvik shows a preferred orientation within the serpentine network and slightly elongated olivine crystals, perpendicular to the vein (Figure 2-23). Extension perpendicular to the vein (and parallel to the preferred orientation) may explain this local phenomenon. Additional EBSD analyses could determine whether there is a preferred crystal orientation. The preferred orientation in a black-white image such as Figure 2-18 can be further analyzed using software programs (ImageJ, NIH). On the whole, the mesh texture does not provide evidence for regional stress. Near the talc veins, the preferred orientation indicates local stress.

Small-scale fracture network (cm scale)

Small (cm-scale in length) fractures have been observed at only one location (Figure 2-22). The veins are parallel to each other and show one particular orientation. They are not likely to be formed due to reaction-induced fracturing. This type of fracturing is expected to be found at more locations, as serpentinization has occurred throughout the peridotite bodies. Moreover, as volume expansion due to

serpentinization occurs in three dimensions, reaction-induced fracturing is expected to occur in all three dimensions as well. A more likely mechanism for these parallel fractures is local stress due to compression or extension.

Fracture networks at outcrop-scale (dm-10m scale)

There is a variety of fracture networks present in the peridotite bodies; dense fracture networks or widely spaced fractures, at dm- to 10 m-scale, including straight and curved fractures, with or without a rim. Most fractures are straight, very thin (1 mm thick) and filled with serpentine. The similar shape of the edges of an 'empty' fracture and crystals that are cut in half but still opposite of each other (Figure 2-19 right), show that the two sides of the peridotite rock have been pushed aside. Lack of solution features like grain indentations and sutured grain boundaries indicate that solution has not taken place. It is very unlikely anyway that pressure solution occurs in dense mantle rocks, certainly not forming a fracture with similar sides and of dm-10m scale. In some cases, the degree of serpentinization is higher near the edge (Figure 2-19 left). The high relief of observed rims may be due to the presence of more resistant minerals. No change in mineralogy was observed, however. Possibly recrystallization has taken place along fracture openings, which are exposed most to fluids. This was suggested by Spengler (2006) for the lip-shaped fractures found in the east of Ugelvik. Yet no difference in the serpentine network is observed in rims either. Thus, no indications are observed for reaction-induced fracturing. Most fractures (perhaps an exception excluded) do not show any shift or sense of shear and appear to be solely cracked apart. Therefore, they can be regarded as extensional fractures. This indicates that space has been created.

It is difficult to specify the relation between fracturing and serpentinization. When a fracture meets another fracture which is empty, it should end at this fracture, because it acts as a free surface. When minerals have grown inside the fracture, another fracture will propagate (Twiss & Moores, 1992). This theory may indicate that cross-cutting fractures have formed one after the other, as serpentine crystals must have precipitated first in the earliest fracture. On the other hand, fractures ending at another fracture may have formed quite rapidly after the already existing fracture, when serpentine crystals did not have the chance yet to crystallize completely.

Exceptions in the homogeneity of the peridotite bodies are compositional banding and pyroxenite layers. There is no direct relation between the banding and fracturing as fractures cut straight through (isoclinal) folds. For the greater part fractures seem to have random orientations with respect to the compositional banding. However, they also occur exactly parallel to the garnet alignment. It may be easiest for the fractures to form in this direction. Especially when the compositional banding is rather thick (~5cm), fractures have been found perpendicular to the banding (Figure 2-13). The lip-shaped fractures, found in the east of Ugelvik, are nearly all orientated parallel to the aligned garnets (Figure 2-8). A second generation was found at a low angle to the compositional banding.

Some of the small-scale fracture patterns observed, may be explained by hierarchical fracturing, a fracturing process described by Lachenbruch (1962, 1963) and Iyer et al. (2008). Initial fractures form randomly, but once they have formed, they are determining for the other subsequent fractures that form. The stress fields around the initial fractures dictate the formation of subsequent fracture generations (Bohn et al., 2005). According to Lachenbruch (1962, 1963), in a system with several generations of fractures, late generation fractures will tend to intersect earlier generation fractures at right angles. When there is frequent nucleation of new fractures a pattern with 120°-angles will form (Toga and Alaca, 2006). The latter is typical for a system consisting of relatively homogeneous material with an isotropic stress field. In the peridotite bodies that are subject of this study, both angles occur in networks (and in combination with each other and with other angles), but not as a consequent and extending pattern. Thus, both mechanisms of fracture network development (90°, 120°) may play a role in the fracture formation in Raudhaugene and Ugelvik, but they seem to be of minor importance.

At the coast of Ugelvik, outcrops are fractured most intensely (Figure 2-5, top right). Fractures are wide and the edges of the blocks of peridotite are rounded. Not all fractures are filled with serpentine. However, when these fracture planes are followed serpentine veins can usually be found. Therefore we assume that originally in all fractures precipitation of mineral deposits has occurred and that lack of mineralogy inside the fracture is probably caused by weathering. This seems likely at the coast, where the rocks are right beside the water and tidal influences play a role. It is remarkable that thick serpentine veins are abundantly present as well. Possibly, precipitation of serpentine still occurs in widened fractures. At low temperatures, the process of serpentinization is expected to occur at a very

slow rate though. The only sign of weathering in thin sections of peridotite, is the oxidation of the serpentine.

The thick fibrous vein found near the coast in Ugelvik, is cut by small perpendicular fractures, indicating a second generation of fractures. They are very thin and in the outcrop it is not clear how they extend into the rock (Figure 2-7 right). The crack-seal structure of these fractures indicates that they formed due to extension. This type of vein forms by subsequent small increments of opening in which serpentine crystals precipitate after every incremental stage (Ramsay, 1980b; Andreani et al., 2004). Serpentinization occurred before these particular crack-seal veins formed, because the fibrous vein already existed. Continued serpentinization may have caused cumulative expansion in the peridotite, which could not be accommodated by the thick serpentine vein, resulting in small fractures. The same mechanism may apply to fractures perpendicular to the compositional banding. A thin section is not available, but further research could determine whether these fractures also formed through a crack-seal mechanism.

The talc veins in the east of Ugelvik, show a different pattern than the serpentine veins. They occur parallel to each other and do not cut each other. As mentioned earlier, the serpentine network in the peridotite around the veins, shows a preferred orientation perpendicular to the talc veins, indicating extension. Some veins show a fracture in the middle of the vein (Figure 2-8 left). Either a fracture was formed and on both sides talc precipitated, or the soft talc veins were cut by a later fracture. The latter seems more likely. This water-bearing mineral phase may indicate another generation of fracturing, as it may have formed under different conditions than the serpentine veins. In one talc vein, a zircon crystal was observed that was probably transported by fluids. Zoning in zircons could provide information on metamorphic events. Possibly, more zircon crystals are present in the talc veins.

Fractures in pyroxenite layers

Thin sections of pyroxenite layers show that minerals are cut in half by the fractures and they appear to be pulled apart by extension (Figure 2-24). The crack-seal mechanism is characterized by small parallel bands within a vein. The process involves subsequent small increments of opening in which serpentine crystals precipitate after every incremental stage (Figure 2-25). The veins appear slightly deformed in the form of kinks. Taking a closer look, the bands of which the vein consists all show the same kink structure. Kinks in this type of vein can be explained by the irregular shape of the crack. Serpentine crystals have grown perpendicular to the crack, from the vein wall to the vein centre. Because of the irregular shape of the crack, crystal growth occurs in different directions from the wall rock. The kinks do not represent deformation features.

The branched nature of the vein, suggesting several opening stages of the fractures is consistent with the formation of crack-seal veins. Cross-cutting relationships in Figure 2-24 show that cracking occurred in very small opening-steps at first (right side in Figure 2-25). Later veins consist of more elongated grains, indicating that serpentine crystals had more time and space to grow.

The lens-shape and the regular parallel alignment of the sub-perpendicular fractures in the pyroxenite layers suggest they accommodate space. Extension of some kind may have taken place, to which the pyroxenite layers have responded in a brittle manner. This is confirmed by the observed microstructures.

Figure 2-28 (left) shows the principal stresses that cause the development of the regular fracture patterns, as found in the pyroxenite layers. A slight angle of the principal stresses could induce fracturing at a small angle (Figure 2-28 right). These patterns were observed in Figure 2-10 a and b.

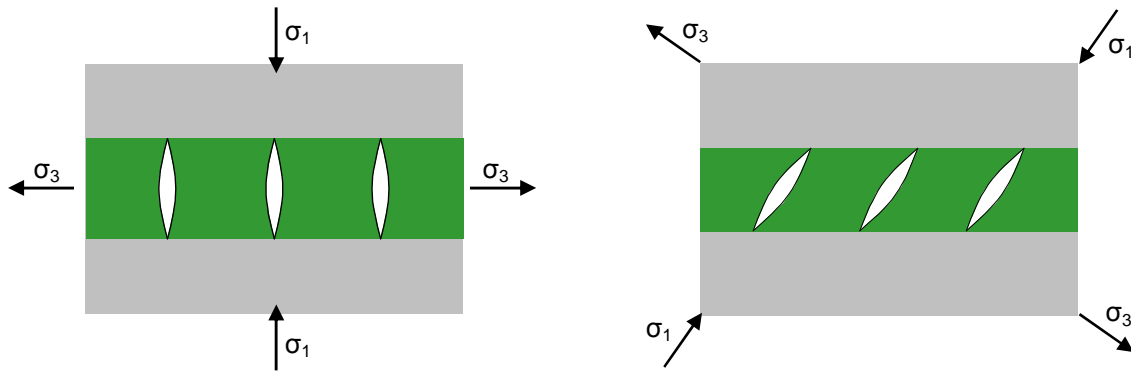


Figure 2-28: Crack-seal veins under stress perpendicular to the pyroxenite layer (left) and at a small angle with respect to the pyroxenite layer (right).

Observations show that fracture spacing is relative to the thickness of the pyroxenite layer. The thinner the pyroxenite layer is, the smaller the spacing is. The characteristic fracture spacing can be explained in several ways (Twiss & Moores, 1992).

Hydrofracturing may have played a role. When a fracture forms, pore fluids from the neighbourhood of the fracture flow into the open fracture, causing a decrease in pore fluid pressure in the rock around the fracture. A decrease in pore fluid pressure causes the effective Mohr circle to move away from the failure criterion. This means that in the vicinity of the fracture, no further fracturing can occur. Only beyond the zone of reduced pore fluid pressure, another fracture can form. This zone defines the minimum distance in fracturing. The more impermeable the rock is, the smaller the fracture spacing is.

When the peridotite bodies expand to a larger extent than the pyroxenite layer in between, shear stress will develop along the boundaries. Tensile stress increases along the boundary until it reaches the tensile strength of the layer and causes the formation of a crack. The crack locally relieves the tension. Away from the crack, along the boundary the stress increases again to be relieved at the next crack. The constant layer strength and build-up of stress cause the development of cracks at a set distance.

The crack-seal type of veins give an indication about the timing of fracturing with respect to serpentinization. The mechanism by which these veins form indicates that serpentine growth occurs directly after a small increment of opening. Thus, serpentinization is going on at the same time as the formation of crack-seal veins.

One way to explain extension is the difference in volume expansion between peridotite and pyroxenite, that occurs as a result of serpentinization. As the peridotite rock expands isotropically, tensile stress is imposed on the pyroxenite layer. In the dimension perpendicular to the pyroxenite layer, forces are exerted on the layer. When the peridotite expansion is restricted in the direction of the pyroxenite layer (by the presence of the pyroxenite layer), additional volume expansion will occur parallel to the pyroxenite layer. This causes even more extension. However, extension occurs in all directions parallel to the pyroxenite layer (Figure 2-29, also in the direction into the paper). Additional boundary conditions due to compositional differences or other stresses may lead to a preferred orientation.

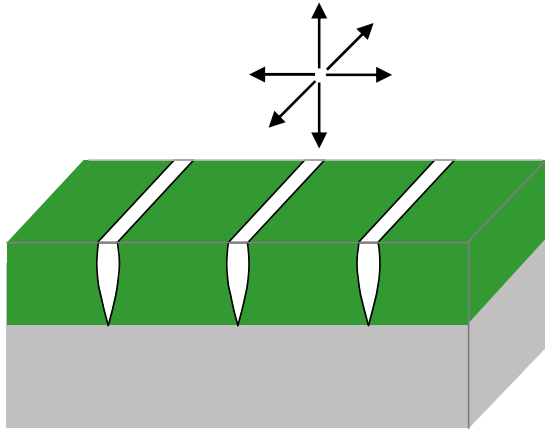


Figure 2-29: 3-dimensional crack seal veins in pyroxenite layer and stresses.

Percentages on volume expansion and linear extension were calculated in section 2.6.2, according to a simplified model (Figure 2-29). From the volume expansion, linear extension was derived. For all scenarios (different serpentinization reactions), these percentages appear to be too low (about 7%) to cause the extension measured in the pyroxenite layers (11% and 13%). There is an additional volume expansion and extension parallel to the pyroxenite layer, due to the restriction of the volume expansion in the direction perpendicular to the pyroxenite layer. This would cause an increase linear expansion parallel to the pyroxenite layer, resulting in sufficient linear expansion to account for the observed extension in the pyroxenite layers. The calculated percentages are indications, as the extent of serpentinization was estimated and the calculations are very sensitive to the molar proportions in the reactions.

Another explanation for the regular fracture pattern in the pyroxenite layers could be thermal contraction. The order of linear contraction is about 0.12% for peridotite and 0.10% for the pyroxenite layers. The percentages are very small. This mechanism does not explain fracturing with linear extension of 11 to 13% (Table 2-2).

The latter two hypotheses do not explain why pyroxenite layers are fractured (and thus stressed) in only one direction. Has the peridotite expanded much more in that particular direction? This seems unlikely as the fractures extend for several meters. One example was observed in the field of a very thin pyroxenite layer with fractures that do not appear to be parallel (Figure 2-10f). Iyer et al. (2008) mention fracturing in pyroxenite layers caused by the expansion of peridotite due to serpentinization. The fracture patterns they find in pyroxenite layers are very different from what we have found, though. The patterns they describe do consist of cracks in all orientations in the pyroxenite plane. The dominant set of fractures in the pyroxenite layers in Ugelvik and Raudhaugene shows that differential expansion is not the only influence. In addition, regional stress may have played a role.

Fracture network peridotite bodies

Figure 2-14 shows the orientations of the pyroxenite layers and their fractures in both peridotite bodies. The orientations of the pyroxenite layers differ for Raudhaugene and Ugelvik. In Raudhaugene they are oriented vertically, but in Ugelvik they are nearly horizontal. Assuming that the pyroxenite layers originally intruded as vertical dykes, this indicates that Ugelvik has been rotated during emplacement in the crust or during its uplift towards the surface, independently from the Raudhaugene peridotite body. The orientations of the pyroxenite layers within each body are very similar.

The overview of main fracture orientations (in both peridotite and pyroxenite) in Raudhaugene (Figure 2-11) does not show a clear pattern. Only the fractures in the two pyroxenite layers are oriented similarly. The similar orientation of the fractures indicates that the pyroxenite layers have experienced the same stress: extension in a N-S direction.

In Ugelvik, around the pyroxenite layers a clear pattern was observed. In the west, pyroxenite fractures have similar orientations. This indicates that the pyroxenite layers have all undergone extension, in this case in NW-SE direction. Fractures in the peridotite show a similar strike. The fractures measured at fieldstop 5.1 all have a strike parallel to the fractures in the pyroxenite layer found at that locality, only the dip varies. In the vicinity of the pyroxenite layers more to the south,

peridotite fractures predominantly have different orientations than the fractures in the pyroxenite layers, but fractures with similar orientations have also been found. In the east, fractures in the two pyroxenite layers have a different orientation than in the west and compared to each other. Among other fracture orientations in nearby outcrops, both orientations are found in the peridotite fracture planes.

For both peridotite bodies peaks in the orientation of fracture planes have been identified (Figure 2-12). The peaks correspond with a N-S strike and steep dip for Raudhaugene and a more NE-SW strike and steep dip for Ugelvik. The more or less similar orientation indicates regional stress may have played a role in the development of the fractures. E-W extension has taken place, which is confirmed in the literature. Several modes of extension have taken place in this region during the Caledonian orogeny (Spengler, 2006), of which the last one was E-W. The fractures in the pyroxenite may show an earlier deformation phase, indicated by a different orientation. Both peaks in the orientation of fractures do not particularly stand out and the number of data on which they are based is limited, making the density plots very sensitive to individual measurements. Fracture orientations should be investigated more extensively to gain more insight. Not all fracture planes that were observed could be measured as they were only visible as a line.

In general, the fractures are very thin and no offsets are visible. This implies that only minor extension could have taken place. Even the thick serpentine veins do not make the difference, since they are only locally found. At grain-scale signs of regional stress are not evident.

The mechanism of extension due to regional stress corresponds to the fact that the fractures in the pyroxenite layers are oriented in one particular direction. Most likely these fracture patterns have been formed due to a combination of volume expansion, through serpentinization, and regional stress. The Ugelvik body was probably rotated before the fracturing.

CO₂ in the system

The presence of calcium carbonate (calcite) indicates incorporation of CO₂ in the peridotites. In theory, this could happen during the process of serpentinization. However, calcite crystals seem to have formed in open spaces only and not within the mesh, which indicates they may have formed very recently. Moreover, the supply of calcium does not seem to be related to reactions involved in serpentinization. If it was inserted into the peridotite as a solute in water, then it would probably have precipitated in the mesh as well. The only other minerals that contain calcium in this system are clinopyroxene and garnet. But these minerals have only been slightly altered, so they could not have provided enough calcium for these calcium crystals to form. In addition, clinopyroxene is only locally present in the pyroxenite layers. Most likely, the calcium and CO₂ have their origin outside the system. In a purely magnesian system, natural carbonation would result in the magnesium carbonate magnesite. However, EMP analyses did not show the presence of magnesite, only calcite was observed. If there was CO₂ present in the infiltrating water as serpentinization occurred, then the content was probably very low.

2.7.2 Evolution of peridotite bodies

The evolution of the peridotite bodies from the Caledonian orogeny until present is summarized below. Different fracture mechanisms have played a role.

Order of events:

- Strong ductile deformation (isoclinal folding of compositional layers and pyroxenite dykes);
- Rotation of Ugelvik peridotite body with respect to Raudhaugene peridotite body during emplacement in subducting crust or exhumation;
- Formation of isotropic micro-fracture network due to thermal contraction as peridotite bodies are exhumed towards the surface;
- Fluid infiltration throughout peridotite bodies along micro-fracture network and formation of serpentine network;
- Volume expansion in peridotite bodies due to serpentinization;
- Extension in pyroxenite layers due to volume expansion and regional stress (N-S extension) causing regularly spaced fracturing in pyroxenite layers;
- Fracturing in peridotite bodies under regional stress (E-W extension) and hierarchical fracturing;
- Continued serpentinization causing small crack-seal fractures perpendicular to thick serpentine veins;
- Weathering and continued serpentinization near coast when peridotite bodies are exposed at the surface.

Determination of different serpentine polymorphs may help establishing PT conditions and therefore restrictions on the timing of formation of the fractures. The polymorphs of serpentine can be distinguished using a Transmission Electron Microscope (TEM) and X-Ray Diffraction (XRD). Stress orientations in the mesh could be derived from the crystal lattice orientations. These can be determined using Electron Backscatter Diffraction (EBSD).

2.8 Conclusions

The geometry and scale of fracturing is studied for the naturally fractured serpentinized peridotite bodies of Raudhaugene and Ugelvik. These characteristics provide insight in the mechanisms that play a role in fracture network development.

The micro-scale fracture network observed in the peridotite has most likely formed due to thermal cracking. Subsequent fluid infiltration enabled the formation of a remarkably homogeneous serpentine network. On a small-scale, no evidence in the form of deformational structures is found, that indicates volume expansion due to serpentinization.

Regular fracture patterns in pyroxenite layers with one dominant orientation can partly be explained by differential expansion due to serpentinization. The predicted volume change in the adjacent peridotite is large enough to cause the observed extension in the pyroxenite layers. The dominant orientation is explained by influences of regional stress. Crack-seal processes, observed in the veins in the pyroxenite layers, indicate several opening stages and that serpentinization occurred when these veins were formed.

Orientations of fractures in the peridotite bodies do not show obvious patterns due to regional stress. Slightly dominant orientations indicate E-W extension. Fracture patterns may have been further influenced by hierarchical fracturing, where earlier fractures dictate the orientation of later fractures. Continued serpentinization resulted in small crack-seal fractures perpendicular to thick serpentine veins. The presence of calcite in fractures indicates incorporation of CO₂, but does not provide evidence that the growth of calcite crystals is involved in fracturing the peridotite.

Several different mechanisms have played a role in fracturing the peridotite bodies. A combination of regional stress, hierarchical fracturing, and mineral reactions involving a volume increase explains the origin of most fractures. The regular fracture patterns in the pyroxenite layers may reveal an earlier phase of extension.

To determine the significance of orientation patterns a larger number of data is required. Crystal lattice orientations, determined using EBSD, can provide insight in the orientation of stress fields and the underlying mechanism. Studying ambiguous cross-cutting relationships microscopically could provide insight on the timing of fracturing.

3. Breccia development and carbonation in the Lherz peridotite (French Pyrenees)

3.1 Introduction

The well-known Lherz peridotite body in the French Pyrenees, located in the Aulus basin north of the North Pyrenean fault (Figure 3-1), has been brecciated intensely. The surrounding Mesozoic limestones are also brecciated. It is remarkable that calcite veins occur abundantly, but only in the outer part of the Lherz body. Different types of breccia are recognized. There are breccias consisting of rounded clasts, in some cases heterogeneous, and a peridotite matrix. In addition there are angular shaped pieces of peridotite that in some cases fit together as a jigsaw puzzle. The question is which mechanism has caused the formation of calcite veins and what is the origin of the breccias. Did the rock fracture in situ, due to a fault mechanism or was fracturing reaction-induced? Could some breccias otherwise be explained by a sedimentary mechanism?

In this research, the hypothesis that the breccias in the Lherz peridotite are formed by CO₂ infiltration and reaction with peridotite is tested. A similar process was identified by Kelemen and Matter (2008) in the Semail ophiolite in Oman, but also suggested by Hansen et al. (2005) at Atlin in British Columbia (Canada). The calcite veins between the breccia look very similar to the carbonates found in Oman. This research gives an account of the distribution of the breccia types, possible implications for the geological evolution of the Lherz body and how these implications fit with hypotheses proposed by other authors.

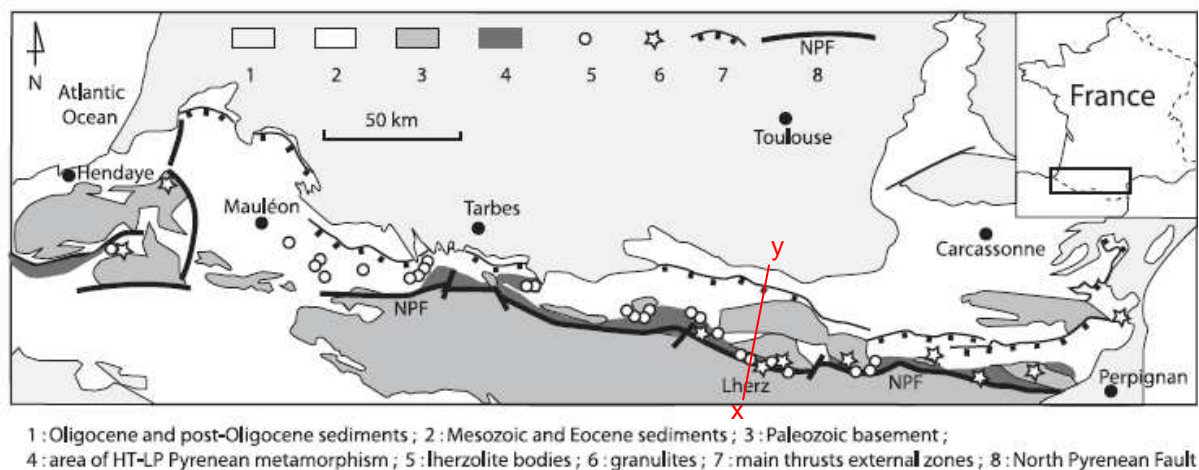


Figure 3-1: Location of mantle bodies including the Lherz peridotite, after Lagabrielle and Bodinier (2008).

3.2 Geological setting

Numerous ultramafic mantle rock bodies occur along the North Pyrenean Fault. These Iherzolites are situated within Mesozoic limestones and dolomites, altogether forming the north Pyrenean zone. The Lherz body is approximately 1.5 km across and one of the larger bodies in this zone. It is mainly composed of spinel-Iherzolite, with intercalated layers of harzburgite up to 20 m thick. Occasionally a pyroxenite layer (websterite) is found (Le Roux et al., 2007). Both the surrounding limestones as well as the peridotite body itself have been brecciated intensely. Near the edge of the body calcite veins are found.

The Lherz body has been studied extensively and its emplacement into the crust has long been debated. In a recent study Lagabrielle and Bodinier (2008) propose that many of the mantle bodies in the surroundings of Étang de Lherz represent fragments of subcontinental mantle material reworked through sedimentary processes within Cretaceous basins of the north Pyrenean zone (Figure 3-2). During the Albian (middle Cretaceous) rifting occurred, which is associated with the rotation of Iberia along the proto-North Pyrenean fault. This was followed by extreme thinning of the crust and the

progressive rise of mantle rocks towards the surface. Eventually, this process led to exhumation of the subcontinental mantle beneath Europe along a detachment, causing a thermal anomaly. As oceanic spreading started in the Bay of Biscay, the region of exhumed mantle on the eastern side is only narrow. Sediments accumulated in deep basins and were metamorphosed in situ. As clasts of the Paleozoic crustal basement are extremely rare in the breccias surrounding the lherzolites, gravity sliding of the Mesozoic cover must have occurred over a tectonic sole of Triassic material (Lagabrielle et al., 2010). The lherzolites occur as clasts of various sizes within monogenic or polymictic debris flow deposits of Cretaceous age. In the Late Cretaceous, a tectonic inversion of the extensional system took place, leading to the incorporation of detachment fault rocks into the Pyrenean orogenic wedge during the contractional phase.

Gravity modelling has been carried out in the past (Anderson, 1985). The results show that the Lherz body is a loose mantle body, detached from its original mantle rocks. It only has a volume of 0.8 km^3 .

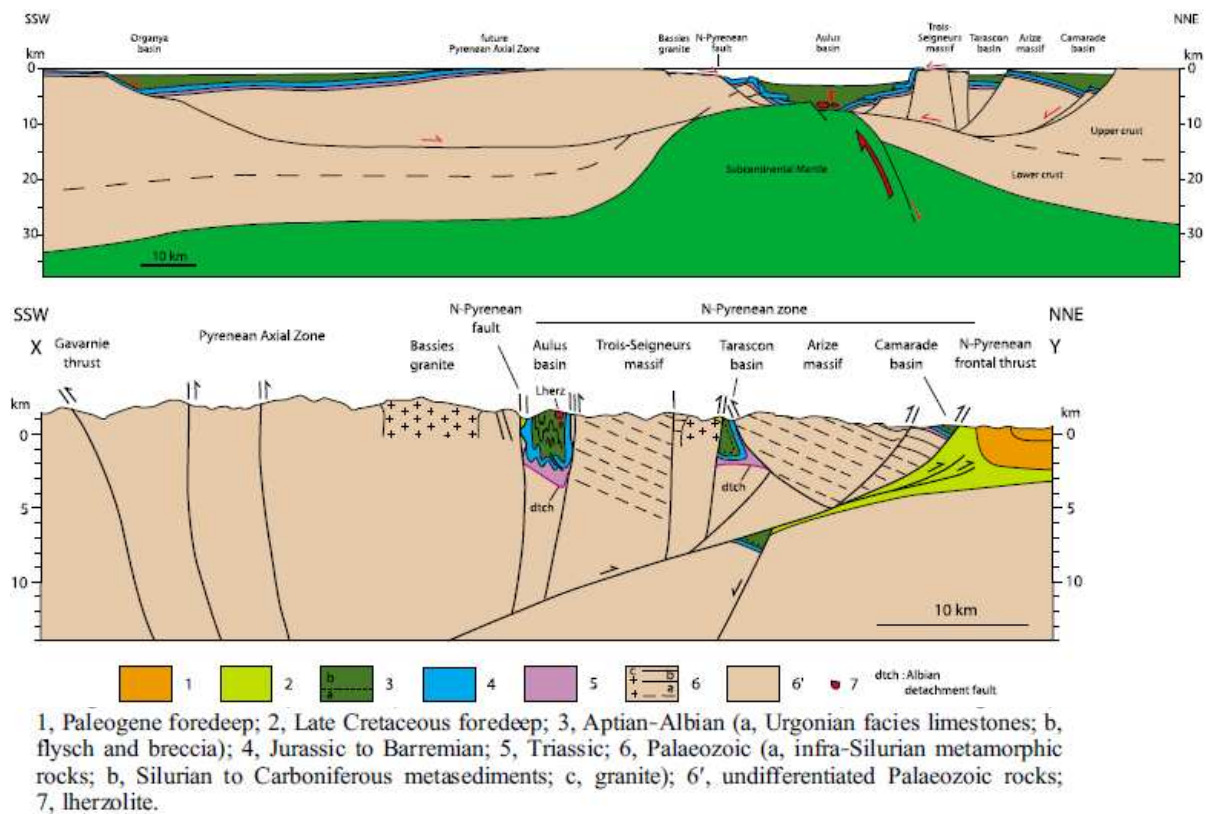


Figure 3-2: Top: model of mantle exhumation during pre-orogenic rifting and gravity sliding of Mesozoic cover into basin. Bottom: cross-section of present geological setting (X and Y are indicated in Figure 3-1). After Lagabrielle et al. (2010).

3.3 Method

Several samples of different breccias were taken at Lherz in the summers of 2009 and 2010. The sampling sites have been plotted on a map by Martyn Drury, Auke Barnhoorn and Côme Levebvre made in the summer of 2009 (Figure 3-3). The samples were studied extensively and special attention was paid to the presence of carbonates and unusual minerals that may indicate specific metamorphic conditions. Thin sections were made and studied under the light microscope for micro-structures. To investigate the chemical contents of some of the samples chemical analyses were performed using micro X-ray fluorescence (μ -XRF) and an electron microprobe (EMP). In addition, on one of the samples electron back-scattered diffraction (EBSD) and X-ray diffraction (XRD) was performed. Based on all analyses the breccias were classified and a conceptual model was developed relating the breccia types to formation mechanisms.

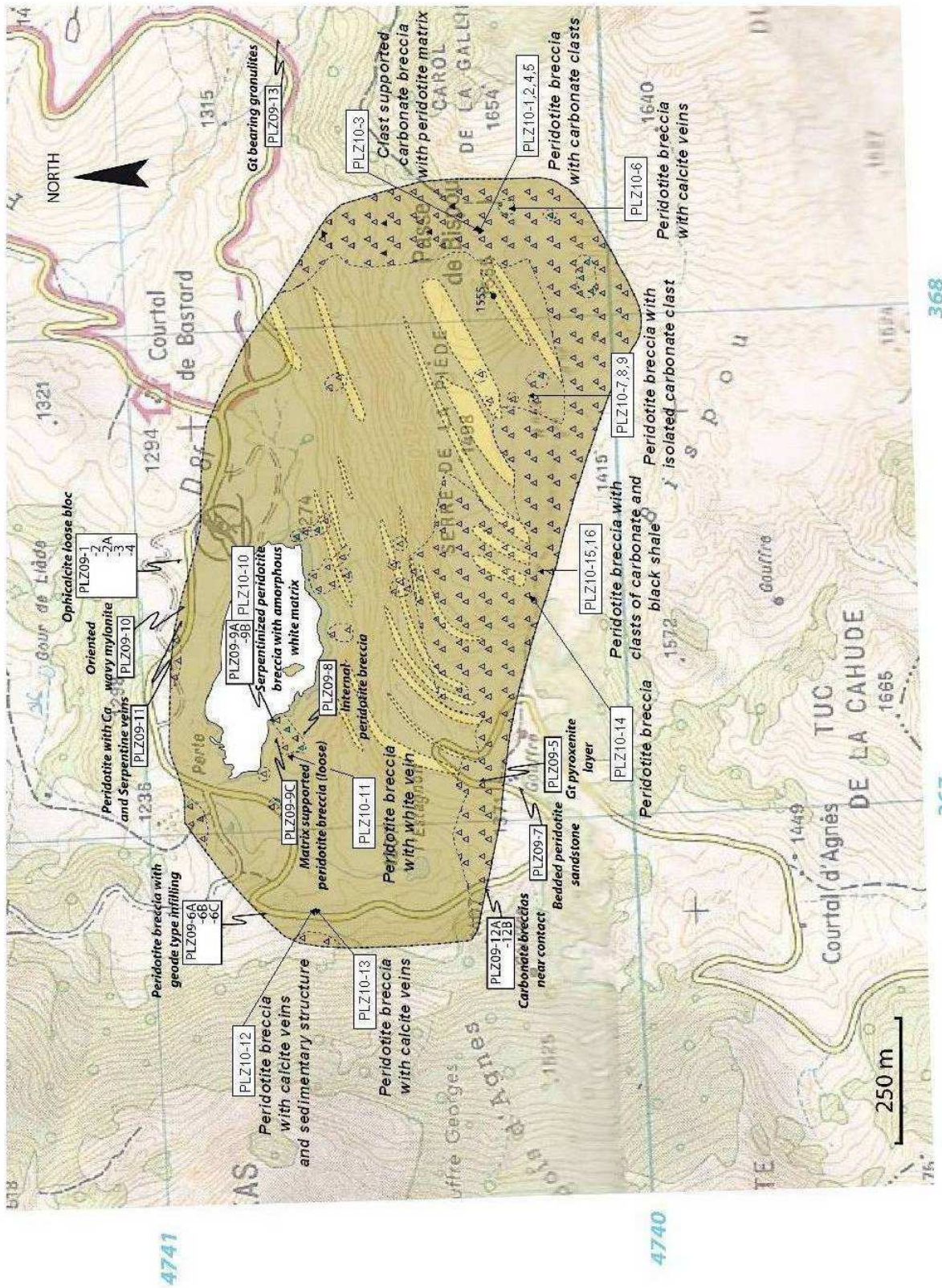


Figure 3-3: Fieldmap with locations of sampling in 2009 and 2010

3.4 Field observations: types of breccias

Different types of breccias could be distinguished in the field. A description of these will be given in the following subsections. The observed breccia-types will be compared to the four types of breccia that Lagabrielle and Bodinier (2008) distinguished (Figure 3-4). Their first and most abundant type are monomictic peridotite breccias, found along the southern and eastern side of the Lherz body. These breccias do not include carbonate clasts and appear to have formed in situ, as mantle structures like websterite layers can be followed throughout. Therefore, the monomictic peridotite breccias are regarded as fault or cataclastic breccias. The second type is similar to the first type, except that these breccias typically contain isolated clasts of limestones and appear more heterogenous. Furthermore, Lagabrielle and Bodinier have recognized some breccias as sedimentary breccias that have filled large fissures in the peridotite body. These breccias are characterized by thin layers of graded ultramafic sandstones that include mainly cm-sized lherzolite clasts and some serpentinite clasts. These are type three breccias, only found in a few specific areas as is indicated on the map. Finally, type four breccias are found in the west of the Lherz body and are also regarded as sedimentary breccias that have filled fissures in the massive peridotite. They consist of angular clasts of serpentinite mostly and (poorly serpentinitized) lherzolites. The breccias are cut by carbonate veins.

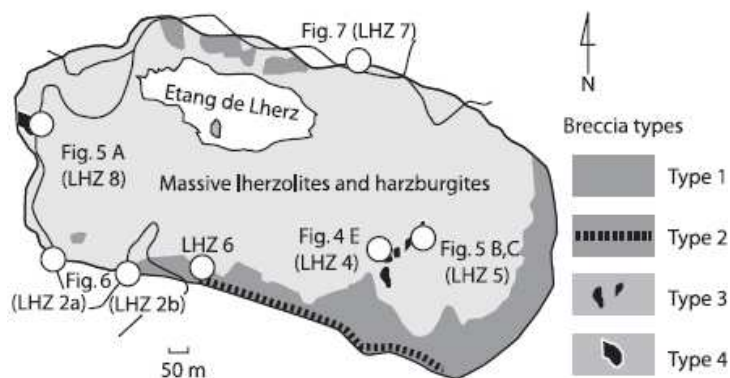


Figure 3-4: Location of main breccia types according to Lagabrielle and Bodinier (2008)

We have observed the following breccias:

1. Peridotite breccia with calcite matrix
 - Jigsaw structure, calcite veins
 - Mix of angular clasts, calcite veins and brown matrix
2. Peridotite breccia with peridotite matrix
3. Polymictic breccias with peridotite matrix
 - Peridotite breccia with isolated limestone clasts
 - Limestone breccia with peridotite matrix
 - Peridotite breccia with clasts of limestone and black shale

3.4.1 Peridotite breccia with calcite matrix

Peridotite breccias with a calcite matrix are abundantly present in the north and west of the Lherz body. At one locality in the east this type of breccia was also found. Two types can be distinguished:

- peridotite breccia consisting of angular clasts that are separated by calcite crystals and fit together like a jigsaw puzzle;
- peridotite breccia consisting of angular clasts that do not fit together, matrix consisting of calcite crystals and a brown material, spaces between clasts and geodes have formed. In some cases, the brown material contains a laminar structure.

Peridotite breccia with jigsaw structure

The first type of peridotite breccia was mainly found in the north of the Lherz body (PLZ09-1,2,3,4 and PLZ09-11 on geological map (Figure 3-3)). The peridotite is cut by serpentine and calcite veins. The calcite veins are far more dominant and cut the serpentine veins. They may also have formed in a (split) serpentine vein. The thickness of the calcite veins ranges from micro- to millimeters. The thicker veins may contain small particles of peridotite (μm to mm scale) and occasionally a small geode has formed. Besides these calcite veins, the matrix consists of a fine-grained brown material. The angular fragments of peridotite, that form the clasts in the breccia, vary in size from μm to dm scale. From the texture on individual clasts (serpentine veins or mylonitic streaks of spinel), which often continues on the other side of a calcite vein, it can be deduced that the clasts used to be joined together. This is confirmed by the similar shape of the rock on both sides of a calcite vein. The pieces fit together like a jigsaw puzzle and only small offsets (~ 0.5 cm) are visible. A loose block found in the west of the peridotite body (PLZ10-13), east of the road, shows clear off-sets (up to a few cm) in its two pyroxenite layers (Figure 3-5). On the eastern side of the Lherz body (PLZ10-6), a peridotite breccia was observed that does not contain straight calcite veins but rather an intense network of calcite veins has formed. As the clasts do not show any texture, it is difficult to determine whether this breccia has formed in situ or that the clasts were transported.



Figure 3-5: Brecciated serpentinized peridotite with calcite matrix, including many peridotite particles (left). Offset of ~ 1 cm in pyroxenite layers in block that is cut by calcite veins (right).

Peridotite breccia with geodes and brown matrix

In the western part of the Lherz body, along the west side of the road, an outcrop of tens of meters containing peridotite breccias was studied. The calcite matrix of these breccias is prominently visible (Figure 3-6). The breccias consist of poorly sorted angular clasts, composed of serpentinized lherzolites or serpentinites. Between clasts geodes (crystal-lined cavities) are commonly found. In some cases clasts fit together, while in other cases the relative position of clasts cannot be reconstructed. This breccia is mostly clast-supported, but not all pieces rest on each other. The matrix consists of a fine-grained brown material. The brown matrix may support the clasts or is enclosed by coarse calcite crystals (Figure 3-6 a). The matrix sometimes contains lherzolitic fragments (μ to mm scale) and in some cases shows clear lamination (Figure 3-6b and c).



(a)



(b)



(c)

Figure 3-6:

- (a) Angular peridotite fragments with calcite crystals between them. A light-brown fine-grained matrix fills up a hole between coarse calcite crystals.
- (b) Small peridotite particles in brown fine-grained matrix. Next to it a geode has formed.
- (c) Laminar structure of fine-grained brown material, surrounded by calcite crystals and between two peridotite fragments.

One sample, coming from a loose block next to the road (PLZ10-12) contains a layered structure of the brown matrix and small peridotite fragments (Figure 3-7 left). A large calcite vein cutting a peridotite fragment is cut by this brown laminated structure. Part of the very fine-grained brown layering is displaced by calcite crystals (Figure 3-7 right). At least two phases of calcite formation have occurred.

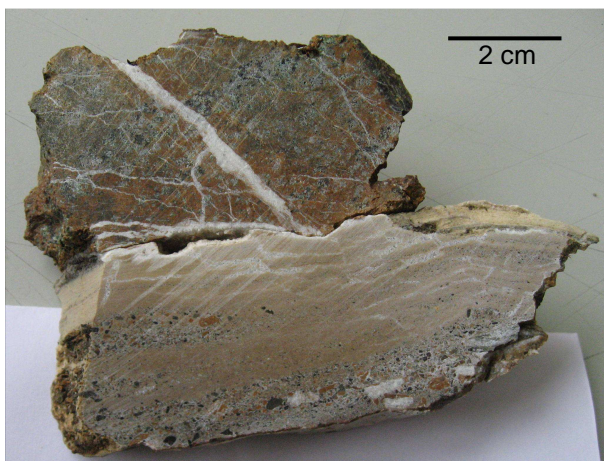


Figure 3-7: Calcite vein in peridotite is cut by sedimentary structure (left). Laminated structure is displaced by calcite crystals as indicated by the arrow (right). The pictures show opposite sides of the same sample.

3.4.2 Peridotite breccia with peridotite matrix

In the centre of the peridotite body and in the south-east, several outcrops consist of peridotite breccias with a (serpentinized) peridotite matrix (Figure 3-8). This type of breccia consists of rounded clasts which vary in size from mm- to cm-scale. The breccia appears heterogeneous as it contains lherzolitic clasts that are serpentinized to different extents and it may include serpentinite clasts. Most often these breccias are matrix-supported and occasionally clast-supported. The clasts are poorly sorted and no bedding is observed



Figure 3-8: Outcrop of peridotite breccia with peridotite matrix (left). Rim of calcite around clast within peridotite breccia (pointed to by pen).

Étang de Lherz (lake) is flanked by intact peridotite, fractured mantle rock and brecciated peridotite. Several samples were taken to investigate whether these different degrees in fracturing could represent different stages of fracturing caused by the same mechanism.



Figure 3-9: White homogeneous material within cracks in peridotite.

Southwest of Étang de Lherz, between cracks of the serpentinized peridotite a homogeneous white/light-green material was found (Figure 3-9). It filled cracks of a few cm wide. The material is hard and does not react with HCl. In this concentration it has only been found at this particular location.

3.4.3 Polymictic breccias with peridotite matrix

Peridotite breccia with isolated limestone clasts

The south-east of the Lherz body is characterized by peridotite breccia, consisting of rounded peridotite and serpentinite clasts and a matrix consisting of similar particles. Within the peridotite breccias limestone clasts are found. Usually they are small (<1 cm), but as Figure 3-10 shows, sometimes they are larger (dm scale). Regardless of the size, there is open space around the clasts which indicates that after they were incorporated into the peridotite breccia they have been partly dissolved.



Figure 3-10:
Large limestone clasts (dm-scale) in peridotite breccia. Space around limestone clasts indicates partial dissolution.

Limestone breccias with peridotite matrix

In the east of the Lherz body (~20 m from the peridotite-limestone contact), the amount of limestone clasts present in the peridotite breccia varies from single clasts (2% limestone; Figure 3-11a) floating in the matrix to a clast-supported monomictic limestone breccia (98% limestone, Figure 3-11b). A cross-section reveals that some calcite-clasts show a crystalline structure, implying that these are marbles (Figure 3-11c). A rim of calcite is visible around a large serpentinite clast.

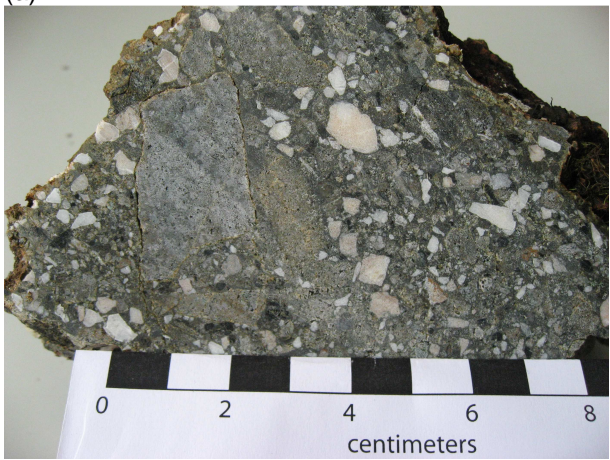
Figure 3-12 shows contacts of a peridotite breccia, including limestone clasts, with a large limestone boulder and of a limestone breccia with a peridotite breccia.



(a)



(b)



(c)

Figure 3-11:
 (a) Cm-scale limestone clasts scattered in peridotite breccias.
 (b) Clast-supported limestone breccia with brown peridotite matrix.
 (c) Some calcite-clasts show a coarse crystalline structure, implying that they are marbles. A rim of calcite is visible around a large serpentinite clast (left).



Figure 3-12:
 On the left: contact of peridotite breccia with a large limestone boulder (these may be loose blocks). Above: contact of limestone breccia and peridotite breccias.

Peridotite breccias with clasts of limestone and black shale

In the south of the Lherz body, polymictic breccias were observed, consisting of rounded clasts of peridotite, serpentinite, limestone and black shale (Figure 3-13, see geological map for location). The matrix consists of peridotite. The black shale has its origin elsewhere.



Figure 3-13:
Polymictic breccia with clasts of peridotite, serpentinite, limestone and black-shale, and a peridotite matrix.

3.5 Mineralogy and microstructures

Light microscopic and EMP analyses were performed on several thin sections to gain insight in the mineralogy and microstructures. Particular attention was paid to the presence of carbonates: calcite (CaCO_3), dolomite ($\text{CaMg}(\text{CO}_3)_2$) and magnesite (MgCO_3). Incorporation of Mg-holding carbonates, like dolomite and magnesite in the veins or matrix of a breccia could indicate that the mantle-body itself was chemically involved in the formation of veins. It might also indicate reaction-induced fracturing. Moreover, the different carbonates form under specific metamorphic conditions. Late fine dolomite grains were observed in the matrix of mylonitic peridotite rock by Palasse (2008). Minerals like sapphirine and kornerepine, which indicate extremely high temperatures at low pressures, were found at the contact of the mantle body and the surrounding limestones by Monchoux (1970), as is mentioned by Minnigh et al. (1980).

3.5.1 Peridotite breccia with calcite matrix

Peridotite breccia with jigsaw structure

Figure 3-14a shows a thin section of a peridotite breccia with calcite matrix. The peridotite is strongly serpentinized and contains several serpentine veins. One black serpentine vein is seen in the lower half of the thin section, that is cut by calcite veins of various thickness (EMP image in Figure 3-14b). Some Fe-oxides are present inside the calcite veins. Later stage cracks are visible, cutting the calcite veins. At a few locations calcite veins have formed along a serpentine vein (Figure 3-14c). The crack formed along the weak contact between serpentine and the calcite vein, and therefore after formation of the veins. In the upper half of the thin section a relatively large calcite vein with coarse grains cuts through a mix of intact peridotite, serpentine and calcite grains (Figure 3-14d). This shows there are at least two stages of carbonation. EMP analyses reveal that no other carbonates are present in the matrix besides calcite.

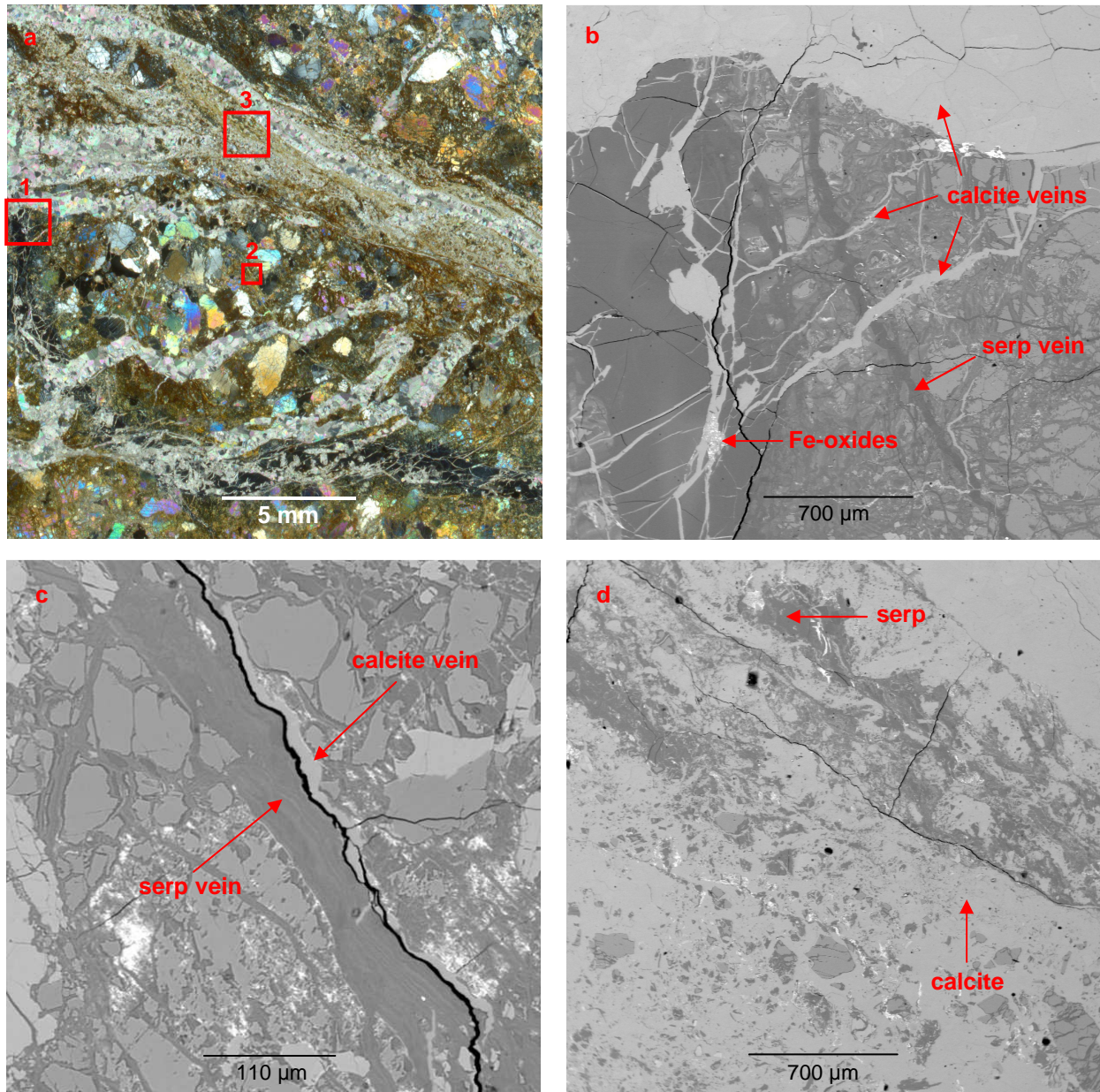


Figure 3-14: (a) Thin section of peridotite breccia with calcite veins. (b) EMP image showing small calcite veins that have cut serpentine veins. Some Fe-oxides are present within a calcite vein. (c) A calcite vein that has formed along a serpentine vein. The crack has formed later. (d) Matrix consisting of grains of peridotite, serpentine and calcite, which is cut by a thick calcite vein.

Peridotite breccia with geodes and brown matrix

The thin section in Figure 3-15a shows angular clasts of serpentinized peridotite in a matrix of calcite crystals and a light-brown material. The textures on the angular pieces show patterns in different directions. If they were rotated and aligned in the same direction, perhaps the pieces could fit together. However, from the orientations of serpentine veins and the way they are distributed, this is not obvious. The clasts are cemented together by very fine to coarse calcite crystals. Within patches of coarse calcite grains there are open spaces forming geodes (Figure 3-15b). The EMP image in Figure 3-15c shows that the fine-grained matrix consists of calcite and particles of a different mineral.

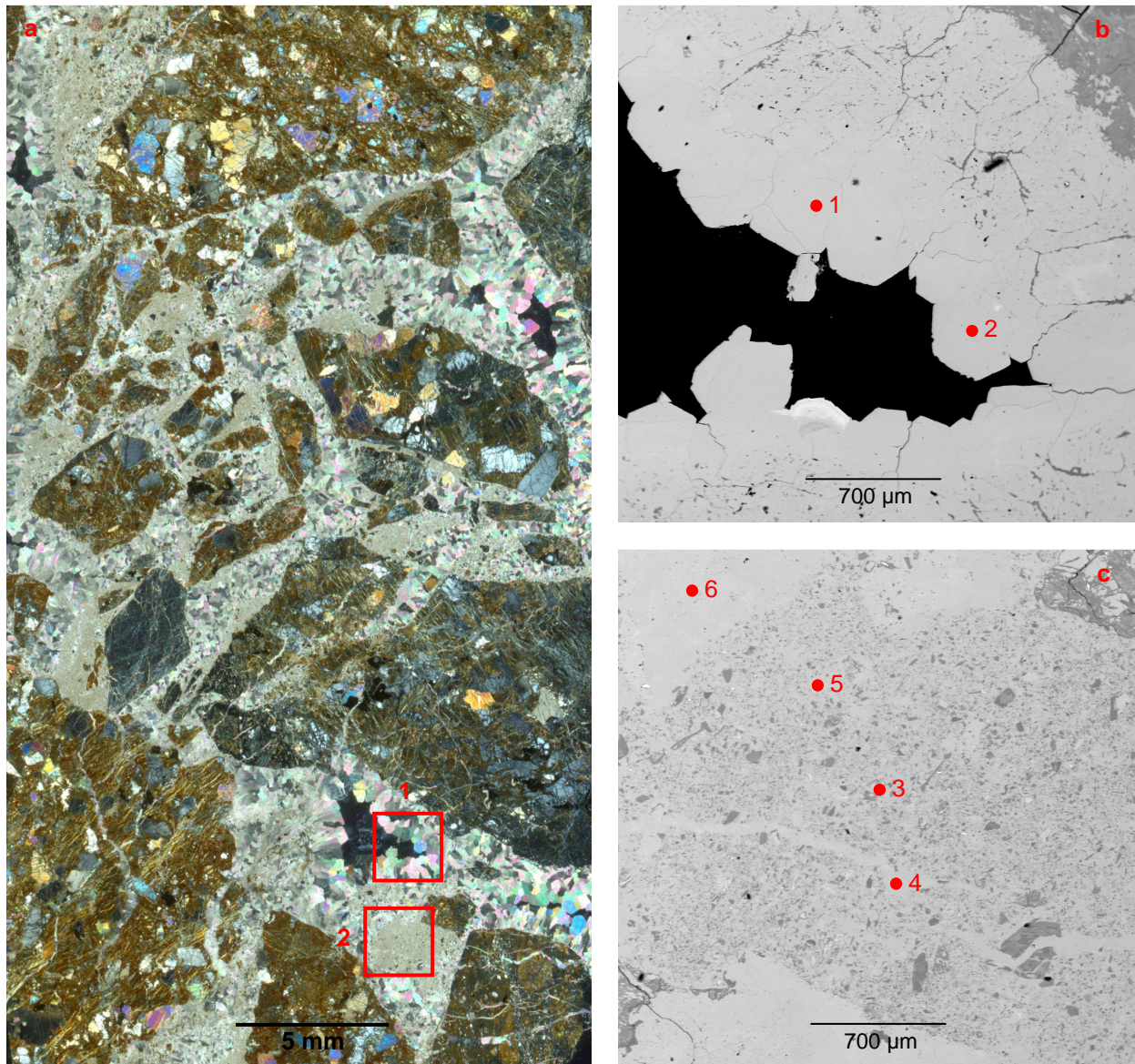


Figure 3-15: (a) Thin section of peridotite breccia with calcite matrix and geodes. (b) Coarse calcite crystals around geode (EMP image). (c) Fine-grained matrix consisting of calcite and μ -sized particles of another mineral (EMP image).

Compound (wt %)	Coarse calcite		Fine calcite			
	1	2	3	4	5	6
SiO ₂	0.000	0.001	0.068	0.035	0.000	0.113
Al ₂ O ₃	0.000	0.000	0.007	0.000	0.000	0.000
FeO	0.289	0.000	0.047	0.016	0.002	0.013
MnO	0.048	0.045	0.000	0.000	0.005	0.024
MgO	0.042	0.027	2.136	2.017	1.873	2.556
CaO	54.557	56.613	56.138	55.063	54.282	56.582
Na ₂ O	0.000	0.000	0.000	0.005	0.000	0.000
TiO ₂	0.006	0.020	0.011	0.012	0.000	0.000
Cr ₂ O ₃	0.000	0.003	0.011	0.000	0.000	0.010
NiO	0.000	0.000	0.000	0.000	0.020	0.000
Total	54.943	56.710	58.417	57.148	56.181	59.298

Table 3-1: Results of WDX measurements done in calcite matrix, given in mass percentages of the oxides. Locations are shown in Figure 3-15.

WDX analyses were done in both the coarse-grained matrix and the fine-grained matrix (Table 3-1). The data show a considerable higher Mg-content in the measurements done within the fine-grained matrix. Except from analysis 5, the Si-content is also slightly higher in the fine-grained matrix. In a later stage a calcite vein cut through this part of the matrix and the serpentinite clast next to it (right bottom in Figure 3-15a).

Sedimentary structure

In the west of the Lherz peridotite a loose block of peridotite breccia was found with a matrix consisting of calcite veins and brown material. Figure 3-7 shows pictures taken of a sample that was cut from this block. EMP analyses point out that the light brown matrix consists of very fine calcite crystals with μm -sized peridotite particles (Figure 3-16). The peridotite particles are embedded in the calcite matrix. The mix of light calcite crystals and brown peridotite particles causes the light brown colour. The EMP image shows that these particles are aligned forming layers.

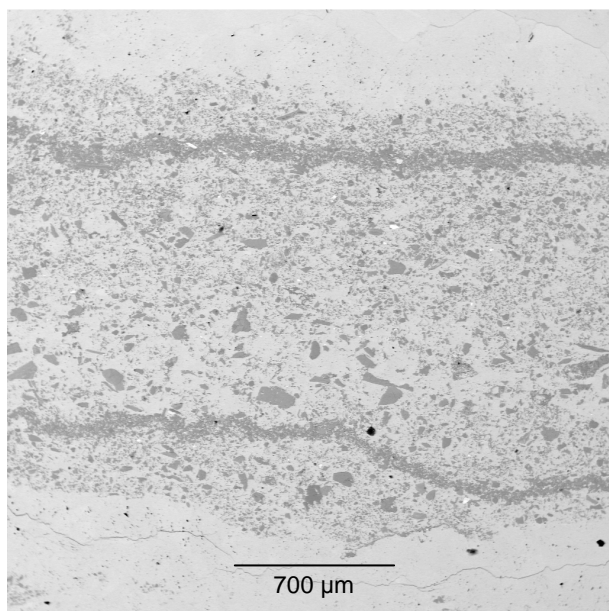


Figure 3-16:
Layers of μm -sized peridotite particles indicating sedimentary processes.

3.5.2 Internal and matrix-supported peridotite breccia

South-west of the lake, a sample was taken from an intact part of the peridotite. A number of very small fractures are present (Figure 3-17). Light microscopy analysis reveals that some parts of the peridotite are brecciated internally, referred to as internal peridotite breccia. Observations done using the light microscope and the EMP both show that there is a serpentine network throughout the peridotite and veins also consist of serpentine. No carbonates have been found.

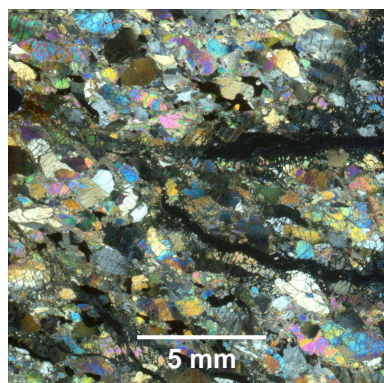


Figure 3-17:
Internal peridotite breccia with serpentine network. No carbonates are present.

Nearby, a sample was taken of a matrix-supported peridotite breccia. Pieces of peridotite, serpentinitized peridotite and single grains float in a brown matrix (Figure 3-18a). EMP analyses show

that the brown and dark brown matrix consist solely of serpentine. On the right side of the thin section a calcite vein is visible. Calcite crystals seem to have grown inside the serpentine network (Figure 3-18b-e). They do not appear within an olivine or clinopyroxene crystal. The calcite veins seem to have followed existing cracks in some cases. A patch of calcite crystals was also found within a serpentine vein in a peridotite clast.

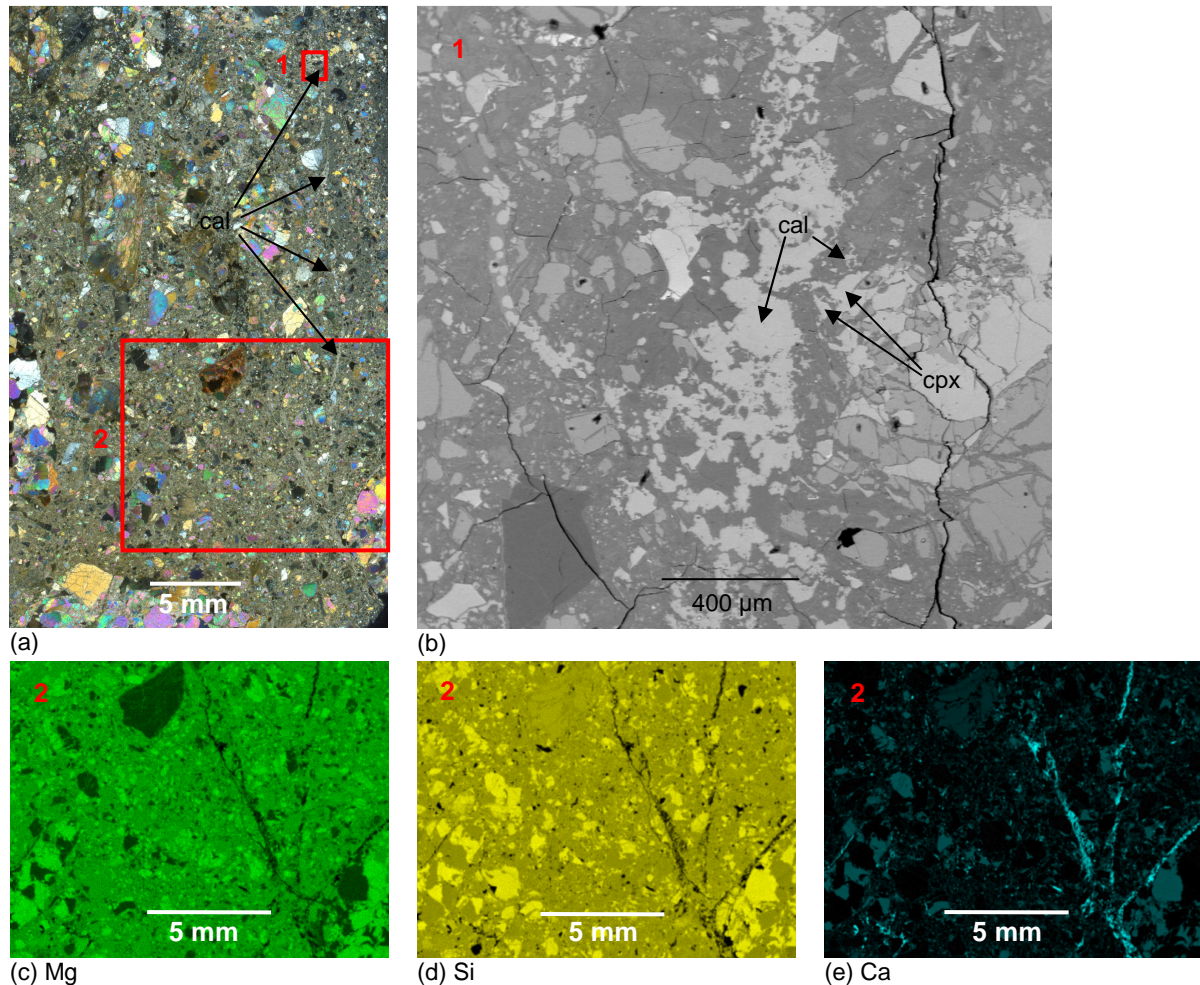


Figure 3-18: (a) Thin section of (serpentinized) peridotite clasts in serpentine matrix. (b) Intergrowth of calcite crystals in matrix, forming a very thin vein. (c,d,e) Mg, Si and Ca contents reveal a calcite vein.

3.5.3 White homogeneous material

On the south-west side of the lake, a white to grey, sometimes greenish, homogeneous material was found between the peridotite (PLZ10-10). Several types of analyses were done to determine the composition of the material.

Micro X-ray fluorescence (μ -XRF)

Using μ -XRF the elemental composition of the material was derived. Maps were made for each element (Figure 3-19). It should be noted that the intensity of the colours cannot be compared one to one for the different elements. A measurement was performed yielding the following values based on 4 oxygen atoms:

Element	Si	Al	Fe	Mn	Mg	Ca	Na	Ti	Cr	K	Total
No. of cations	1.009	0.011	0.017	0.001	1.928	0.000	0.053	0.001	0.000	0.000	3.020

Measurements using μ -XRF are known to be less accurate than using the EMP. The ratio Mg:Si of nearly 2:1 is indicative for olivine. The extraordinary low content of iron is remarkable. This means that the substance would be almost pure forsterite.

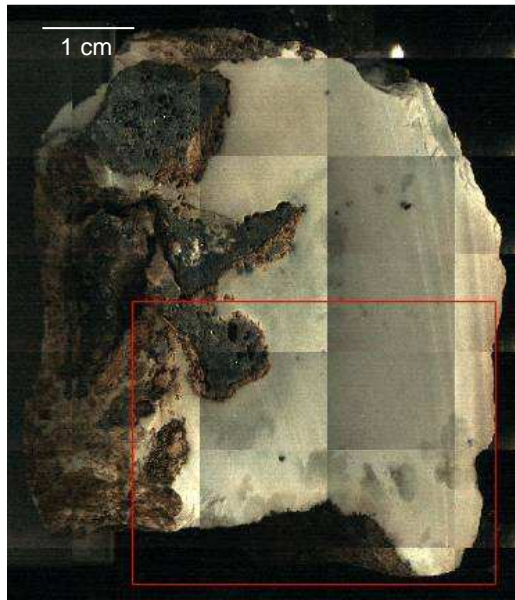
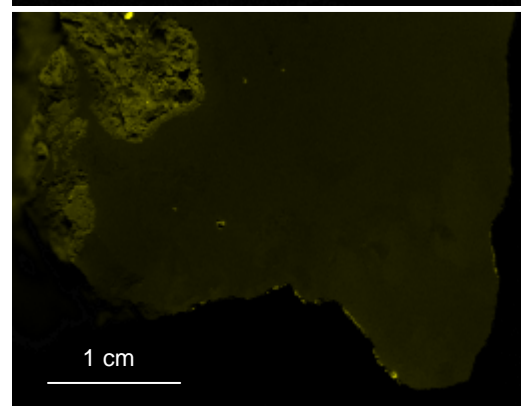
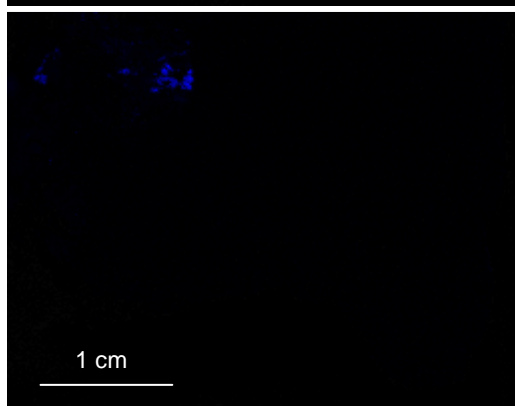
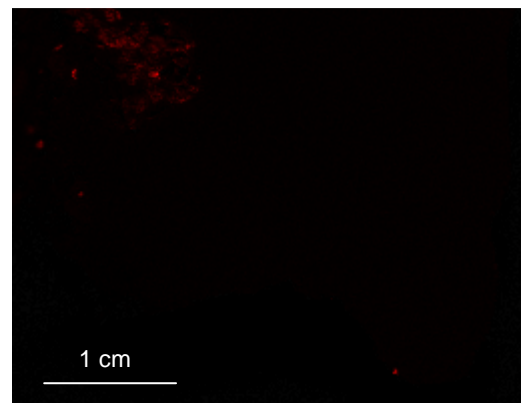
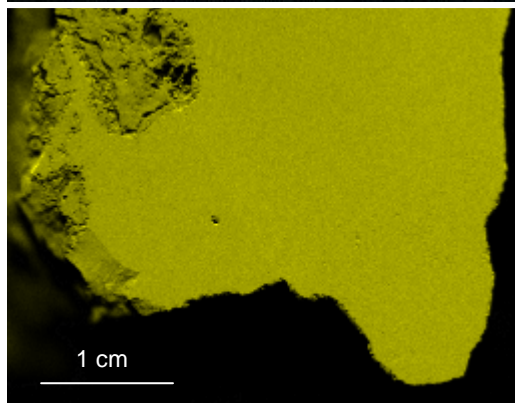
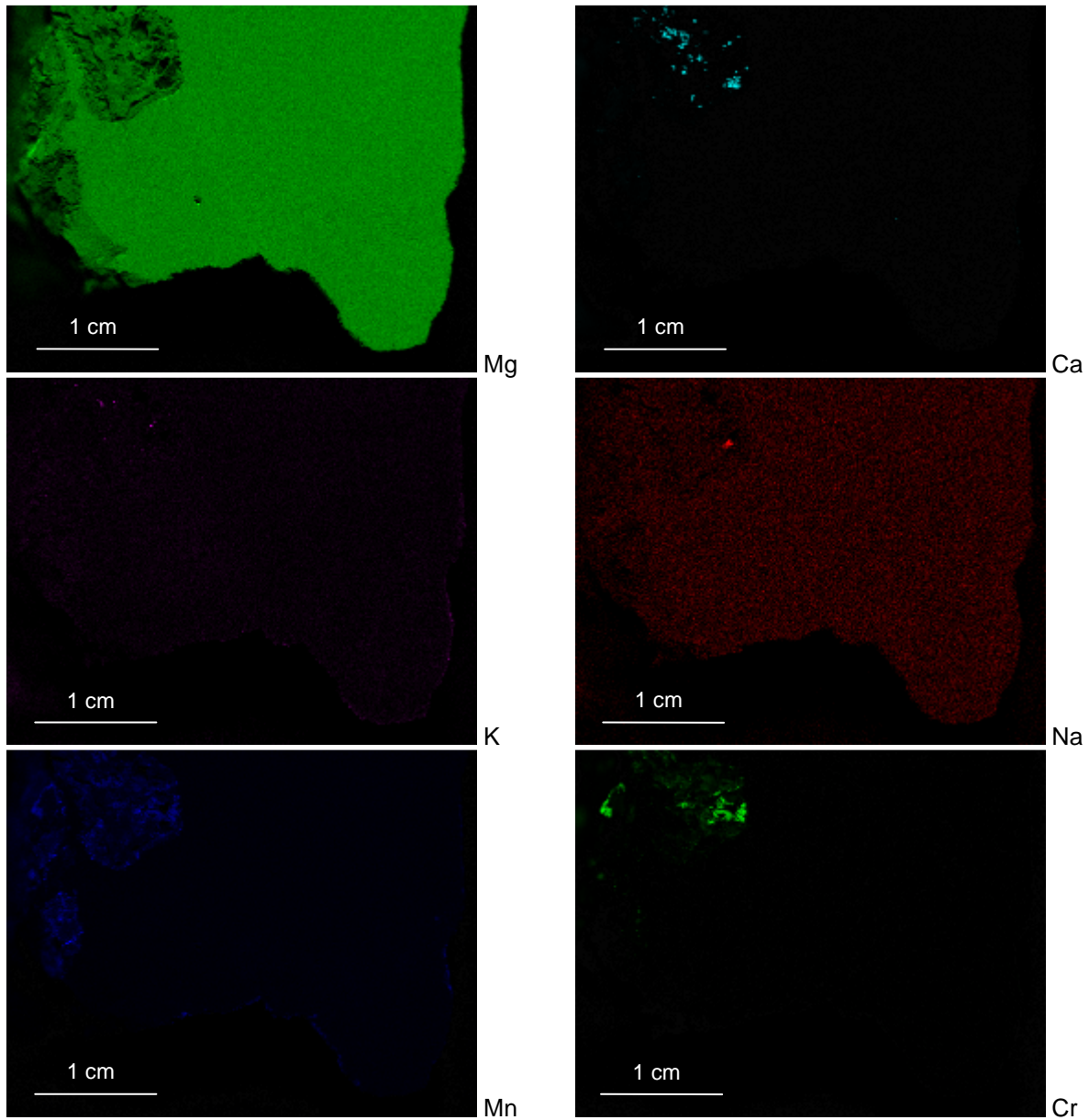


Figure 3-19:

Left: sample of homogeneous material with surrounding peridotite. The substance seems to have filled small holes. The red box indicates the mapping area.

Below and on the next page: maps for each element.





Light microscopy

Observations done using the light microscope reveal that the homogeneous material looks pale brown in plane polarized light (PPL). The relief is low and crystals are difficult to distinguish. The substance has a low birefringence. A sort of tweed or knitting pattern is observed when the thin section is viewed in cross polarized light (XPL) and with a gypsum plate (Figure 3-20a, b). Two orientations, perpendicular to each other, are visible. None of these characteristics is typical for olivine. Olivine is transparent in PPL, has a moderate to high relief and a high birefringence. Moreover, olivine crystals are equant. The observed characteristics match better with the chemically (almost) similar mineral serpentine. Near the contact with the peridotite small circles with a radial pattern were observed (Figure 3-20c, d).

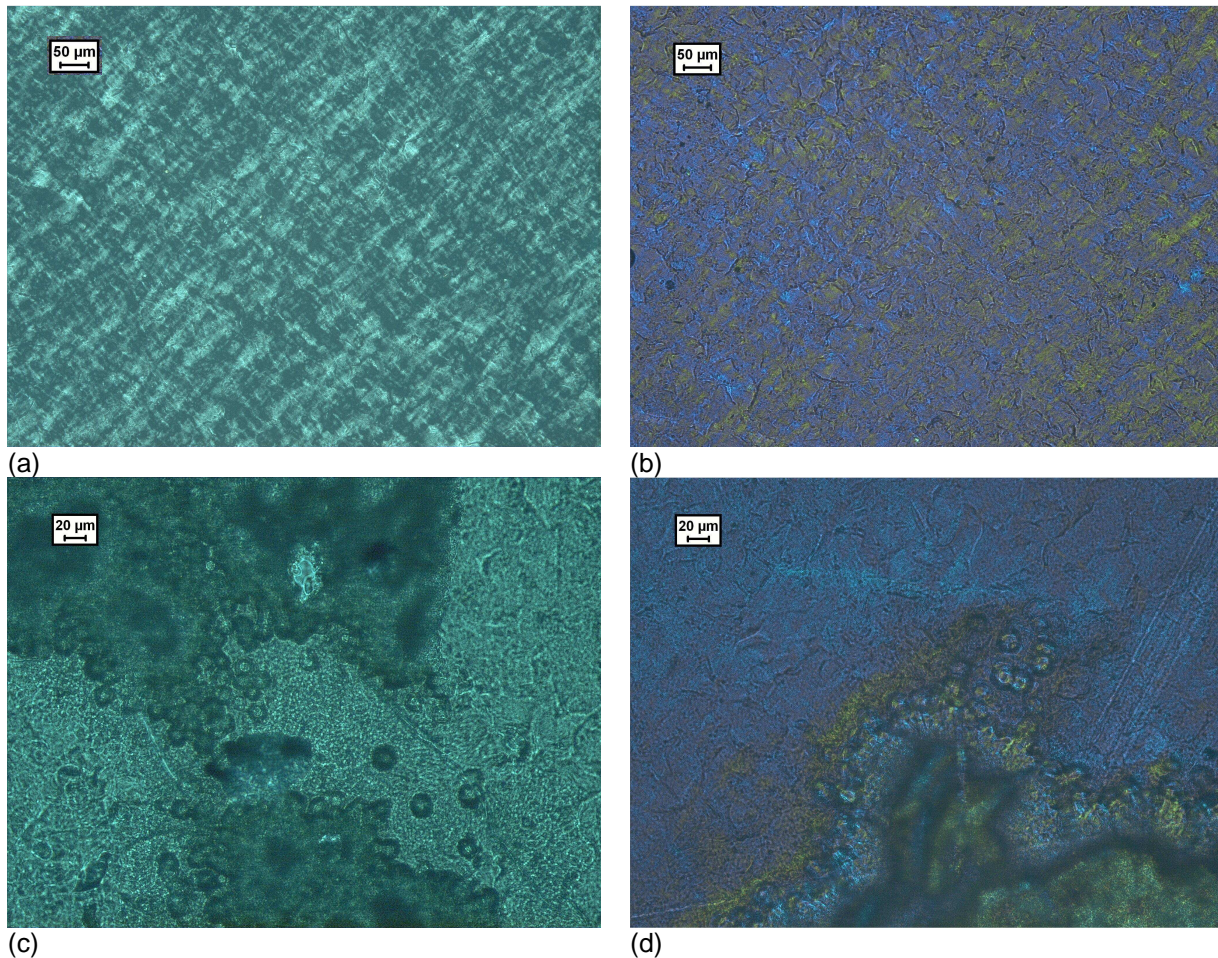


Figure 3-20: (a) and (b) Tweed pattern in XPL and using gypsum plate. (c) Circular shapes at edge of homogeneous material and peridotite in PPL. (d) Using a gypsum plate the circles show quadrants in blue and orange on opposite sides.

EMP

EMP analyses were performed to get more precise results on the chemical contents of the homogeneous material. Table 3-2 shows the results of a few measurements in the homogeneous matrix (analyses 2,6 and 12) and two measurements in the peridotite, near the contact with the matrix (analyses 4 and 7). The chemical contents of this material and the cation ratios that have been calculated ((Mg,Fe):Si is close to 3:2) show that the mineral is most likely serpentine. A total of ~85%, much lower than 100%, indicates that either water evaporated or a gas like CO₂ escaped during the measurements. It fits with serpentine being a water-bearing mineral. These results, however, do not correspond with the results from the μ-XRF.

Compound (wt %)	No. of cations (based on 7 oxygen atoms)									
	2	4	6	7	12					
SiO ₂	42.800	42.808	42.871	42.888	42.909	2.039	2.049	2.043	2.061	2.054
TiO ₂	0.000	0.000	0.000	0.000	0.000	0.000	0.000	0.000	0.000	0.000
Al ₂ O ₃	0.000	0.000	0.047	0.443	0.000	0.000	0.000	0.003	0.025	0.000
FeO	2.229	1.266	2.159	6.055	1.994	0.089	0.051	0.086	0.243	0.080
MgO	39.696	39.890	39.495	35.957	39.314	2.819	2.847	2.806	2.575	2.805
CaO	0.000	0.000	0.000	0.204	0.013	0.000	0.000	0.000	0.011	0.001
K ₂ O	0.004	0.000	0.000	0.000	0.000	0.000	0.000	0.000	0.000	0.000
Na ₂ O	0.099	0.017	0.171	0.029	0.000	0.009	0.002	0.016	0.003	0.000
MnO	0.159	0.085	0.022	0.260	0.017	0.006	0.003	0.001	0.011	0.001
Cr ₂ O ₃	0.040	0.000	0.141	0.000	0.120	0.002	0.000	0.005	0.000	0.005
Total	85.028	84.068	84.907	85.837	84.367	4.965	4.952	4.961	4.928	4.944

Table 3-2: EDX analyses of homogeneous material and peridotite edge. Analyses 2,6 and 12 were performed on homogeneous matrix. Analyses 4 and 7 correspond with the peridotite edge.

Regardless whether the mineral is serpentine or olivine, the low Fe-content is remarkable. In a system like this, the ratio Mg:Fe is usually about 9:1. Iron is found in concentrated patches of Fe-oxides in the matrix (Figure 3-21).

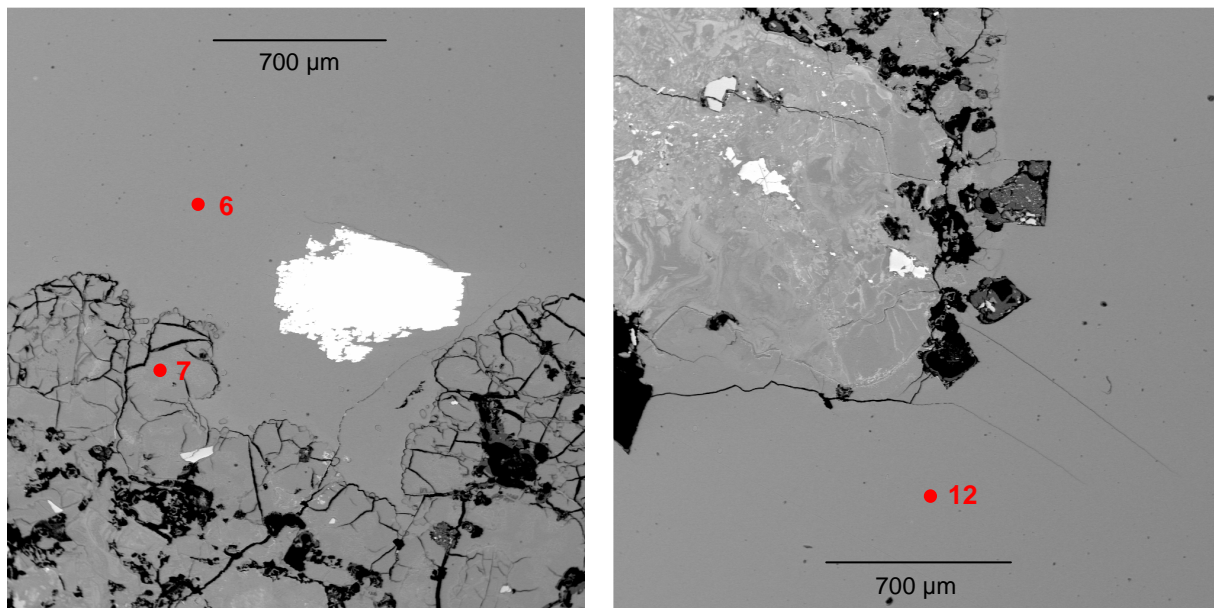


Figure 3-21: Locations of EMP measurements. The back-scattered images of the homogeneous material show a consistent chemical composition throughout the matrix. The white mineral is an Fe-oxide.

Two additional techniques were used to determine the exact mineralogy of this substance. EBSD was performed to see if crystal lattice patterns could be recognized. In addition, an XRD-analysis was done.

Electron Back-Scattered Diffraction (EBSD)

Figure 3-22 shows back-scattered Scanning Electron Microscope (SEM) images of the homogeneous matrix and the small circles near the contact with the peridotite. The matrix does not show any texture, only some polishing scratches are visible. The circles show a clear edge, but the inside looks homogeneous as well. No patterns were found in the matrix. On the edges of the circles only a few patterns were recognized.

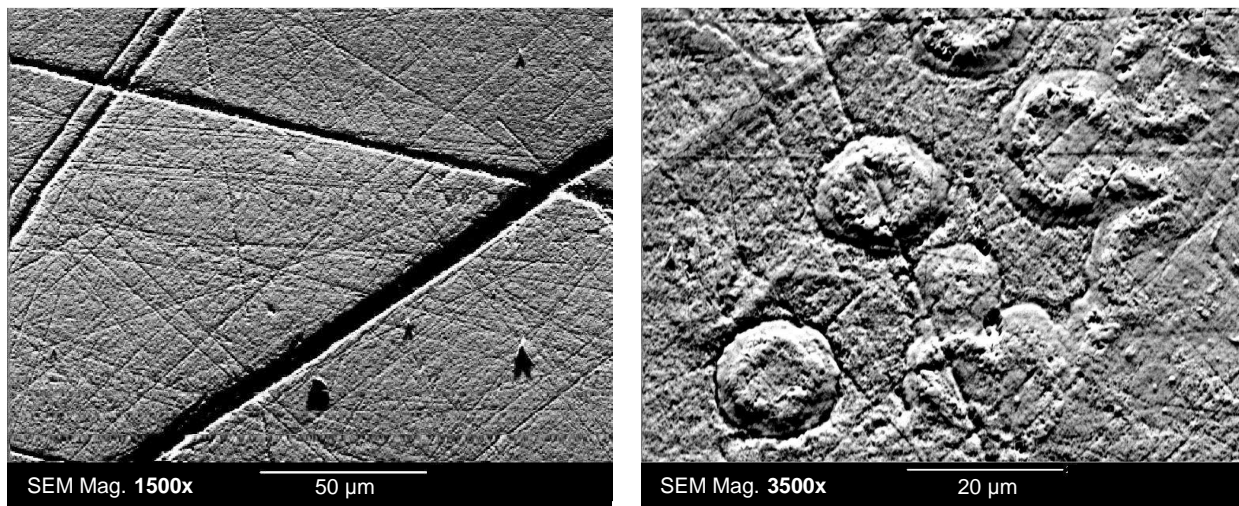


Figure 3-22: Back-scattered SEM images of homogeneous matrix (left) and circles near the edge of the peridotite (right).

Several hundreds of measurements were done on and around the circles. Only at very specific locations, patterns were found that were clear enough to index (Figure 3-23a). Around these locations extra measurements were done, which only resulted in two more patterns (at locations 5 and 91).

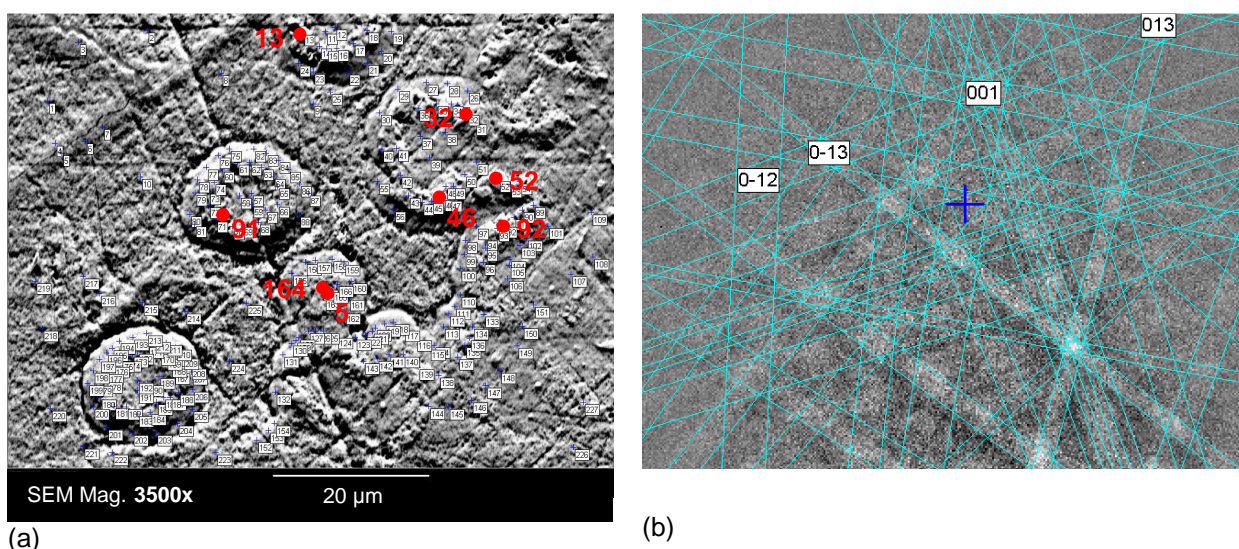


Figure 3-23: (a) Locations of measurements; red dots indicate locations of indexed patterns. (b) Clear pattern at location 164. Indexed as antigorite SG Pm $m=1$ (blue).

Table 3-3 contains information on the patterns that were indexed. The clearest pattern was obtained at location 164 (Figure 3-23b). Like the other patterns, it is indexed as antigorite. Patterns of other locations are included in Appendix E. The patterns at locations 13 and 52 could also be indexed as forsterite with MAD values of 1.1 and 0.9 respectively. However, to fit with the forsterite pattern not all visible lines were included. Antigorite fits better with the observed patterns.

Image	Location	Index colour	Manually	MAD	Euler angles		
circles	13	purple	x	0.7	59	137	204
	32	purple	x	0.6	12	23	168
	46	purple	x	0.9	29	97	108
	52	blue	x	1.1	180	86	89
	92	blue	x	0.9	172	125	2
	164	blue	x	0.6	8	15	282
circle 3	91	blue	x	0.1	127	68	196
circle 4	5	purple	x	0.9	153	9	263

Table 3-3: Index colour: purple = Antigorite SG C2/m m; blue = Antigorite SG Pm m=1 (antigorite files after D. Mainprice, Université Montpellier).

X-ray diffraction (XRD)

Results of the XRD-analysis are shown in Figure 3-24. The black line represents the measurement of the homogeneous material. The red line shows the results corrected for background scatter. A clear pattern with distinct peaks is observed. The XRD results are compared to known patterns of chemically similar minerals (purple and blue). The purple plot fits very well with the measured peaks. It represents a type of serpentine with chemical formula $Mg_{2.83}Fe_{0.08}Fe_{0.03}Si_{1.97}Al_{0.03}O_{4.90}(OH)_4$, related to the polymorph clinochrysotile. The purple plot does not explain the highest peak (left). Another mineral phase may account for this peak, most likely another serpentine polymorph: lizardite (represented by the blue plot) or antigorite. The plots of neither of these polymorphs, however, can explain the peak fully.

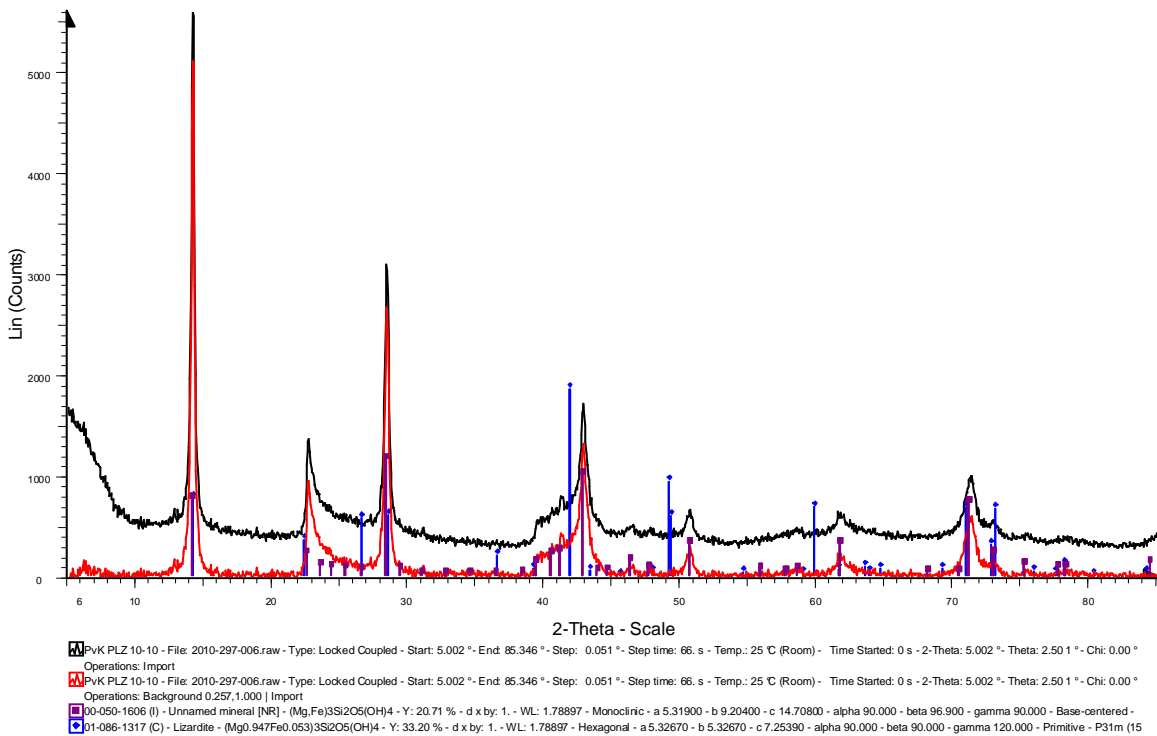


Figure 3-24: XRD results on powdered homogeneous material. Original results are represented by the black line. The red line represents the measured results corrected for background scatter. The purple and blue patterns represent clinochrysotile and lizardite respectively.

3.6 Discussion

3.6.1 Geological implications of classified breccias

Development of peridotite breccia with calcite matrix: phase 1

The northwest of the Lherz peridotite is characterized by an abundance of calcite veins. Two different types of peridotite breccias with a calcite matrix were distinguished: jigsaw breccia and breccia where the clasts only partially fit together. These breccias have a number of characteristics in common. Both have angular clasts. The jig-saw structure in the first type of the breccias can be interpreted as an in-situ breccia. Cross-cutting relations show that the process of serpentinization was taking place before carbonation. Only slight offsets are visible, but the clasts on a whole have barely been moved (cm-scale). The angular shapes have been preserved. The breccia formation that consists of a mix of angular clasts apparently has undergone more movement. We refer to this as a 'disturbed' breccia. However, since the angularity has been preserved, here too movement has played a limited role. The clasts may have been moved and rotated on cm-scale. A gradual transition between these types of breccia was observed.

Two main mechanisms could cause the formation of in situ breccia: fracturing due to tectonics and reaction-induced fracturing. Both mechanisms could be accompanied by hydrofracturing. Fracturing due to tectonics is the result of external stress, forming a fault breccia. Reaction-induced fracturing results from internal stress, caused by expansion due to chemical processes. Hydrofracturing is caused by internal hydraulic overpressures.

Tectonic origin

The Lherz body is part of a complex geologic history. Coming from deep (a few hundreds of kilometers) in the earth, it now rests on top of a mountain. In theory, the mantle body could represent an intrusion, having intruded as a ductile body. The large-scale brecciation however, implies that the peridotite body has undergone mechanical processes as brittle rock. It has experienced at least three phases of deformation:

1. When it was exhumed to the surface;
2. When it was detached from the rest of the mantle;
3. When it was involved the orogeny of the Pyrenees and was uplifted to its present location.

Either one of these three events may have put the peridotite body under great external stress. Therefore, a cataclastic (or tectonic) breccia is very plausible.

Moreover, fluids may have played a role in weakening the rock. Higher pore fluid pressure causes tensile stress, which reduces the required amount of external stress needed for fracturing. Once a crack has formed, there is an immediate pressure drop. Fluids from the adjacent rock enter the crack due to a pressure gradient. The fluids may contain minerals dissolved from the host rock, that precipitate in the crack due to supersaturation. This causes a decrease in available space and an increase in fluid pressure, resulting in the propagation of the fracture (Etheridge et al., 1984).

Reaction-induced

Neither magnesite nor dolomite has been found in the samples. Therefore reaction-induced fracturing due to Mg-carbonation has not taken place. On the other hand, calcite is largely present inside large veins and small cracks. The origin of calcium could be the peridotite rock, as Kelemen and Matter (2008) suggest for the formation of the abundant calcite veins in the Semail ophiolite in Oman. Serpentinization of clinopyroxenes would provide calcium-rich fluids that, under certain circumstances, precipitate as calcium-carbonates. Lherzolite, that makes up most of the Lherz body, contains approximately 15% clinopyroxenes in mass percentage (Le Roux et al., 2007). The total amount of CaO in the body is only 3% (mass percentage) and cannot account for the abundance of calcite veins present. In addition, lherzolite contains much more magnesium, 36-40% of MgO (mass percentage). One would expect to find even more magnesite and dolomite than calcite. Kelemen and Matter suggest that Ca-carbonation occurs after Mg-carbonation and the formation of dolomite. It is therefore likely that peridotite has chemically not taken part in the formation of calcite veins in the Lherz body. Moreover calcite veins are only found near the edges of the peridotite body. If peridotite was chemically involved, calcite veins are expected to be present throughout the Lherz body.

Another origin for the calcium could be the Mesozoic limestones in which the Lherz body is now embedded. Water may have transported Ca^+ and CO_3^- ions dissolved from the limestones into small cracks in the peridotite. Precipitation of calcite occurred and formed calcite veins. Possibly the growth of calcite crystals can propagate small (cm-scale) fractures. Small off-sets have been observed that seem to be the result of the growth of calcite crystals. Some small fractures may have formed after initial brecciation had already taken place. Reaction-induced fracturing, however, does not explain rotation of clasts and the formation of geodes. For both phenomena space is required. Perhaps the growth of calcite crystals have propagated small fractures, but fracturing to the extent that was observed is not likely the result of merely calcite crystal growth. Reaction-induced fracturing is therefore not the origin of the abundant peridotite breccias.

Back-scattered images show that serpentine veins are cut by calcite veins (Figure 3-14b). Occasionally fractures or calcite veins have developed along serpentine veins. Most likely this was the weakest part in the rock and most likely to fracture. These observations indicate that there is no relation between serpentinization and calcite veining.

Development of peridotite breccia with calcite matrix: phase 2

Sedimentary structures have been found in the disturbed breccia. They fill in spaces between clasts, indicating sedimentary deposition has occurred after the positioning of the clasts. From cross-sections it cannot conclusively be determined whether the breccia is fully clast-supported or locally matrix-supported. Apart from the lamination structures in Figure 3-6c and Figure 3-7 (loose block), no other geopetal structures were observed that could indicate the orientation of the breccia at the time of deposition.

The brown matrix between the clasts consists of calcite and peridotite particles. Peridotite particles are often observed 'floating' in the fine-grained calcite matrix (Figure 3-16). At the time of deposition, they must have been supported by calcite grains. This means that calcite most likely entered the breccia system both in solution and as small particles. The calcite particles may represent detrital material from the Mesozoic limestones. As no pore spaces are observed, calcite has most likely precipitated inside pores cementing the particles, after the limestone and peridotite particles were deposited.

The slight Mg-content of the calcite in the fine-grained matrix in Figure 3-15 can be interpreted in several ways. Either the measurements are 'contaminated' by the other particles, which are presumably peridotite particles. Analysis 6 however, was measured within a single calcite grain, yet also some magnesium was measured. Another possibility is that impurities within the calcite crystals contain magnesium. This indicates a higher temperature during crystallization.

Some spaces between clasts were not filled with either calcite or a mix of calcite and peridotite. Large calcite crystals cover the surface of the clasts forming so-called geodes. The availability of space resulted in the formation of large crystals. Moreover, they had time to grow this large. Some geodes are filled with a mix of fine-grained calcite and peridotite. Therefore deposition also occurred after the formation of geodes.

In the in-situ breccia no clear sedimentary structures are found, but some small geodes and a mix of calcite crystals and peridotite particles is observed to a lesser extent.

Cross-cutting relationships show that several stages of carbonation have taken place, the latest of which formed pure calcite veins. They are characterized by their bright white appearance and do not contain any peridotite particles. This may be a result of fluid circulation after deposition. The different generations of calcite veining may be distinguished by a difference in chemical contents.

Development peridotite breccia with peridotite matrix

The peridotite breccia with peridotite matrix, found in the centre and south-east of the Lherz body, is made up of peridotite pieces of various sizes (ranging from cm-size clasts to grain-size particles). The breccia has a relatively large amount of matrix. The clasts in this type of peridotite are rounded and have therefore experienced some movement after formation. The particles of peridotite that make up the matrix, is presumably residual material of the rounded clasts. These observations match: we find much more fine material together with rounded clasts than with angular clasts (in the previously

discussed breccia type). It also suggests that the material within one type of breccia has a common origin.

The peridotite rock may originally have been brecciated due to tectonics. Because no veins are present, reaction-induced fracturing can be excluded. As mentioned earlier, large-scale brecciation is not likely the result of expansion due to chemical processes. Water must have played a role in rounding the clasts. The netto transport distance that is involved does not have to be far. The limited transport distance is also confirmed by the many peridotite clasts which have their provenance in the Lherz peridotite itself. There is a very gradual transition in size of the clasts in these peridotite breccias. It is therefore debatable whether they are matrix- or clast-supported. As the clasts are poorly sorted and there is no internal structure, the sedimentary process involved is likely to be a debris flow. However, no large clasts (larger than one or two decimetres) are included, so it must have been a rather small-scale event in a moderately low energy environment. Further studies should reveal the exact circumstances under which deposition took place. We regard this breccia as a sedimentary breccia. Apparently, almost no calcium-carbonate was involved in this process, as the matrix consists mainly of serpentine and individual peridotite grains. Only a few very thin calcite veins (μ -scale) are present. Even in the middle of the Lherz body some influences of carbonation are noticeable.

The internally brecciated peridotite could represent an earlier stage before carbonation occurred in terms of brecciation and the formation of (minor) veins, but during these processes no carbonation is involved. This would imply that carbonation was not reaction-induced. In this internal breccias no carbonation has been going on at all. Therefore, it does not seem to represent a former stage of brecciation before carbonation. External stress causing very small-scale fault breccia is the most likely mechanism.

Development of polymictic peridotite breccia

The incorporation of exotic clasts in a peridotite breccia clearly implies transportation and a sedimentary origin. Moreover, all clasts in these breccias (peridotite, serpentinite, limestone and black-shale) are rounded and have thus undergone some transport. The peridotite and serpentinite clasts are likely to come from the Lherz body itself. They may have formed through tectonic brecciation. Movement of the fragments has probably resulted in the rounded shape of the clasts and the large amount of finer material which makes up the matrix. The peridotite sediments must have been reworked so that limestone clasts could be incorporated. The presence of calcite in the matrix of these breccias is not obvious, although some was found at the rim of clasts. If water has transported limestone clasts into a zone of loose peridotite fragments, one would expect the water to be carbonate-rich. Perhaps gravity sliding has played a role here, which resulted in the incorporation of limestone clasts but not the infiltration of calcium carbonate-rich water. Again, as the clasts are poorly sorted and no sedimentary structures are observed, the sedimentary process involved is likely to be a debris flow. In the case that gravity has played a role, the rock may be regarded as an olistostrome. Lithification has occurred and rules out the possibility of recent incorporation of the limestone clasts.

In the east both limestone-bearing peridotite breccias and a limestone breccia was found, not far from the contact of the peridotite body with the surrounding limestones. The contact of a limestone breccia with a limestone-bearing peridotite breccia shown in

Figure 3-12 shows a very abrupt transition. It has the appearance of a small channel. Towards the center of the peridotite body, transport of limestones has still taken place, as isolated clasts show. The large limestone clasts in Figure 3-10 were a relatively heavy transport for which gravity sliding may have played a role. After deposition one of them was broken and subsequently surrounded by peridotite sediments.

In the south, even clasts of black shale were incorporated into the breccia. They probably come from the Lias formation (Early Jurassic). Outcrops of this formation can be found within two kilometres south and west of the Lherz body.

Quite obviously, this type of breccia can be regarded as a sedimentary breccia, although the peridotite was originally fragmented by a different mechanism.

Sedimentary processes

Regarding the breccias that have been discussed above, sedimentary processes have played a major role in their formation. For effective movement of clasts, as is the case here, water is the main means of transport. Further investigation should investigate if sedimentary structures in the field (bedding, grading, channels, etc.) can support these findings. Clear examples of bedding or lamination in the neighbourhood of Lherz have been found by previous authors. Choukroune (1980) showed a clear example of sedimentary stratified breccia and of slumping in fine-grained material near Lherz.

Calcium carbonate

It is remarkable that calcium carbonate-influences can be found throughout the Lherz body, but in different forms, namely: calcite veins, calcite sediment and limestone clasts. Limestones do not occur together with calcite veins, although they probably have the same origin (the Mesozoic limestones in which the peridotite is now embedded). Only one outcrop with brecciated peridotite and calcite veins was observed in the neighbourhood of limestone-bearing breccias in the east. Moreover, it appears that no calcite is present in the matrix of the breccias that include limestone. This can be studied in more detail. Between the outcrops where limestones are found (in the south-east) and the sites where calcite veins are found (in the north-east) there is a part where there is very little calcium carbonate. Although calcite veins have formed by precipitation from fluids, while limestone clasts entered the system mechanically, they have in common that water is the most probable means of transport. Less limestones are found farther into the peridotite body. This is a gradual transition. From the middle of the body, where peridotite breccia with rounded clasts have been found together with intact peridotite, to the north-east, where abundant calcite veins are found between angular clasts of peridotite, the transition appears to be more abrupt. Hydrothermal fluid circulation may have provided suitable metamorphic conditions for the growth of calcite crystals at this particular location.

3.6.2 Serpentine or white olivine?

A Mg, Si-bearing homogeneous material was found at Étang de Lherz. The results of the different analyses on this material are summarized below:

- The XRF-analysis shows a Mg-Si ratio of 2:1, typical for olivine. The very low Fe-content indicates forsterite.
- The optical properties such as relief (low) and polarization colour (pale brown in PPL and grey in XPL) indicate serpentine. This is supported by the tweed pattern observed in XPL (rather an elongated structure as opposed to equant olivine crystals).
- EMP analyses show Mg-Si ratios of 3:2, which indicate serpentine. The total of 85% fits with a hydrous mineral.
- The scarce EBSD patterns indicate the presence of antigorite crystals. These are found on the edges of μ -scale spheres along the boundary of the homogeneous material and peridotite. No patterns have been found for the homogeneous phase.
- The XRD-results indicate serpentine: clinochrysotile and possibly lizardite or antigorite.

The results of the analyses are in favour of serpentine. The presence of this mineral is consistent with the retrograde path the Lherz body has undergone. Only the large amount of this homogeneous serpentine, found at one specific location, and the low Fe-percentage are unusual.

The XRF-analysis showed results that are not consistent with the other results. This can be explained by the nature of this method, i.e. results depend on boundary conditions set by defining constituent elements in advance. Moreover, the accuracy of calibration may not be sufficient to distinguish these chemically similar minerals.

Although the homogeneous material looks amorphous, the tweed pattern observed under the light microscope (XPL) and the distinct pattern from the XRD analysis (no amorphous bulge) show that it does have a crystal structure. As single grains could not be distinguished under the light microscope and SEM, and EBSD patterns were not measured within the matrix, the crystals are presumably very small. This indicates there was little time and space to grow. Serpentine may have precipitated from a very saturated fluid in a short period of time.

The micro-spheres along the boundary of the serpentine and peridotite may represent small gas bubbles. These spheres could provide more space for crystals to grow. This could explain why EBSD patterns were specifically found on the edge of these spheres.

3.6.3 General model for breccia development

Phase 1: Tectonic brecciation

The breccias all have in common that after tectonic fracturing, sedimentary reworking has occurred to a certain extent. This implies that tectonic brecciation has taken place before the peridotite rocks were involved in a sedimentary setting. Exhumation of the mantle rock must have occurred before and is therefore the likely mechanism that caused cataclastic brecciation. For exhumation to occur, space has to be created. The formation of a basin due to extension could explain the sedimentary setting. There is no evidence that the rocks have experienced brecciation after the sedimentary reworking. The Lherz body may have been protected by the surrounding Mesozoic limestones during the contractional phases of the Pyrenean orogeny. It may have been located on top of Mesozoic limestones in the sedimentary setting. Alternatively, the Lherz peridotite may have been thrust over the limestone formation during the initial stages of the Pyrenean orogeny.

Phase 2: Sedimentary reworking

The characteristics of the different breccias can be related to the energy that is associated with their formation. Roughly, from the north-west to the south-east a sequence is observed: from large angular clasts to smaller rounded clasts (an increase in movement) and from solely peridotite clasts to the incorporation of sporadic exotic clasts to numerous exotic clasts (an increase in transport). One exception on the abovementioned sequence is the presence of an (apparently) in situ peridotite breccia with angular clasts and calcite veins found in the east of the Lherz body. The sequence is described below and summarized in Table 3-4.

- Peridotite jigsaw structure: barely any movement, so either there was not much water or the rocks were trapped somehow. There was a large calcite supply however, so possibly these rocks were stuck in a fissure;
- Disturbed peridotite breccia: little movement, more space but possibly also trapped, a large calcite supply;
- Peridotite breccia with rounded clasts: free movement, transport over small distances;
- Peridotite breccia with rounded clasts and sporadically a limestone clast: free movement, transport over large distances, for large limestone clasts gravity sliding may have played a role;
- Peridotite breccia with rounded clasts and exotic clasts: free movement, transport of exotic clasts, sometimes over very large distances;
- Limestone breccia with peridotite matrix: well-sorted, little matrix, no calcite, water with high energy, deposition in one place, for example small channel.

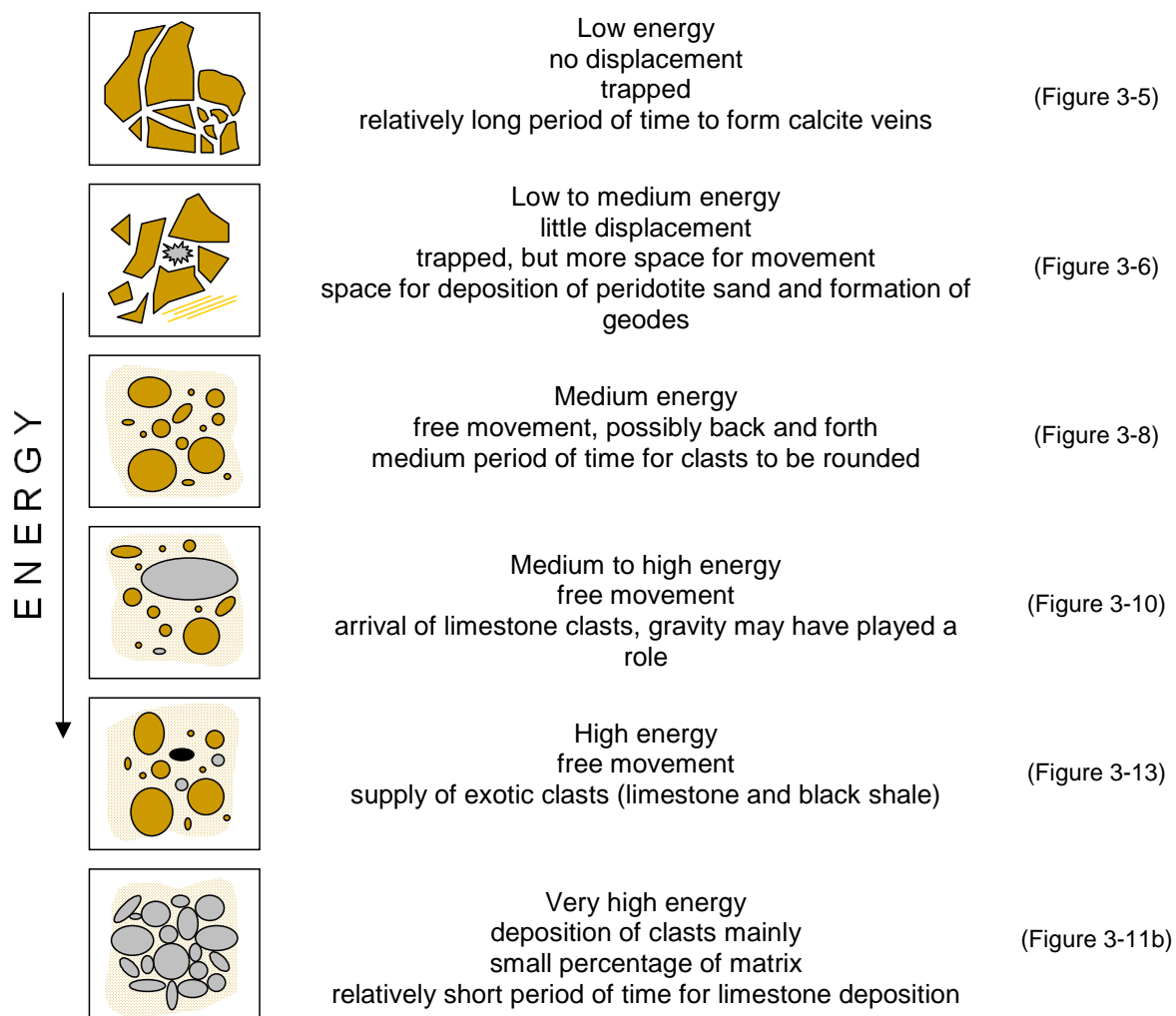


Table 3-4: Conceptual model for development of breccias in the Lherz body.

Literature

The peridotite breccia of type 1, as distinguished by Lagabrielle and Bodinier (2008), with little displacement between the clasts, has not been recognized in the south or east by us. Rather, in the south-east peridotite breccia was found with rounded clasts that must have undergone some movement. Breccias including isolated clasts of limestone (type 2 according to Lagabrielle and Bodinier) were observed at a location nearby. However they consist of rounded peridotite clasts. Therefore we have not been able to determine the original relative positioning of the clasts. The type 3 breccia, characterized by thin layers of graded ultramafic sandstone that filled large fissures and found only at specific locations, was not observed. Breccias in this vicinity are assumed to have experienced sedimentary reworking though. Type 4 seems to correspond with the peridotite breccia consisting of angular clasts and calcite veins. In the field the fissures which this type has filled proposedly, were not obvious.

The observations of Lagabrielle and Bodinier are consistent with our findings. They have visited other parts of the Lherz body, but their findings are complementary. The hypothesis of Lagabrielle and Bodinier about the emplacement of the Lherz body as described in the section 3.4 seems very plausible.

An overview of geological events and breccia development along with a geological time scale is given below:

<i>Time</i>	<i>Geological events</i>	<i>Breccia development</i>
Albian (Cretaceous)	Preorogenic rifting	
	Mantle rocks progressively rise to surface along detachment fault; thermal anomaly → HT LP metamorphism	mylonitic streaks of spinel, serpentinization
	Exhumation of mantle rocks	fault breccia
	Formation of narrow, deep basin	transport of loose fragments
	Gravity-sliding of Mesozoic carbonate platforms and some Early Jurassic black shale	exotic clasts are transported into peridotite basin
	Calcium carbonate dissolved in water	Calcite crystals form → propagation of micro-cracks due to precipitation of calcite (reaction-induced fracturing)
	Transportation of detrital calcite particles by water	Deposition of peridotite and calcite particles
–	–	Formation of calcite veins
–	–	Lherz body is detached from mantle
Late Cretaceous	Compressional phases during orogeny of Pyrenees	Uplift together with Mesozoic limestones
Tertiary to present		Weathering and erosion

Table 3-5: Influences of geological events on breccia development in Lherz body.

3.7 Conclusions

Several types of breccias were distinguished in the field, among which are peridotite breccias with angular clasts and a calcite matrix, peridotite breccias consisting of rounded clasts and possibly containing carbonate clasts or even black shale, and a clast-supported carbonate breccia with a peridotite matrix.

Cross-cutting relations show that the process of serpentinization occurred before carbonation. EMP analyses point out that calcite veins include μ -sized peridotite particles causing a light brown colour. Lamination structures were found within this type of matrix, indicating sedimentary deposition of peridotite and calcite particles. The presence of this matrix inside geodes indicates deposition after formation of geodes. The matrix is cut by pure calcite veins, indicating later stage calcite veining.

The absence of magnesium-rich carbonates and the low amount of calcium present in lherzolite, largely excludes reaction-induced fracturing as an explanation for the origin of the breccias found in the Lherz body. Rotated clasts and the presence of geodes are not explained by reaction-induced fracturing either.

The breccias most likely have a cataclastic origin, after which clasts were reworked through sedimentary processes. The presence of large exotic clasts (dm-scale) in the middle of the mantle body suggests that gravitational mass movements played a role. Local differences in the sedimentary setting are responsible for a difference in clast movement and energy. This results in the types of breccias mentioned above, with different amounts and appearance forms (vein, clast, matrix) of carbonate.

Very fine-grained, homogeneous serpentine, present at one specific locality, is consistent with the retrograde path the Lherz body has followed.

Tectonic brecciation took place during exhumation of the mantle rock. No later-stage brecciation is observed after the sedimentary reworking. This implies that the Lherz body was protected from faults during the Pyrenean orogeny. The findings and their geological implications correspond to the geological history of the emplacement of the Lherz body that is proposed by Lagabrielle et al. (2010).

It remains to be investigated how exactly carbonate was incorporated in the proposed setting and what causes the appearance of calcite veins only near the contact of the peridotite with the Mesozoic limestone. Different generations of calcite veining could possibly be distinguished by a difference in chemical contents. Thin sections of polymictic breccias can be made to investigate whether and to what extent calcite is present in the matrix together with limestone clasts.

4. Summary

Studying naturally fractured mantle rocks contributes to ongoing research on possibilities of in situ CO₂ sequestration in mantle rocks. Two case-studies were done on the development of fracture networks in peridotite and the role of serpentinization and carbonation in fracturing. The peridotite bodies of Raudhaugene and Ugelvik, in the Western Gneiss Region (Norway), and the Lherz body (French Pyrenees) were investigated. In this summary the main findings are listed and compared with other geological settings where in situ carbonation has taken place.

What general types of fracture patterns are found in the peridotite bodies in the Western Gneiss Region and Lherz?

The peridotite bodies of Raudhaugene and Ugelvik are characterized by a variety of fracture networks at different scales:

- Homogeneous fracture network at microscale.
- Absence of fracture networks at cm scale.
- Regular fracture pattern with a dominant orientation in pyroxenite layers.
- Outcrop scale fractures are very thin (1 mm) extensional fractures with various orientations and are filled with serpentine. They cut each other and the compositional banding fairly randomly, although fractures at angles of 60, 90 and 120 degrees also occur. At some localities thick serpentine veins with a second generation of perpendicular fractures were found and parallel talc veins have been observed.
- Although no clear fracture pattern is observed on a regional scale, the preferable orientation indicates E-W extension.

The Lherz peridotite body is fractured extensively and outcrops consist mainly of characteristic breccias:

- Peridotite breccias with angular clasts, calcite veins and a matrix of calcite, and peridotite sediments. Clasts are either in-situ or they have rotated. Calcite and peridotite sediments show laminar structures and geodes have formed in open spaces.
- Peridotite breccias consisting of rounded clasts of peridotite and serpentinite and a matrix consisting of similar rock particles. In some parts of the Lherz body, limestone clasts are included in the breccia, this varies from sporadic limestone clasts to a clast-supported carbonate breccia with a peridotite matrix.
- Peridotite breccias consisting of rounded clasts of peridotite, serpentinite, carbonate clasts and black shale.

In the Semail ophiolite in Oman and Atlin in British Columbia, Canada, extensive dense fracture networks are found at predominantly right angles and (mainly magnesium rich) carbonate veins are abundantly present (Kelemen & Matter, 2008; Hansen et al., 2005).

What do the fracture patterns reveal about the process(es) that formed them?

In the Raudhaugene and Ugelvik peridotite bodies multiple mechanisms play a role in creating stress fields in the rock that result in fracturing:

- Thermal cracking is the most likely mechanism for the formation of the micro-fracture network. This network enabled fluids to infiltrate deep into a rock, resulting in a homogeneous serpentine network.
- The angles at which fractures in the peridotite have formed with respect to each other suggest that hierarchical fracturing has played a role.
- The crack-seal structure observed in the fractures in the pyroxenite layers shows extension has taken place during serpentinization. The regularly spaced fractures are partly explained by differential volume expansion due to serpentinization. The predicted volume change in the adjacent peridotite is large enough to cause the observed extension in the pyroxenite layers. The dominant orientation is explained by influences from regional stress.
- The fracture patterns with various orientations have probably formed by multiple phases of regional extension. The thin fractures and lack of off-sets suggest only minor extension.

The Lherz peridotite body is intensely fractured due to tectonic stress and subsequently reworked by sedimentary processes:

- Intense fracturing has most likely occurred to tectonics, strongly suggested by its tectonic history; a mantle body on top of a mountain.
- Lamination structures in the calcite-peridotite matrix and the incorporation of limestone clasts in the peridotite breccia indicate sedimentary processes.
- Cross-cutting relationships show that serpentinization has occurred before the formation of calcite veins and is not involved in fracturing.
- Calcite veins have formed before and after deposition of calcite and peridotite particles.
- The presence of limestone clasts in the breccias, calcite sediment and calcite crystals in the form of veins and geodes indicate that the origin of the calcite is most likely the Mesozoic limestones in which the peridotite is now embedded. Large limestone clasts have most likely entered the system by gravitational processes.

Did reaction-induced fracturing play a role in the development?

The fractures in the peridotite bodies of Raudhaugene and Ugelvik show no evidence for reaction-induced fracturing. The fractures in the pyroxenite layers were formed due to volume expansion in the surrounding peridotite and are therefore indirectly reaction-induced.

- No micro-structural evidence for reaction-induced fracturing in peridotite rock in the form of deformational features has been found.
- The presence of calcite in open fractures does not provide evidence that the crystal growth of the calcite minerals are involved in fracturing the peridotite. No carbonates have been observed in the mesh.

Reaction-induced fracturing has not played a role in brecciating the Lherz body.

- The absence of Mg-rich carbonates and the low amount of calcium in lherzolite indicate that the peridotite was chemically not involved in carbonation.
- Rotated clasts and the presence of geodes in open spaces cannot be explained by reaction-induced fracturing.

Mg-rich carbonates in the mesh and veins of the upper mantle rocks in the Semail ophiolite (Oman) and Atlin (British Columbia, Canada), indicate involvement of the peridotite in the chemical processes that have taken place. Carbonation in the mantle rocks in Atlin is preserved in the form of distinct mineralogical zones separated by reaction fronts. In both geological settings, in situ carbonation has caused extensive fracturing.

Concluding

In Raudhaugene and Ugelvik, the fractures in the peridotite and pyroxenite layers cannot be explained by a simple model of regional stress or reaction-induced fracturing. More mechanisms play a role in the development of a large variety of fracture networks: regional stress, hierarchical fracturing, volume expansion due to serpentinization and thermal contraction. The fractured pyroxenite layers indicate that expansion has taken place due to serpentinization, but the role of serpentinization in the formation of fractures in peridotite cannot readily be determined. Brecciation of the Lherz peridotite is the result of tectonic stress and sedimentary reworking. In both geological settings, carbonates are present in the form of calcite in fractures, but their origin is most likely outside the system. No evidence has been found that they are involved in fracturing.

In other geological settings, like the Semail ophiolite and mantle rocks in Atlin, evidence of in situ carbonation and reaction-induced fracturing is given by the presence of Mg-rich carbonates in both mesh and veins. All carbonate mineral reactions involved, occur at very low pressure and temperature conditions, corresponding to shallow levels in the crust. The permeability of the rock plays an important role in fluid infiltration. The continuity of the mineral reactions and volume expansion is hampered by a strong decrease in permeability as observed in experiments in the High Pressure and Temperature Laboratory at Utrecht University (Van Noort, pers. comm.). In natural settings, hydrothermal fluids may play an important role in sustaining the optimal temperatures for a sufficient amount of time, which are needed for in situ carbonation to occur. In addition, a CO₂-rich fluid is favourable for carbonate reactions to take place. The development of reaction-induced fracture networks can best be studied in natural examples of mineral-carbonation systems with optimal conditions for carbonate reactions.

5. References

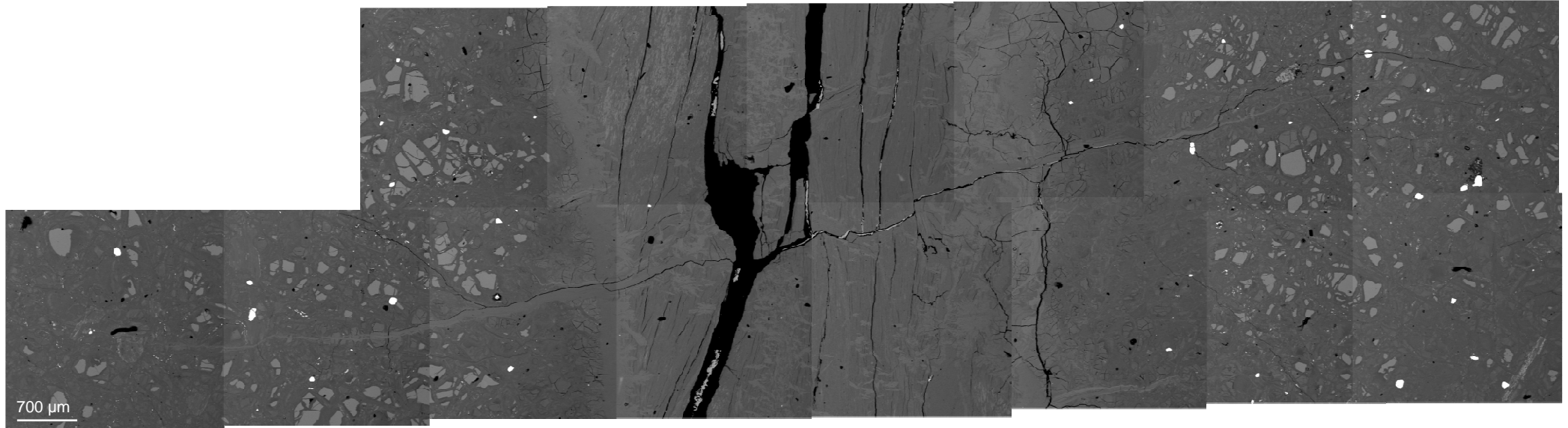
- Ahrens, T.J. (1995). *Mineral physics & crystallography, a handbook of physical constants*. American Geophysical Union, Washington.
- Anderson, H.J. (1985). Gravity modelling of the Iherzolite body at Lers (French Pyrenees); some regional implications. *Geol. Mag.* 122 (1), 51-56.
- Andreani, M., Mével, C., Boullier, A.-M. and Escartín, J. (2007). Dynamic control on serpentine crystallization in veins: Constraints on hydration processes in oceanic peridotites. *Geochemistry, Geophysics, Geosystems*, 8, Q02012, doi:10.1029/2006GC001373.
- Andreani, M., Baronnet, A., Boullier, A.-M. and Gratier, J.-P. (2004). A microstructural study of a "crack-seal" type serpentine vein using SEM and TEM techniques. *European Journal of Mineralogies*, 16, 585-595.
- Bohn, S., Platkiewicz, J., Andreotti, B., Adda-Bedia, M. and Couder, Y. (2005c). Hierarchical crack pattern as formed by successive domain division. II. From disordered to deterministic behaviour. *Phys. Rev. E* 71, 046215.
- Carswell, D.A. (1968). Possible primary upper mantle peridotite in Norwegian basal gneiss. *Lithos*, 1, 322-355.
- Carswell, D.A. (1973). Garnet pyroxenite lens within Ugelvik layered garnet peridotite. *Earth and Planetary Science Letters*, 20, 347-352.
- Choukroune, P. (1980). Comment on 'Quenching: an additional model for emplacement of the Iherzolite at Lers (French Pyrenees)'. *Geology*, ?, 514, November 1980.
- Drury M.R., Van Roermund, H.L.M., Carswell, D.A., De Smet, J.H., Van den Berg, A.P. and Vlaar, N.J. (2001). Emplacement of deep upper-mantle rocks into cratonic lithosphere by convection and diapiric upwelling. *Journal of Petrology*, 42, 131-140.
- Etheridge, M.A., Wall, V.J. and Cox, S.F. (1984). High fluid pressures during regional metamorphism and deformation: implications for mass transport and deformation mechanisms. *Journal of Geophysical Research*, 89, 4344-4358.
- Hansen, L.D., Dipple, G.M., Gordon, T.M. and Kellett, D.A. (2005). Carbonated serpentinite (listwanite) at Atlin, British Columbia: a geological analogue to carbon dioxide sequestration. *The Canadian Mineralogist*, 43, 225-239.
- Iyer, K., Jamtveit, B., Mathiesen, J., Malthe-Sørenssen, A. and Feder, J. (2008). Reaction-assisted hierarchical fracturing during serpentinization. *Earth and Planetary Science Letters*, 267, 503-516.
- Jamtveit, B., Malthe-Sørenssen, A. and Kostenko, O. (2008). Reaction enhanced permeability during retrogressive metamorphism. *Earth and Planetary Science Letters*, 267, 620-627.
- Jamtveit, B., Putnis, C.V. and Malthe-Sørenssen, A. (2009). Reaction induced fracturing during replacement processes. *Contributions to Mineralogy and Petrology*, 157, 127-133.
- Kelemen, P.B. and Matter, J. (2008). In situ carbonation of peridotite for CO₂ storage. *Proceedings of the [US] National Academy of Sciences*, 105, 17295-17300.
- Lachenbruch, A.H. (1962). Mechanics of thermal contraction cracks and ice-wedge polygons in permafrost. *Geol. Soc. Amer. Spec. Paper* 70 (69 p).
- Lachenbruch, A.H. (1963). Contraction theory of ice-wedge polygons: a qualitative discussion. *Permafrost international conference. Proc. Natl. Acad. Sci.*, vol. 63-71 (Washington), (563 p).
- Lagabriele, Y. and Bodinier, J.-L. (2008). Submarine reworking of exhumed subcontinental mantle rocks: field evidence from the Lherz peridotites, French Pyrenees. *Terra Nova*, 20, 11-21.
- Lagabriele, Y., Labaume, P. and De Saint Blanquat, M. (2010). Mantle exhumation, crustal denudation, and gravity tectonics during Cretaceous rifting in the Pyrenean realm (SW Europe): Insights from the geological setting of the Iherzolite bodies. *Tectonics*, 29.

- Le Roux, V., Bodinier, J.-L., Tommasi, A., Alard, O., Dautria, J.-M., Vauchez, A. and Riches, A.J.V. (2007). The Lherz spinel lherzolite: refertilized rather than pristine mantle. *Earth and Planetary Science Letters*, 259, 599-612.
- Mével, C. (2003). Serpentinization of abyssal peridotites at mid-ocean ridges. *C. R. Geoscience*, 335, 825-852.
- Minnigh, L.D., Van Calsteren, P.W.C. and Den Tex, E. (1980). Quenching: an additional model for emplacement of the lherzolite at Lers (French Pyrenees). *Geology*, 8, 18-21.
- Monchoux, P. (1970). Les lherzolites Pyrénées: contribution à l'étude de leur mineralogy, de leur genèse et de leurs transformations [thèse]. Toulouse, France, Université Paul Sabatier, 180 p.
- O'Hanley, D.S. (1992). Solution to the volume problem in serpentinization. *Geology*, 20, 705-708.
- Palasse, L.N. (2008). Microstructural evolution and seismic anisotropy of upper mantle rocks in rift zones. Phd thesis, Universiteit Utrecht, The Netherlands.
- Prichard, H.M. (1979). A petrographic study of the process of serpentinisation in ophiolites and the ocean crust. *Contributions to Mineralogy and Petrology*, 68, 231-241.
- Ramsay, J.G. (1980). The crack-seal mechanism of rock deformation. *Nature* 284, 135-139.
- Rudge, J.F., Kelemen, P.B. and Spiegelman, M. (2010). A simple model of reaction-induced cracking applied to serpentinization and carbonation of peridotite. *Earth and Planetary Science Letters*, 291, 215-227.
- Schuilng, R.D. and Krijgsman, P. (2006a). Enhanced weathering: an effective and cheap tool to sequester CO₂. *Climatic Change*, 74, 349-354.
- Spengler, D. (2006). Origin and evolution of deep upper mantle rocks from Western Norway. Phd thesis, Universiteit Utrecht, The Netherlands.
- Toga, K.B. and Alaca, B.E., (2006). Junction formation during desiccation cracking. *Phys. Rev. E* 74, 021405.
- Twiss, R.J. and Moores, E.M. (1992). *Structural Geology*. W.H. Freeman and Company, New York.
- Van Roermund, H.L.M. and Drury, M.R. (1998). Ultra-high pressure (P>6 GPa) garnet peridotites in western Norway: exhumation of mantle rocks from more than 185km. *Terra Nova*, 10, 295-301.
- Van Roermund, H.L.M., Drury, M.R., Barnhoorn, A. and De Ronde, A.A. (2000a). Super-silicic garnet microstructures from an orogenic garnet peridotite, evidence for an ultra-deep (>6 GPa) origin. *Journal of Metamorphic Geology*, 18, 135-147.

Appendix A: List of mineralogy

				Mg : Si
Hydrous minerals				
	serpentine	serp	$(\text{Mg, Fe})_3\text{Si}_2\text{O}_5(\text{OH})_4$	3:2
	<i>chrysotile</i>		$\text{Mg}_3\text{Si}_2\text{O}_5(\text{OH})_4$	
	<i>lizardite</i>		$(\text{Mg}_{2,8}\text{Fe}_{0,1}\text{Al}_{0,1})(\text{Si}_{1,9}\text{Al}_{0,1})\text{O}_5(\text{OH})_4$	
	<i>antigorite</i>		$\text{Mg}_{48}\text{Si}_{34}\text{O}_{85}(\text{OH})_{62}$	
T↓	talc	tlc	$\text{Mg}_3\text{Si}_4\text{O}_{10}(\text{OH})_2$	3:4
	chlorite	chl	$(\text{Mg, Fe, Al})_3(\text{Si, Al})_2\text{O}_5(\text{OH})_4$	3:2
	<i>clinochlore</i>		$(\text{Mg}_5\text{Al})(\text{AlSi}_3)\text{O}_{10}(\text{OH})_8$	
	amphibole	amp		5:8
	<i>actinolite</i>		$\text{Ca}_2(\text{Mg, Fe})_5\text{Si}_8\text{O}_{22}(\text{OH})_2$	
	<i>tremolite</i>		$\text{Ca}_2\text{Mg}_5\text{Si}_8\text{O}_{22}(\text{OH})_2$	
	<i>hornblende</i>		$\text{Ca}_2(\text{Mg, Fe, Al})_5(\text{Al, Si})_8\text{O}_{22}(\text{OH})_2$	
	<i>anthophyllite</i>		$(\text{Mg, Fe})_7\text{Si}_8\text{O}_{22}(\text{OH})_2$	7:8
Minerals in peridotites and pyroxenites				
	olivine	ol	$(\text{Mg, Fe})_2\text{SiO}_4$	2:1
	<i>forsterite</i>		Mg_2SiO_4	
	<i>fayalite</i>		Fe_2SiO_4	
	orthopyroxene	opx		1:1
	<i>enstatite</i>		$\text{Mg}_2\text{Si}_2\text{O}_6$	
	clinopyroxene	cpx		1:2
	<i>diopside</i>		$\text{CaMgSi}_2\text{O}_6$	
Al-bearing minerals				
	plagioclase	plag		
P↓	spinel	spi	$(\text{Mg, Fe})(\text{Al, Cr})_2\text{O}_4$	
	<i>spinel</i>		MgAl_2O_4	
	<i>hercynite</i>		FeAl_2O_4	
	<i>magnesiochromite</i>		MgCr_2O_4	
	<i>chromite</i>		FeCr_2O_4	
	garnet	grt		
	<i>pyrope</i>		$\text{Mg}_3\text{Al}_2(\text{SiO}_4)_3$	
	<i>almandine</i>		$\text{Fe}_3\text{Al}_2(\text{SiO}_4)_3$	
Possible reaction products				
	brucite		$\text{Mg}(\text{OH})_2$	
	magnesite		MgCO_3	
	dolomite		$\text{CaMg}(\text{CO}_3)_2$	
	calcite		CaCO_3	
	nickel sulfate		NiSO_4	
	magnetite		Fe_3O_4	

Appendix B



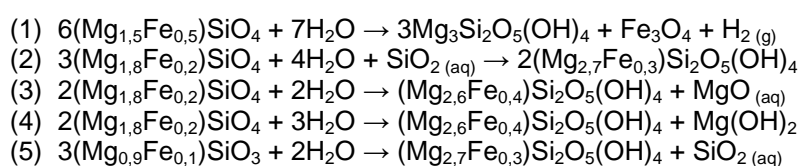
EMP picture of peridotite rock along the coast of Ugelvik cut by two generations of fractures. Thick fibrous serpentine vein in the center, running vertically. Rim is marked by a band of star-shaped serpentine crystals grown over the fibrous serpentine crystals. On both sides olivine relicts and some orthopyroxene crystals (darker) are surrounded by a serpentine network. In between olivine relicts rims of magnetite (white) are visible. Some randomly scattered spinel crystals (white) are also present. A second generation serpentine vein cuts the thick vein, running from lower left to upper right of this picture. It does not have marked edges and disappears into the matrix on both sides. Along both the thick vein and the thin vein cutting across it, calcite crystals are found. They are found in open spaces within these fractures.

Appendix C: Volume change calculations

Volume increase in peridotite

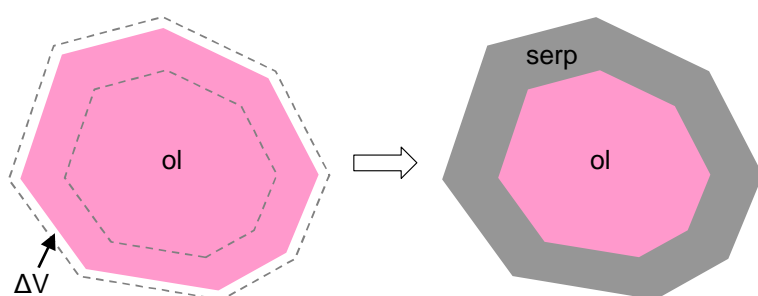
Volume change calculations have been done for two samples (R422 and U631) of peridotite adjacent to the pyroxenite layers (Figure 2-24) to determine how much expansion may have taken place and whether this could be responsible for the extension in the pyroxenite layers. The calculations were done for each sample separately.

First, for each of the reactions below the volume expansion was derived by calculating the molar volume of solids before and after the reaction. The proportions of the elements per mineral are based on EMP measurements. Some assumptions had to be made for the reactions to be balanced. Furthermore, the thin sections of both samples were analyzed to determine the composition of the peridotite and to what extent serpentinization has taken place. To be able to compare the volume increases (3D) with the two-dimensional percentages in the thin sections the volume increase for two dimensions was also calculated.



Reaction	Mol. vol. reactants (dm ³)	Mol. vol. products (dm ³)	Volume expansion 3D (%)	Area expansion 2D (%)
1	0.2673	0.3771	41	26
2	0.1322	0.2293	73	44
3	0.0871	0.1159	33	21
4	0.0871	0.1402	61	37
5	0.0940	0.1146	22	14

For both samples, the peridotite adjacent to the pyroxenite layer was analyzed to estimate the relative amounts of olivine and enstatite and to determine to which extent these minerals have been serpentinized. As we assume volume expansion due to serpentinization, the thin sections represent the expanded peridotite. Originally, the volume of the peridotite rock and area in thin section was slightly smaller (see schematic drawing below). In both samples the olivine has partially been serpentinized. The schematic drawing shows an olivine crystal (or crystal fragment) that is serpentinized along the outer rim. Only the part of the olivine crystal involved in the reaction has undergone a slight volume increase.



Schematic drawing of original olivine crystal (left) and serpentinized olivine crystal (right). ΔV indicates the volume change with respect to the part of the olivine crystal that reacted to form serpentine.

Both samples consist of approximately 95% olivine and 5% enstatite. Enstatite is usually less altered than olivine. The relative amount of serpentine reacted from enstatite crystals is 30 or 40%, while for olivine this is 50 or 60% (see table below).

Thin section	Ol + serp.ol (%)	En + serp.en (%)	Serp. ol (%)	Serp. en (%)
R422	95	5	60	30
U631	95	5	50	40

Taking into account these percentages, the expected volume change in the peridotite can be calculated using one of the first four reactions in combination with the fifth reaction. When ΔO = area expansion 2D for olivine (the result of one of the reactions involving olivine) and ΔE = area expansion 2D for enstatite (the result of the reaction involving enstatite), then

$$\text{volume expansion 2D (in \%)} = 95 * (\Delta O / ((\Delta O + 100) * \frac{40}{60} + 100)) + 5 * (\Delta E / ((\Delta E + 100) * \frac{70}{30} + 100))$$

and

$$\text{volume expansion 2D (in \%)} = 95 * (\Delta O / ((\Delta O + 100) * \frac{50}{50} + 100)) + 5 * (\Delta E / ((\Delta E + 100) * \frac{60}{40} + 100))$$

for R422 and U631 respectively.

From the derived 2-dimensional area expansion the linear expansion was calculated, so that the results can be compared to the (linear) extension in the pyroxenite layers.

Thin section R422

Reactions	Area expansion 2D (%)	Linear expansion 1D (%)
1+5	14	7
2+5	22	10
3+5	11	5
4+5	19	9

Thin section U631

Reactions	Area expansion 2D (%)	Linear expansion 1D (%)
1+5	11	5
2+5	18	8
3+5	9	5
4+5	15	7

Extension in pyroxenite layer

Finally, for both samples the thickness of the fractures in the pyroxenite layers were measured to determine how much extension has taken place.

Sample R422

Total length pyroxenite layer	65 mm
4 x 1mm thick FR	4 mm
5 x 0.5 mm thick FR	2.5 mm
4 x 0.25 mm thick FR	1 mm
Total linear extension (in mm)	7.5 mm
Total linear extension (in %)	13 %

Sample U631

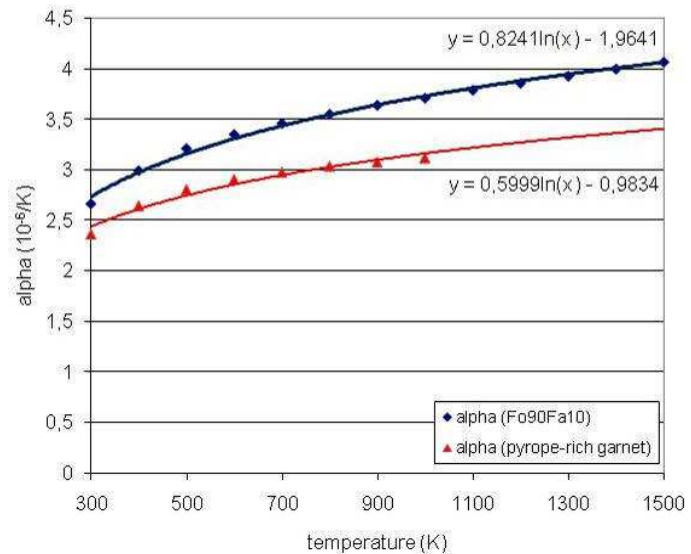
Total length pyroxenite layer	83 mm
6 x 1mm thick FR	6 mm
3 x 0.5 mm thick FR	1.5 mm
4 x 0.25 mm thick FR	1 mm
Total linear extension (in mm)	8.5 mm
Total linear extension (in %)	11 %

For all reactions the linear expansion in the peridotite is less than the extension in the pyroxenite layer.

Appendix D: Thermal contraction calculations

Thermal expansion coefficients are given by Ahrens (1995). Olivine represents peridotite rock. For the pyroxenite layers thermal expansion coefficients for pyrope-rich garnet have been used.

T in K	α_v (Fo90Fa10) in $10^{-6}/^{\circ}\text{C}$	α_v (Pyr-rich Grt) in $10^{-6}/^{\circ}\text{C}$
300	2,66	2,36
400	2,99	2,64
500	3,21	2,8
600	3,35	2,9
700	3,46	2,97
800	3,55	3,03
900	3,64	3,07
1000	3,71	3,11
1100	3,79	
1200	3,86	
1300	3,93	
1400	4	
1500	4,07	



For the peridotite, calculations have been done in the following way. The curve that fits best with these data is given by $\alpha_v(T) = 0.8241 \ln(T) - 1.9641$.

The change in volume is given by:

$$\frac{\Delta V}{V} = \int_{T_0}^{T_1} \alpha_v(T) dT = [0.82417 \ln(T) - 2.78827]$$

where $\Delta V/V$ is the fractional change in volume, T_0 is the starting temperature, T_1 is the final temperature and $\alpha_v(T)$ is the thermal expansion coefficient as a function of temperature T .

If we consider the uplift of the peridotite body from regions of about 1000 to 10°C (1300 to 300K), we can calculate the fractional change in volume $\Delta V/V = -0,35\%$.

Analogue, a general formula for the thermal expansion coefficients of the pyroxenite layer is given by $\alpha_v(T) = 0.5999 \ln(T) - 0.9834$.

The change in volume is given by:

$$\frac{\Delta V}{V} = \int_{T_0}^{T_1} \alpha_v(T) dT = [0.59997 \ln(T) - 1.58337]$$

For a change in temperature from 1000 to 10°C (1300 to 300K) the fractional change in volume is $\Delta V/V = -0,30\%$.

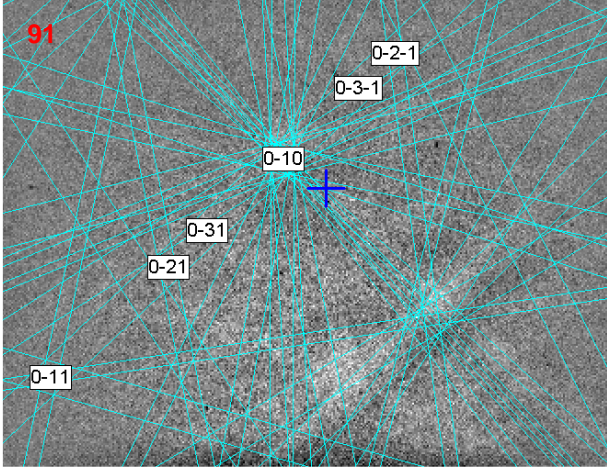
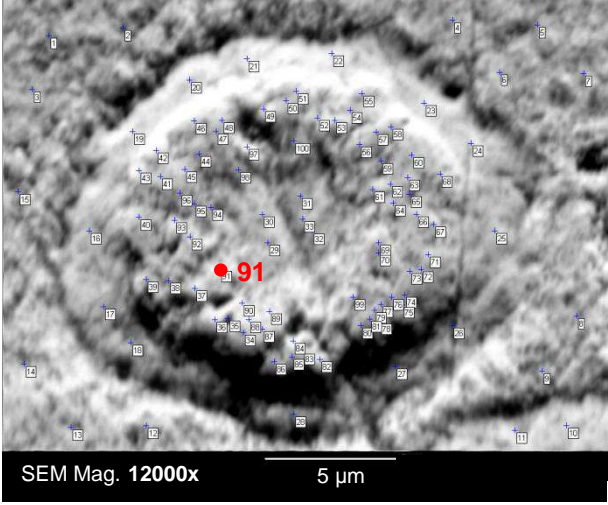
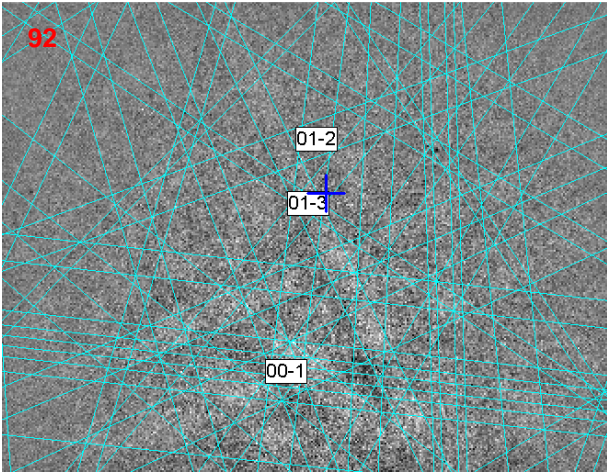
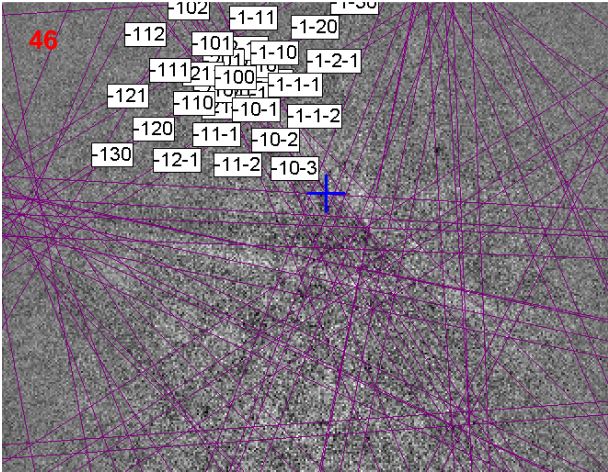
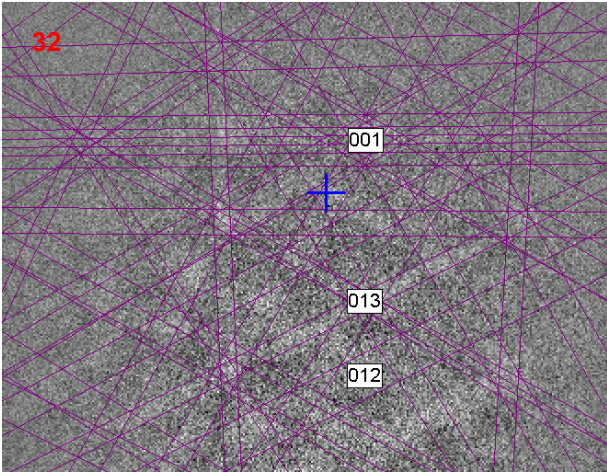
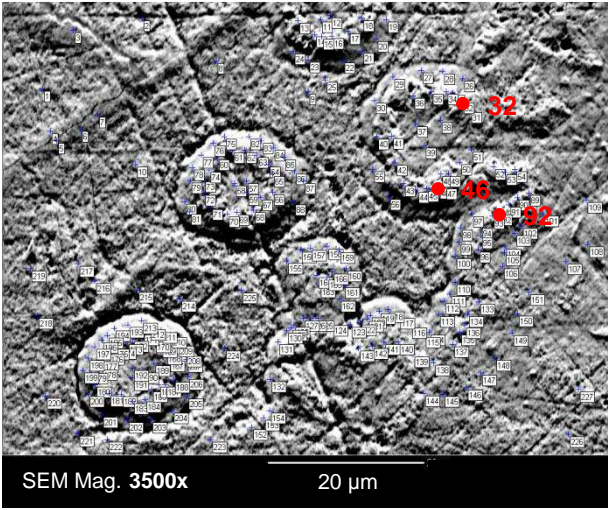
Assuming isotropic materials, the linear thermal expansion coefficient is given by $\alpha L \approx \frac{1}{3} \alpha_v$. This means that the change in linear dimension can be computed as follows:

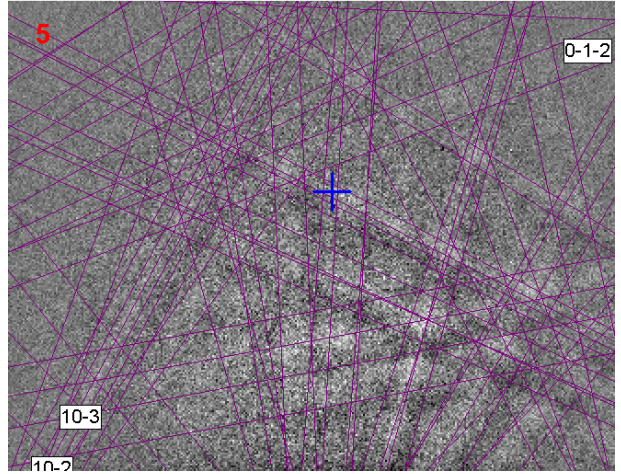
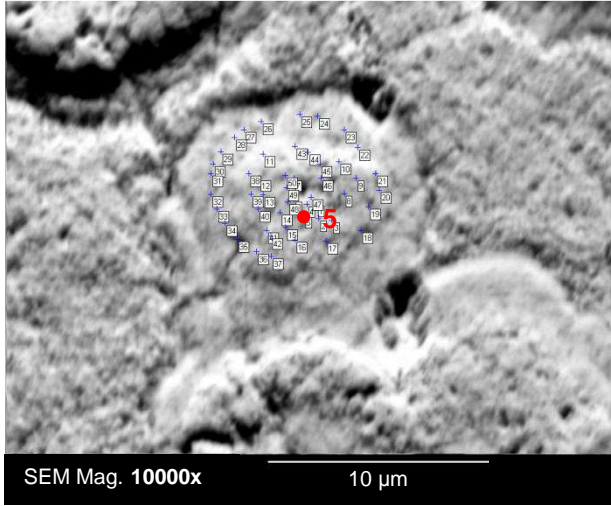
$$\frac{\Delta L}{L} = \int_{T_0}^{T_1} \alpha L(T) dT = \frac{1}{3} \int_{T_0}^{T_1} \alpha_v(T) dT = \frac{1}{3} \frac{\Delta V}{V}$$

So the order of linear contraction is about -0,12% for peridotite and -0,10% for the pyroxenite layers.

Appendix E: EBSD patterns

EBSD-patterns in rim of circles found along contact homogeneous matrix and peridotite rock:





Acknowledgements

I would like to thank Martyn Drury and Chris Spiers for giving me the opportunity to do this research project and for their support and critical feedback. In addition, I thank my fieldwork partner Karen Oud, Auke Barnhoorn for his useful comments and support, Reinier van Noort for valuable input and assisting with XRD-analyses, Côme Lefebvre for helpful discussions and support, Herman van Roermund, Tilly Bouten for assisting with EMP and μ -XRF analyses, Saskia ten Grotenhuis for helping with the SEM, Maartje Hamers for joining me in the field for two rainy days and helping me with EBSD measurements, David Mainprice from Université Montpellier for providing serpentine structure files, Kalijn and Annelies for support and nice lunch breaks and especially Maarten for everlasting support.